Gas phase heterogeneous catalyst performance testing in laboratory fixed-bed reactors.

by

Dawid Kruger

Submitted in partial fulfilment of the requirements for the degree of

Master of Science in Engineering

University of Cape Town

University of Cape Town

Department of Chemical Engineering

Catalysis Institute

Supervisor: Prof. Jack C. Q. Fletcher

Co-supervisor: Mr Stephen J. Roberts

The copyright of this thesis vests in the author. No quotation from it or information derived from it is to be published without full acknowledgement of the source. The thesis is to be used for private study or non-commercial research purposes only.

Published by the University of Cape Town (UCT) in terms of the non-exclusive license granted to UCT by the author.

University of Cape Town

Abstract

Activity, selectivity and stability are invariably among the key factors of the performance of a catalyst. In the development of catalysts these properties are often screened for a range of materials and formulations. Interpretation of these key performance indicators are prone to various confounding effects. Here, performance testing of solid, porous catalysts for gas phase reactions in tubular fixed bed reactors is considered. Transport limitations and particularly internal mass transfer limitations are often cited in this case. Many have given general discussions and guides for effective catalyst performance testing, reviewed or put forward theoretical descriptions for transport phenomena and have measured and correlated associated transport coefficients. Some quantitative requirements and the relative importance of different effects have been found to remain unclear.

Here, some of these aspects are addressed by the development of 3 catalyst testing criteria. Specifically, an upper limit is derived for the chemical conversion in a first-order reaction such that differential rate conditions are established, a lower limit on the chemical conversion is applied to limit the loss of precision in conversion measurements, and an expression is derived to limit the effect of pressure drop across a catalyst bed on the observed rate of a first-order reaction.

The prevalence and sensitivity of these and other transport limitation criteria were investigated theoretically in the context of the low-temperature (LT) water-gas shift (WGS) reaction over a $Cu/ZnO/Al_2O_3$ catalyst in a laboratory scale performance test. Factorial combination of some commonly manipulated experimental parameters (reactant feed rate, temperature, catalyst particle size, catalyst loading, dilution fraction and reactor tube size) was employed in this regard. The upper conversion limit, the internal mass transfer criterion and the radial heat transfer criterion were found to be particularly severe. So too, to a lesser extent, were the axial dispersion and pressure drop criteria, and the lower conversion limit. The sensitivity analysis indicated optima in the varied experimental parameters and yielded insights into effective control of different effects by selection of process conditions.

Application of the set of criteria in an experimental performance test was demonstrated using a proprietary medium-temperature (MT), WGS catalyst under reaction at temperatures of 275 °C, 300 °C and 375 °C, 1 atm total pressure, dry feed composition of 10% CO, 10% CO_2, 70% H_2, 10% N_2, steam-to-dry gas ratio of 0.5 and 158 h^{-1} weight hourly space velocity (WHSV). The catalyst was found to have near total selectivity towards the WGS reaction with activities of 12.2 ± 1.1, 17.1 ± 0.5 and 24.9 ± 1.5 μmol/s.g_{cat} at 275 °C, 300 °C and 375 °C respectively. This corresponds to an activation energy of 39 ± 2 kJ/mol; a value within range of what is reported in literature for similar catalysts.

This experiment also served to compare experimental and predicted internal mass transfer limitations by testing catalyst particles of different mean sizes. This catalyst as well as a $CuO/ZnO/Al_2O_3$ catalyst precursor was characterised in respect of their pore size distributions (N_2 physisorption and mercury intrusion porosimetry (MIP)), particle size distributions (by photo- and microscopic analysis), bulk and particle densities and product gas compositions (by gas chromatography) to enable evaluation of the various criteria employed.

Evaluation of the various criteria indicated that, theoretically, the considered confounding effects had a negligible effect on the measured catalytic activities for the catalyst sample with the smallest mean particle size, while the larger particles experienced only internal mass transfer limitations. Different models considered for effective diffusivities all under-predicted values when compared to the effective diffusivities inferred from the reaction-diffusion experiments. Predictions ranged to within factors of 3 – 20 of the experimental values, depending on whether pore size distribution data were derived from MIP or physisorption data. Here, the lack of characterisation of the macro-porosity by N_2 physisorption resulted in more severe under-estimations of the effective diffusivities than the equivalent estimations made with MIP data. The best prediction was made by the 'parallel-path pore' model by Johnson & Stewart (1965) using MIP data. Predictions of internal mass transfer limitations varied in a similar manner. It is noted that the simplifications of the highly complex porous catalyst by these model combinations introduce large sources of error in the prediction of internal mass transfer limitations.

Acknowledgements

I would like to thank my supervisor Prof. Jack Fletcher and co-supervisor Stephen Roberts for their guidance and unwavering support, faith and patience.

Special thanks must also be given to the members of the Fuel-to-Hydrogen group who have also helped greatly, Niels Luchters, Dr. JV Fletcher, Waldo Koorts and Marianne Werle van der Merwe. I would also like to thank the catalysis technical staff, the Catalysis Institute and the Department of Chemical Engineering at UCT for making this possible. For performing MIP analysis, I would like to acknowledge and thank Sasol Ltd.

For the equally needed non-technical support, my love and thanks to my friends and family.

This work is based on research supported by the National Research Foundation of South Africa (Grant Number: 113571), the Catalysis Institute, UCT and Ada and Berty Levenstein Bursars, who have my gratitude for their financial support.

Plagiarism declaration

I know the meaning of plagiarism and declare that all the work in the document, save for that which is properly acknowledged, is my own. This thesis/dissertation has been submitted to the Turnitin module (or equivalent similarity and originality checking software) and I confirm that my supervisor has seen my report and any concerns revealed by such have been resolved with my supervisor.

Signed by candidate

Dawid Kruger

22 April 2019

Content

List of figures

List of tables

List of Abbreviations

Abbreviation	Description
AR	(Particle) Aspect Ratio
BET	Brunauer-Emmett-Teller (Physisorption analysis)
BJH	Barrett-Joyner-Halenda (Physisorption analysis)
CSTR	Continuous Stirred-Tank Reactor
FIC	Flow Indication and Control
FT	Flow Transmitter
GC	Gas Chromatography
ID	(Tube) Internal Diameter
LT	Low-Temperature (of reaction)
LPG	Liquified Petroleum Gas
MARR	Mean Absolute Relative Residuals
MFC	Mass Flow Controller
MinFeret	Minimum Feret (diameter); Minimum calliper diameter
MIP	Mercury Intrusion Porosimetry
MS5A	Molecular Sieve 5 Angstrom (gas chromatography column)
MT	Medium-Temperature (of reaction);
OD	Outer Diameter
PFR	Plug-Flow Reactor
PIC	Pressure Indicator Controller
PPQ	PoraPLOT Q (gas chromatography column)
PPP	Parallel-Path Pore (model); See equation 34
RP	Random Pore (model); See equation 35
SCCM	Standard Cubic Centimetres per Minute
SP	Single Pore (model); See equation 32
TIC	Temperature Indicator Controller
TOS	Time On-Stream
UMW	University of Cape Town, Medium-temperature, Water-gas shift catalyst
WGS	Water Gas Shift (reaction)
WHSV	Weight Hourly Space Velocity

Notation

Symbol	Description	Units
A	Area of Pre-exponential factor in the Arrhenius equation	
a_m	Volume specific surface area, ($A_{p,external}/V_p$)	m^{-1}
Bo	Bodenstein number	-
b	Volume fraction of bed diluent	-
C	Molar concentration	mol/m^3
$\hat{C}_p$	Specific heat capacity	J/kg.K
D	Diffusion/dispersion coefficient	m^2/s
d	Diameter	m
E_a	Apparent activation energy	J/mol
F	Molar flow rate	mol/s
ΔH_r	Enthalpy change of reaction	J/mol
h_f	External heat transfer coefficient	W/m^2
J	Diffusive flux	$mol/s.m^2$
K_{eq}	(Reaction) Equilibrium constant	
k_c	External mass transfer coefficient	m/s
k	Reaction kinetic constant	
L_{bed}	Bed length	m
M	Molar mass	kg/mol
N	Molar flux	$mol/s.m^2$
N_c	The total number of components in a mixture	-
$\bar{N}$	Success/Failure rate of criteria/criterion	-
Nu	Nusselt number	-
n	Reaction order/number of repeats	-
P	Pressure	Pa
Pe	Peclet number	-
Pr	Prandtl number	-
q	Heat flux	W/m^2
R	Universal gas constant	J/mol.K
$\Re$	Reaction rate per volume (catalyst particle or bed)	$mol/m^3.s$

Symbol	Description	Units
$\Re'$	Reaction rate per catalyst mass	mol/kg.s
Re	Reynolds number	-
r	Radius or radial position	m
Sc	Schmidt number	-
Sh	Sherwood number	-
t_{crit}	Critical T-value	-
T	Temperature	K
$\bar{u}$	Superficial flow velocity	m/s
V	Volume	m^3
v	Diffusion volume (of molecules)	m^3/mol
W	Catalyst weight	kg
X	Conversion	-
y	Gas phase mole fraction	-
z	Length co-ordinate in slab geometry	m
	Greek letters	
α	Maximum allowable relative deviation from ideality	-
β	Prater number	-
γ	Dimensionless temperature	-
ε	Void fraction (voidage)	-
η	Effectiveness factor	-
ϑ	Independent experimental variable	
κ	Bed permeability	m^2
λ	Thermal conductivity	W/m.K
μ	Viscosity	Pa.s
ρ	Density	kg/m^3
σ	Standard deviation	
σ_i	Lennard-Jones collision diameter	m
τ	Tortuosity	-
υ	Stoichiometric coefficient	-
φ	Thiele modulus	-
Ω_μ	Lennard-Jones collision integral for viscosity	-

Subscripts

Symbol	Description	Symbol	Description
0	Initial	LL	Lower limit
b	Bulk	m	Mixture
ax	Axial	obs	Observed
bed	Bed of (catalyst) particles	p	Particle
cat	Catalyst (including support)	pf	Pycnometric fluid
D	Dry	pr	Pore
dil	Diluent	$proj$	Projected (area)
e	Effective	rad	Radial
ex	External/Inter-particle	s	Surface
g	Gas	T	Total
i	Species identifier	t	(Reactor) tube
int	Internal/Intra-particle	UL	Upper limit
j	Other species in a mixture	tur	Turbulent
K	Knudsen	w	(Reactor) Wall
L	Bed Length		

1 Introduction

1.1 Background

Heterogenous catalytic processes are integral to many, vast chemical industries, which are major contributors to the global economy (Petrov, 2002) and, as such, catalyst discovery and development, as well as fundamental catalysis research continues to impact the chemical industry. Catalyst development is mainly driven by economic interests, either for cheaper or better catalysts to replace existing ones or as the key to a new chemical process or product.

Discussions on general strategies for catalyst development can be found in Dautzenberg (1989), Derouane (2002), Petrov (2002), Dumesic, Huber & Boudart (2008) and Kapteijn & Moulijn (2008). Catalyst development strategies and structures are approached somewhat differently by different researchers, but can typically be simplified into the following overall structure:

(1) Combinatorial catalyst synthesis,

Informed by fundamental knowledge of catalysis generating a material 'library'. Key catalyst parameters are identified (active metal species/concentration, crystallite size, promoter species/concentration, support material) and varied in combination to generate a structured variety of potential catalysts.

(2) Screening and characterisation

To unambiguously identify top performing catalysts in terms of specified performance criteria. A catalyst's activity, selectivity and stability (resistance towards deactivation) are invariably among the most important factors that determine its performance. Other desirable characteristics include high mechanical strength, low cost of materials and manufacture, ability to be regenerated and low safety, health and environmental risks.

Characterisation, such as by elemental analysis, physisorption, chemisorption, etc., allows for comparison of performance on a normalised basis, such as on the mass or cost of the key active ingredient(s).

In the measurement of catalyst performance, observed reaction rates can be significantly affected by mass and heat transfer, and fluidic effects, which are to be avoided to allow facile, simple interpretation of experimental results.

(3) Iterative synthesis and continued screening and characterisation

Top performing catalyst formulas are further investigated to gain insight on their physical and mechanical properties, deactivation mechanisms and mode of action and consequently and otherwise refined and optimised.

(4) Scale-up

The economic and practical feasibility of incorporating a new catalyst into a process is investigated. Process and reactor designs are considered, built and demonstrated at lab-scale, pilot-plant scale and eventually commercial scale.

The scale and duration of catalyst developments may vary widely and will more often than not fail before commercial implementation (Derouane, 2002) for various reasons (the process or product becomes obsolete, thermodynamic barriers, material costs, etc.). However, the economic advantage that successful catalysts bring justifies the resources and time spent on development.

1.2 Context of present study

The present study is concerned with catalyst performance testing in the context of (2) and (3) in section 1.1. Preliminary catalyst screening typically involves chemical characterisation for a particular reaction, in terms of activity, stability and selectivity (Moulijn, Tarfaoui & Kapteijn, 1991) and physical characterisation (specific surface area, porosity, pore size distribution, dispersion of the active phase, etc.) of the catalyst. It aims to compare performances of different catalyst types, formulations and preparations to narrow down development efforts to optimise catalyst(s) performance (Dumesic, Huber & Boudart, 2008). Many authors have provided general guidelines for catalyst performance testing, however, some quantitative requirements of practical aspects of catalyst performance testing remain unclear.

In preliminary screening (and especially in kinetic and mechanistic studies), it is vital for the researcher to be aware of the potentially confounding and limiting effects in the reaction system due to intra-particle, inter-particle and reactor scale mass, heat and momentum transfer phenomena. Commonly it is desired to run a laboratory reactor in the absence of these effects such that the true catalytic performance of catalysts may be compared. These effects can be characterised with various theoretical criteria derived from simplified mathematical models. In particular, intra-particle mass transfer limitations are often addressed in kinetic studies. The accuracies of these criteria and their prevalence and extent of their influence are often unclear.

In this study, literature is reviewed regarding principles and guidelines of performance testing of heterogeneous catalysts in gas phase reactions, potentially limiting transport effects therein and the estimation of various physico-chemical parameters needed for the characterisation of transport effects. Additional practical criteria are developed where quantitative requirements were unclear. The sensitivity and prevalence of different confounding effects towards commonly controlled experimental parameters are investigated numerically for a theoretical system. Lastly, experimental internal mass transfer limitations are compared to model predictions for a novel catalyst.

2 Literature review

In the following sections, literature regarding testing of heterogenous catalysts for gas phase reactions is reviewed. General, practical considerations and guidelines for experimenters are given first. This is followed by summaries of important potentially confounding transport effects (heat, mass and momentum transfer) with criteria for their observed absence. Lastly, methods for calculating various transport coefficients, which are needed for the evaluation of transport criteria, are given.

2.1 Experimental performance testing of heterogenous catalysts in tubular reactors.

Texts on the general subject of performance testing of heterogeneous catalysts are few. Among them are the works of Dautzenberg (1989), Derouane (2002), Flank (1989), Kapteijn & Moulijn (2008), and Petrov (2002). Although these authors have approached the subject somewhat differently, there is good agreement on common concepts and guidelines. Here, a summary is given of important concepts in the testing of heterogenous catalysts for gas phase reactions in tubular laboratory reactors.

Heterogeneous catalysts accelerate reactions which are otherwise relatively slow by providing reaction pathways having a lower activation energy (compared with homogeneous reaction) on a catalytically active surface. To make efficient use of the active material (often a transition metal), a high surface area to mass ratio is desired. Generally, this is achieved by producing small particles (often nano-scale) of the active material. These particles would cause excessive pressure-drop if used directly in flow reactors and they are, therefore, either agglomerated into larger, porous particles or dispersed and supported on surfaces of larger porous particles.

The rate of a catalytic reaction depends on the chemical conditions (concentration of chemical species, pressure, and temperature) present at the active surfaces. The activity of a catalyst gives an indication of its ability to speed up a given reaction, at specified conditions. More specifically, it refers to the normalised rate of the catalytic reaction, usually given as the rate per active site, catalyst mass, bed volume, or the mass or surface area of the active material.

The selectivity and stability of a catalyst are also critical to the viability of its use in industrial chemical processing. A more selective catalyst will often be chosen over a more active (but less selective) catalyst, the decision being dependant on the resulting practicality and economics of the wider chemical process. In terms of stability, as noted by Dautzenberg (1989), the catalyst with the highest initial activity does not necessarily perform the best overall, a better measure being its average activity over a longer (~1500 h) time frame.

In the measurement of the activities of a set of catalysts there are many factors to consider and decisions to be made. These are not necessarily straight forward. The selection of equipment that is put together to make the test unit or 'rig' (flow controllers, pumps, reactor(s), chemical analysers, heaters/coolers, vessels, etc.) and the range of conditions that the catalytic system is to be exposed to (temperature, feed composition, total pressure, flow rate, catalyst mass, particle size, dilution of the bed), must be considered in detail. These decisions affect the quality of data generated by measurements in various ways and should be made carefully.

It is important for the researcher to be aware of the different transport processes and confounding effects occurring in the experimental reactor facilitating the catalytic reaction. This is especially important in kinetic and mechanistic studies, since transport processes can disguise the intrinsic chemical and kinetic behaviour of a catalytic reaction system. For instance, mass transfer limitations, within the catalyst particle interior or at the exterior, can cause local species concentrations to differ significantly from that of the bulk fluid. Similarly heat transfer limitations can create local hot or cold spots in exothermic or endothermic reactions, respectively. The determination of kinetic parameters, reaction mechanisms and activity screening of catalysts can thus be misled if these effects are ignored. Therefore, it is important that the extent of the influence of transport effects on experimental observations are characterised. These considerations of mass, heat and momentum effects are illustrated in figure 1 at different scales. This subject is more fully elaborated upon in section 2.2.

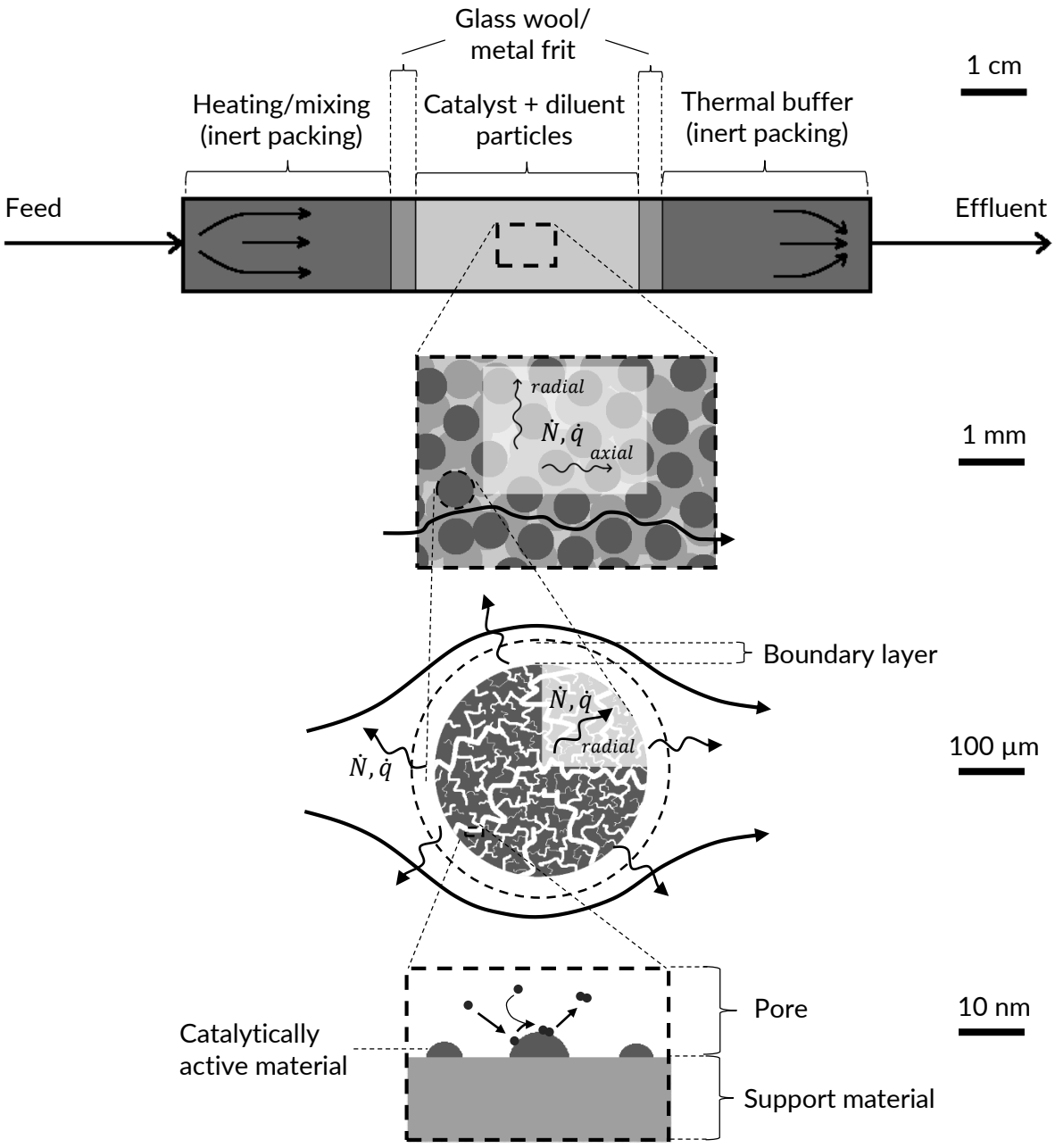

Figure 1 – Illustration of different fluidic, diffusive and heat transport effects occurring at different scales in a laboratory packed bed reactor.

2.1.1 The catalytic test unit

A test unit must be appropriate to the volume and number of catalysts being tested and will often need to be specifically designed or adapted for a particular catalyst/reaction system. The main functions of the test unit are the supply and mixing of feed streams, facilitation of the catalytic reaction(s) and the handling of downstream

functions, such as sampling, separation, venting and analysis. The range of test conditions achievable during testing will be limited on the equipment providing heating, cooling and pressure management and the materials that make up the test unit. More detail on these considerations can be found in Weitkamp & Gläser (2008) and a review of different reactors and guidelines for their selection are given by Dautzenberg (1989) and by Kapteijn & Moulijn (2008).

2.1.2 Guidelines for catalytic activity experiments

2.1.2.1 Measurement of catalyst activity

Activity is typically inferred from measuring concentration changes between feed and effluent streams of the catalytic reactor, or in other terms, the conversion of one or more chemical species. Petrov (2002) discusses the effect of the degree of conversion on the sensitivity of rate measurements. It can be shown that the rate constant (k) is sensitive to the conversion at the limits of high and low conversions, while at intermediate conversions precision is better preserved (Petrov, 2002). This can be explained intuitively for high conversions. When a conversion is measured that approaches the equilibrium conversion, it becomes increasingly hard to determine the catalyst activity since an infinitely active catalyst and one that is just active enough to achieve equilibrium conversion would have produced indistinguishable observed overall rates. Thus, testing should be done with an expected range of conversions in mind. However, since the objective of the experiment, is the measurement of activity, the conversion is unknown prior to analyses. Activities of catalysts being tested must be guessed at and approximated as best as possible so that decisions such as the temperature and the catalyst mass used can be made. Except for the most novel catalysts and reactions, this can readily be achieved by approximating from what has been found in literature for chemically similar catalysts.

Since the activity of a catalyst is specific to the conditions it is exposed to, it is convenient to avoid pressure, concentration and temperature gradients at all scales. The reactor can also then be described by a very simple model and intrinsic rate data can easily be interpreted from experiments. An ideal plug-flow, fixed-bed reactor may be described by:

$$\frac{dF_i}{dW} = \frac{dX_i}{d\left(\frac{W}{F_{i0}}\right)} = \Re_i'(C,T) = k(T).f(C,T) \quad (1)$$

When plug flow conditions can be assumed, equation 1 can be used in kinetic studies, with a wide range of experimental rate data, to find the functional dependence of the rate on process conditions. However, since the conversion is typically only measured across the entire reactor (the overall conversion) and the functional form of $f(C,T)$ is typically unknown at the screening stage of catalyst development, equation 1 is not suited for direct, quantitative interpretation of single rate measurements.

The observed, overall (or integral) rate of reaction across a flow reactor can be calculated with equation 2. When there is little spatial variation in the chemical flows, temperatures and pressures in the catalyst bed the integral reaction rate approaches the 'differential' reaction rate (Kapteijn & Moulijn, 2008). Although it is clear that such conditions are achievable at low conversions the quantitative requirements thereof are unclear. This is addressed in part in section 4.1 and 4.3.

Under differential conditions equation 1 reduces to the equation for a perfect continuous stirred-tank reactor (CSTR):

$$\Re_{i,obs}{}'(C,T) = \frac{\Delta F_i}{W} = \frac{X_i}{\left(\frac{W}{F_{i0}}\right)} \quad (2)$$

Equation 2 can be used to extract intrinsic rate data ($\Re_i$) given that measurements are free from transport limitations and differential conditions are achieved.

2.1.2.2 Selecting process conditions

If the catalyst is to replace an existing one, for ease of comparisons, it is advantageous to choose testing temperatures, pressures and compositions as close as possible to what would be used in the industrial process, or, in the case of kinetic studies, a range of conditions centred on nominal industrial conditions. However, limitations of the different materials making up a catalyst, especially its thermal stability, must be noted. As an example, industrial water-gas shift (WGS) catalysts have been developed for

'high' and 'low' temperature operation and comparisons made between the two at the high temperature conditions could yield a false result since the low temperature catalyst could undergo deactivation by thermal sintering at temperatures below high-temperature shift conditions.

The material flow rate can be used to some extent to control the conversion. This should be checked with what can be handled and accurately supplied and by the test unit (especially mass flow controllers). The catalyst mass may be adjusted to balance the flow and conversion requirements as long as the catalyst sample remains representative of the batch and effects such as bypassing are avoided. In addition, the conversion level must be considered in the context of the precision with which it is measured and the information it is desired to yield (either qualitative or quantitative). The requirements on the conversion level in this context is addressed in section 4.2.

Catalysts which can selectively consume or produce a specific chemical species, or class thereof, are very valuable. Thus, in catalytic systems where multiple reactions occur, characterisation of the selectivity of catalysts towards the different reactions is very important. Evaluation of catalyst selectivity requires broad chemical analysis of the reactor effluent, accurate accounting of the mass balance and a good model of the reaction network and sensible definitions for selectivity. To avoid misinterpretation, inference of the selectivity must be made from measurements at equal conversion, temperature, pressure and composition (Flank, 1989, Kapteijn & Moulijn, 2008), since these variables affect selectivity. For sequential reactions where the intermediate product is desired, a more active catalyst may appear to be less selective due to a higher conversion of the intermediate product (Kapteijn & Moulijn, 2008). Furthermore, selectivity comparisons for different catalysts should be made under equal spatial distributions of process conditions. The condition should be met for catalysts with equal rate forms ($f(C,T)$) at equal conversion and process conditions. Otherwise, it is achievable by effecting differential conditions.

Since temperature dependencies vary for different reactions in a multi-reaction system, catalyst selectivities are temperature dependant. It is thus very useful to conduct experiments at a range of temperatures such that the optimal selectivity for

each catalyst may be found, allowing for comparisons on the basis of maximum selectivity (Kapteijn & Moulijn, 2008).

Transport limitations may also affect selectivity (Kapteijn & Moulijn, 2008) and must be eliminated, unless the aim is to control selectivity through transport limitations. To some extent, process conditions may also be adjusted to reduce the effect of transport limitations. Further discussion on this may be found in sections 2.2, 2.3, and 5.

2.1.2.3 Experimental design

In the context of catalyst screening, there are many catalyst parameters, such as the composition of the active catalytic material, its dispersion on a porous support, its crystallite size, support material and its properties, and promoters and their concentrations, which influence its performance. Experimental programmes must aim to identify which of these variables are important (Dautzenberg, 1989) and, in the broader context of catalyst development, must find the optimum combination. In this case, factorial experimental designs are recommended (Dautzenberg, 1989). For development and discrimination of kinetic models, Froment, Bischoff & DeWilde (2011) note that sequential experimental designs have gained popularity due to their ability to use preceding experimental results to inform on requirements for subsequent experiments.

An overview on experimental design and factorial methods for catalyst screening can be found in Finlayson & Biegler (2008). In factorial design, all possible combinations of variables are investigated, often at only 'high' and 'low' levels to limit the number of experiments needed, and statistical techniques then used to identify key variables and potential interactions between them (Finlayson & Biegler, 2008).

2.2 Transport phenomena and criteria for the absence of transport limitations

Criteria for the relative absence of intra- and inter-particle concentration and temperature gradients as well as other potentially confounding effects are numerous and are reported by various researchers. These criteria often only consider one transport process at a time, neglecting compounding effects, and make use of various

approximations. A selection of these criteria, applicable to fixed-bed catalytic reactors with gas-phase reactions, are discussed in the following sections.

With the use of a criterion, the aim is to qualitatively gauge if a phenomenon influences observed measurements. Across literature on transport limitation criteria, there is a general approach in defining a criterion. A ratio of an observed quantity (potentially under influence from some physical phenomenon) to the same quantity in an ideal system is defined. Commonly the reaction rate is used. For instance, the ratio of reaction rate per catalyst volume under transport influence, to the reaction rate under particle surface conditions (ideal) is used when dealing with intra-particle mass or heat transfer. In this context the ratio is known as the effectiveness factor. The ratio indicates that the influence of a phenomenon is weak when the ratio deviates very little from unity and indicates significant influence otherwise. Many criteria from literature can be formulated as:

$$\Delta_{effect} = \left| 1 - \frac{Quantity, under\ \ effect}{Quantity, intrinsic} \right| < \alpha \tag{3}$$

The value, Δ_{effect}, is the (absolute) deviation value for the effect of interest. Across literature, drawing perhaps from common practises in statistics, a standard value of 5% is used for α, the maximum allowable deviation of the ratio from unity. This ratio is usually expressed in terms of a mathematical model, utilising various degrees of approximations and simplifications. A criterion is more useful when expressed in terms of readily observable or calculable quantities. Various physical parameters are needed in the evaluation of criteria. In the absence of experimental values, these quantities can be estimated to varying degrees of accuracy. This is discussed further in section 2.3.

Methods exist for experimental diagnostic tests for external and internal mass transfer limitations. A well-known test for internal mass transfer limitations can be made by measuring catalyst activity for a range of catalyst particle sizes. Such a test can aid in finding the particle size required to eliminate internal mass transfer limitations where the catalyst activity should stabilise for small particle sizes (i.e. not a function of the particle size). This should be done with care since other transport effects may simultaneously limit the observed catalyst activity.

2.2.1 Mass transfer

In conventional chemical systems, mass transport occurs mainly by diffusive and convective mechanisms. Diffusion occurs due to the stochastic motion of particles and their collisions. This results in the net transport of species from high to low concentration. The driving force for diffusion is the gradient of concentration. Diffusion is described by Fick's first law:

$$J_i = -D_{ij} \frac{dC_i}{dx} \tag{4}$$

Here x is an arbitrary spatial coordinate to be replaced by the relevant coordinate of the system of interest. The proportionality constant, D, is termed the diffusion coefficient and is a function of the properties of the species in the fluid, temperature and total concentration (or pressure). The estimation of the diffusion coefficient for different contexts is discussed in section 2.3.1.

A catalytically active surface facilitates chemical reactions and acts to push the reactive fluid towards chemical equilibrium. In a steady-state, reactive heterogeneous system, reactants continuously diffuse from the bulk fluid (high chemical potential) to the active catalytic surfaces (lower potential) inside and on the exterior of the porous catalyst particle, and products continuously diffuse from the catalytic surfaces back into the bulk fluid. When the reaction rate is fast compared to the diffusive rate, the local concentration of reactants at the catalytically active surface will be significantly less than in the bulk fluid. Similarly, product concentrations at these surfaces will be higher than in the bulk. Reaction rates are controlled by just a few parameters, namely, the concentration or partial pressure of chemical species present (apart from zero-order reactions) and temperature. Generally, higher reactant concentrations increase reaction rates. Slow mass transfer thus generally limits reaction rates. When such diffusion limitations are present and not given due consideration, kinetic data are prone to misinterpretation (Mears, 1971a). Commonly used criteria which are helpful in identifying mass transfer limitations are given by Mears (1971a) as well as (Moulijn, Tarfaoui & Kapteijn, 1991).

2.2.1.1 Intraparticle mass transfer

The subject of diffusion and reaction in porous catalysts and its effect on the observed reaction rate was first analysed by three independent authors in the period of 1937 to 1939, (Satterfield, 1970). A brief account of the pioneering and subsequent work is given by Satterfield (1970). The simple treatment for the description of intraparticle mass transfer and reaction is summarised here.

Due to the reactive nature of the interior surfaces of a catalyst particle (which results in counter diffusion of reactants and products) and the high resistance to convective flow in the generally narrow pores of porous catalysts, mass conservation for catalyst particles is generally described by diffusion and reaction terms only. For a spherical particle:

$$-D_{i,e}\left[\frac{d^2C_i}{dr^2}+\frac{2}{r}\frac{dC_i}{dr}\right]=\upsilon_i\Re_p \tag{5}$$

Here an effective diffusivity (D_e) must account for various factors affecting the effective rate of diffusion inside a complex porous structure (see section 2.3.1 for methods of estimating its value). Equation 5 can be solved analytically for a first-order irreversible reaction:

$$\frac{C_i(r)}{C_{i,S}}=\frac{r}{r_S}\left(\frac{\sinh\left(\varphi\frac{r}{r_S}\right)}{sinh(\varphi)}\right) \tag{6}$$

An important parameter, the Thiele modulus (φ), yields information about the relative rates of reaction and intraparticle diffusion and is defined for simple power-law kinetics by:

$$\varphi=r_S\sqrt{\frac{k\ {C_{i,s}}^{n-1}}{D_{i,e}}} \tag{7}$$

When φ is small ($\varphi \ll 1$) the concentration inside the particle can be expected to be very near that of the surface, when φ is large ($\varphi \gg 1$) the concentration diminishes

significantly toward the centre of the particle and hence the reaction rate therewith. Intraparticle mass transfer limitations thus reduce the overall 'effective' reaction rate of the catalyst particle.

The internal effectiveness factor (η_{int}) is the ratio of the overall effective reaction rate per particle to the rate which would be expected if the particle interior is entirely exposed to surface conditions. The overall effective reaction rate per particle can be equated to the molecular flux at the particle surface.

$$\eta_{int} = \frac{\int \Re_p(C,T)\, dV_p}{\Re_p(C_S,T_S)\, V_p} = \frac{-\left(A\, D_{i,e} \frac{dC_i}{dr}\right)_{r=r_S}}{\Re_p(C_S,T_S)\, V_p} \tag{8}$$

For the isothermal reaction described by simple power-law kinetics $\left(\Re_p = kC_i{}^n\right)$, the internal effectiveness factor can be expressed as a function of the Thiele modulus:

$$\eta_{int} = \frac{3}{\varphi^2}(\varphi.coth\varphi - 1) \tag{9}$$

The reaction order and the rate constant, needed to calculate the Thiele modulus, may, however, not have been determined at the stage of experimentation where characterization of the internal mass transfer limitations is of interest. The Wheeler-Weisz modulus ($\eta_{int}\varphi^2$) can be used to compare relative reaction and diffusion rates in terms of observable quantities. In fact, the internal effectiveness factor can instead be plotted as a function of the Wheeler-Weisz modulus.

The internal effectiveness factor deviates by less than 5% from unity, for a spherical catalyst particle when:

$$\eta_{int}\varphi^2 = \frac{\Re_{obs,p}\, {d_p}^2}{4\, D_{i,e}\, C_{i,S}} < 0.77 \tag{10}$$

For slab geometry the criterion is met when the Wheeler-Weisz modulus is smaller than 0.15.

The form of equation 9 does not allow the deviation value for intraparticle mass transfer, Δ_{IntMT}, (taken as the deviation of the effectiveness factor from unity) to be expressed directly in terms of the observable, Wheeler-Weisz modulus. The deviation value can, however, be found numerically given the Wheeler-Weisz modulus.

$$\Delta_{IntMT} = |1 - \eta_{int}| = f(\eta_{int}\varphi^2) < 0.05 \tag{11}$$

This criterion is derived for an isothermal, first-order, irreversible reaction and spherical geometry. Heterogeneous reaction kinetics are not often described by first-order expressions. However, this assumption may sometimes hold satisfactorily over small changes in conversion (see appendix A). The assumption that the particle is isothermal can be evaluated separately (see section 2.2.2.1). This criterion can be evaluated assuming that the concentration at the external surface equals that of the bulk fluid ($C_{i,S} = C_{i,b}$), subject to evaluation of the interfacial mass transfer criterion discussed in section 2.2.1.2.

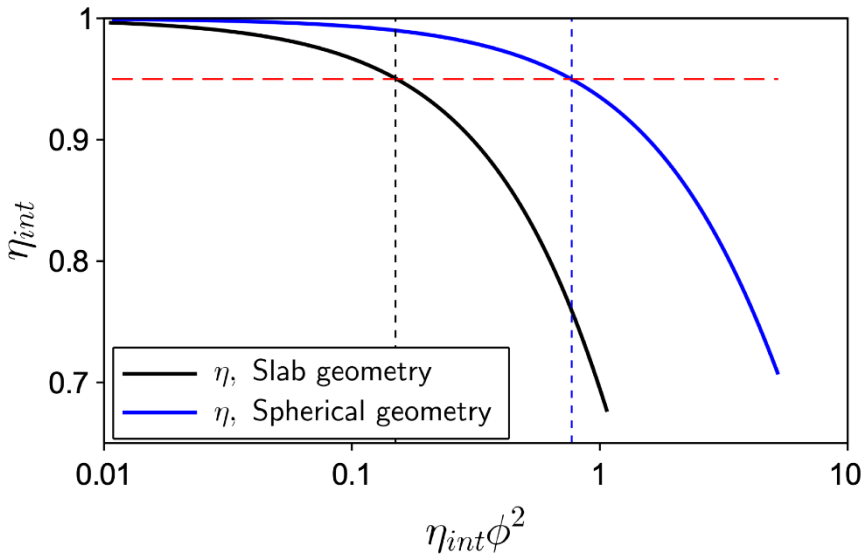

Figure 2 – The internal effectiveness factor for mass transfer as a function of the Wheeler-Weisz modulus for slab and sphere geometries.

2.2.1.2 Interfacial mass transfer

Mass transfer between a particle and the bulk fluid stream is complicated by the boundary layer around the particle where the fluid velocity changes rapidly. Assuming a no-slip boundary conditions, the fluid velocity diminishes to zero at the surface of the particle. Sufficiently high flow velocities enable rapid molecular transport by fluid

mixing (non-diffusive) while transport occurs via molecular diffusion in more stagnant regions. Thus, external mass transfer rates are enhanced by increasing the fluid velocity. This can be considered as a decrease in the thickness of the boundary layer. This complex system is commonly described by semi-empirical correlations through the film-model:

$$N_i = k_c\left(C_{i,b} - C_{i,S}\right) \tag{12}$$

At steady-state, a mass balance over a catalyst particle yields:

$$\Re_{p,obs} = a_m k_c\left(C_{i,b} - C_{i,S}\right) \tag{13}$$

As with the internal effectiveness factor, an external effectiveness factor can be defined as the ratio of reaction rates evaluated at surface and bulk conditions:

$$\eta_{ex} = \frac{\Re_p(C_S, T_S)}{\Re_p(C_b, T_b)} \tag{14}$$

If isothermal conditions and first-order kinetics are assumed the deviation value, termed the Carberry number (Ca) in the context of external mass transfer (Moulijn, Tarfaoui & Kapteijn, 1991), can be expressed as:

$$\Delta_{ExMT} = Ca = |1 - \eta_{ex}| = \left|1 - \frac{C_{i,S}}{C_{i,b}}\right| \tag{15}$$

The right-hand side of equation 15 can be conveniently expressed in terms of observable quantities by combining it with equation 13 (Kapteijn & Moulijn, 2008):

$$\Delta_{ExMT} = \frac{\Re_{p,obs}}{a_m k_c C_{i,b}} < 0.05 \tag{16}$$

For most catalytic systems, transport limitations external to the catalyst particle will only be present if intraparticle diffusion limitations are also present (Petersen, 1965).

2.2.1.3 Axial dispersion

In packed bed reactors, axial mixing can occur due to axial eddy dispersion (Mears, 1971b) and diffusion (Wakao & Kaguei, 1982). This phenomenon causes deviation from plug-flow and increases the space time required to achieve the same conversion that is achievable in a reactor with perfect plug-flow (Mears, 1971b). This effect is less pronounced in vapour phase reactions than in liquid phase and two-phase reactions (Mears, 1971b). Axial mixing can be described by a material balance over a differential volume element, considering axial diffusion, reaction and bulk (convective) flow:

$$D_{i,ax}\frac{d^2C_i}{dl^2} - \bar{u}\frac{dC_i}{dl} + \upsilon_i\Re_{bed} = 0 \tag{17}$$

Burghardt & Zaleski (1968) have derived an approximate solution for equation 17 from perturbation theory. A criterion has been derived by Mears (1971b) from the truncated perturbation solution which, in its final form, expresses the deviation in the length of the real reactor and that required in plug flow (both achieving the same conversion):

$$\Delta_{AxDisp} = \left|1 - \frac{L_{PF}}{L_{bed}}\right| = \frac{n}{Pe}ln\left(\frac{1}{1-X}\right) < 0.05 \tag{18}$$

With:

$$Pe = \frac{\bar{u}L_{bed}}{D_{i,ax}}$$

In the derivation of this criterion first-order kinetics were assumed, interfacial and intraparticle mass transfer resistances were assumed to be negligible and mathematical approximations (such as truncated Taylor expansions) were employed. Gierman (1988) found, experimentally, that limiting the deviation to less than 12.5% (1/8), was sufficient for the extraction of rate constants with an accuracy of about 10%. Mears (1971b) notes that axial concentration gradients are lowered when a bed is lengthened, and that axial dispersion can thus be diminished.

2.2.2 Heat transfer

Generally, temperature differentials in heterogeneous catalytic reactors are unavoidable (Gierman, 1988). They are a consequence of the thermodynamic changes

that occur in any reaction and the spatial separation of reaction and bulk fluid. In other words, reactions absorb or release heat (being either endo- or exothermic) and thus, at the solid-fluid boundary, will create temperature differentials.

The nature of the reaction, the conditions present and the properties of the materials involved determine the severity of the temperature gradients. A reaction with a small heat of reaction, occurring in a reactor with good thermal transport, over a catalyst with good thermal conductivity, is likely to be practically isothermal. On the other hand, significant temperature variations may be formed during highly energetic vapour phase reactions in the catalyst interior, in the stagnant film around particles and at the reactor wall.

Due to the strong effect of temperature on reaction rates, care must be taken to characterise the thermal distribution of a reactor. Wehinger, Eppinger & Kraume (2014) have demonstrated how incorrect assumptions in this regard have led to misinterpreted kinetic data. Furthermore, they note that accurate prediction of thermal distributions is exceedingly important for the estimation of product distribution.

2.2.2.1 Intraparticle heat transfer

Heat transfer inside porous catalysts is usually described by the conduction mechanism. By Fourier's law of heat conduction:

$$q_z = -\lambda_P \frac{dT}{dz} \tag{19}$$

A heat balance over a catalyst particle of slab geometry yields:

$$-\lambda_p \frac{d^2T}{dz^2} = (-\Delta H_r)\Re_p \tag{20}$$

Temperature gradients inside a catalyst particle will affect the effectiveness factor through the effect of temperature on the local reaction rate (Froment, Bischoff & DeWilde, 2011, Moulijn, Tarfaoui & Kapteijn, 1991). This is usually described by an Arrhenius dependence of the kinetic rate constant on temperature. The following criterion can be used for restricting the effectiveness factor to less than 5% deviation

from unity ($\eta \approx 1 \pm 0.05$) in a first-order irreversible reaction (Moulijn, Tarfaoui & Kapteijn, 1991) :

$$\Delta_{IntHT} = \beta_{Int}\gamma_S(\eta\varphi^2) < 0.05 \qquad (21)$$

With:

$$\beta_{Int} = \frac{(-\Delta H)D_e C_S}{\lambda_p T_S} \;; \qquad \gamma_S = \frac{E_a}{RT_S} \;; \qquad \eta\varphi^2 = \frac{\Re_{p,obs} {d_p}^2}{4D_e C_S}$$

2.2.2.2 Interfacial heat transfer

Intraparticle temperature gradients are likely to be more severe than interfacial temperature gradients (Froment, Bischoff & DeWilde, 2011). Interfacial heat transfer can be treated in an analogous way to interfacial mass transfer since their transport occurs through similar mechanisms (Satterfield, 1970). Combining an energy balance over a catalyst particle with the film model for external heat transfer yields:

$$(-\Delta H_r)\Re' \rho_p = h_f a_m (T_S - T_P) \qquad (22)$$

As with external mass transfer, the external heat transfer rates are enhanced by increasing the fluid velocity.

As before, a criterion is given for restricting the overall effectiveness factor to within 5% of unity ($\bar{\eta} \approx 1 \pm 0.05$) in a first-order irreversible reaction (Moulijn, Tarfaoui & Kapteijn, 1991) :

$$\Delta_{ExHT} = \beta_{ex}\gamma_b Ca < 0.05 \qquad (23)$$

With: $$\beta_{ex} = \frac{(-\Delta H_r)k_c C_{i,b}}{h_f T_b} \qquad \gamma_b = \frac{E}{RT_b} \qquad Ca = \frac{\Re_{p,obs}}{k_c a_m C_{i,b}}$$

With this criterion, the effect of temperature on the reaction rate is assumed to be much larger than concentration effects (which is hence neglected) and a truncated

Taylor expansion is used to estimate the exponential arising from the Arrhenius expression.

2.2.2.3 Radial heat transfer

Severe temperature gradients may exist both axially and radially in a tubular fixed bed reactor and cause deviation from ideal isothermal conditions. Temperatures along the reactor axis may be measured and controlled with zonal heating (see section 6.1.5) to be practically isothermal. It is much more difficult to measure and control the radial thermal distribution.

The following energy balance is applicable to a tubular reactor at the axial coordinate where the maximum temperature deviation occurs (Mears, 1971a):

$$\lambda_{rad}\left(\frac{d^2T}{dr_t{}^2}+\frac{1}{r_t}\frac{dT}{dr_t}\right)=(-\Delta H_r)(1-\varepsilon_{bed})(1-b)\Re_p \qquad (24)$$

From an analytical solution to equation 24, Mears (1971c) derived a criterion for the deviation in the reaction rate due to temperature differences between the reactor wall (T_W) and the maximum or minimum catalyst bed temperature:

$$\Delta_{RadHT}=\frac{|-\Delta H_r|(1-\varepsilon_{bed})(1-b)\Re_p d_t{}^2 E_a}{32\lambda_{rad}RT_w{}^2}<0.05 \qquad (25)$$

The criterion is contingent on the assumption that intraparticle, interfacial and wall heat transfer limitations can be neglected, and that the radial temperature profile can be approximated to be parabolic.

2.2.3 Fluid flow

It is useful to consider two extreme cases of fluid mixing in a reactor: a perfectly mixed reactor (e.g. a perfect CSTR) and a perfect plug-flow reactor (PFR). The mixing characteristics of a real reactor will be bound by these two mixing extremes. Fluid flow in a heterogeneous catalytic reactor is influenced by a number of factors, such as viscous effects, reactor geometry, turbulence and wall effects (Froment, Bischoff & DeWilde, 2011). Froment, Bischoff & DeWilde (2011) note that plug flow is

approximated in long, narrow tubular reactors carrying fluids of low viscosity at a high flow velocity. Stagnant regions may be formed at baffles and corners and fluid bypassing can occur when streamlines do not experience the same flow resistance (Froment, Bischoff & DeWilde, 2011). Bypassing occurs at reactor walls where the catalyst bed void fraction is higher than in the bulk catalyst bed (Chu & Ng, 1989).

2.2.3.1 Radial dispersion

Chu & Ng (1989) studied, through experimentation and simulation, random packing geometries in packed tubes having particle-to-tube diameter ratios (d_p/d_t) in the range 0.025 - 0.35. It is well known that the local voidage near the tube walls inside a packed bed is higher than in the bulk of the bed. This leads to higher fluid permeabilities near the wall and overall (Chu & Ng, 1989) and is illustrated in figure 3. The value of κ_0 is given by the Blake-Kozeny equation for the permeability of a large porous bed.

Chu & Ng (1989) noted that there is a marked increase in bed permeability when the inverse ratio, the tube-to-particle diameter ratio, is less than about 8 $(d_p/d_t < 0.125)$. This observation has been used by some authors as a criterion for the absence of radial concentration gradients due to bypassing. Moulijn, Tarfaoui & Kapteijn (1991) have

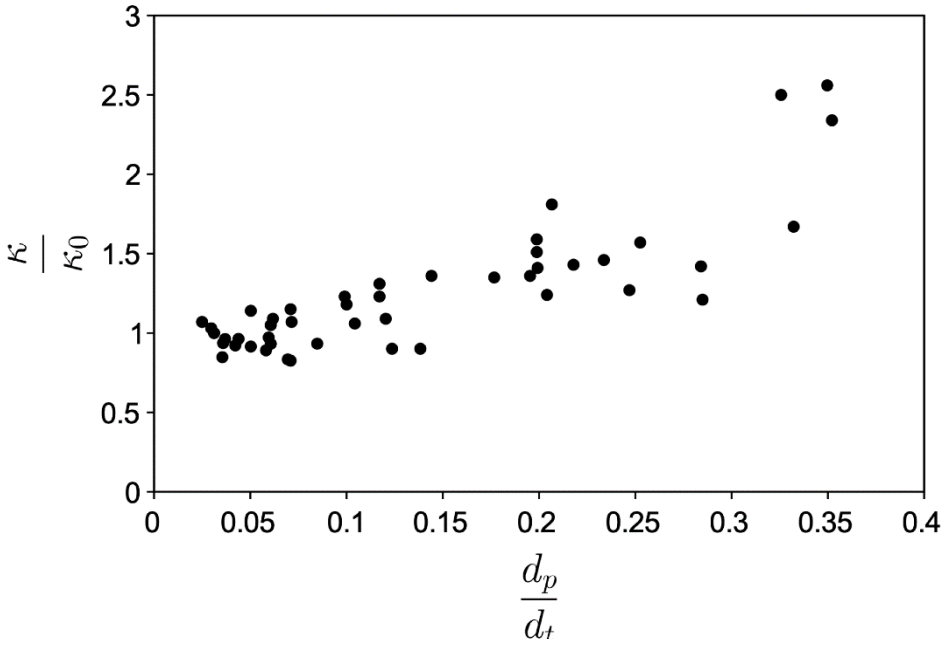

Figure 3 - Effect of particle-to-tube diameter ratio (d_p/d_t) on the overall relative permeability (κ/κ_0) of packed beds of spherical particles. Replotted from Chu & Ng (1989).

suggested that the tube-to-particle diameter ratio should be larger than 15 (d_p/d_t< 0.067). As can be seen from the scatter of experimental data points in figure 3, beds with random packings show relatively large variations in the permeability obtained during packing (Chu & Ng, 1989).

Here a simple approach is taken favouring consistency with other criteria. Hence, the criterion for absence of effects caused by low tube-to-particle diameter ratios is taken as:

$$\Delta_{RadDisp} = \frac{d_p}{2d_t} < 0.05 \tag{26}$$

In contrast to other criteria, the value of $\Delta_{RadDisp}$ in equation 26 does not represent a theoretically derived deviation from ideality. It is used only as an indication of the empirical observation that radial flow dispersion is unlikely to be observed if this criterion is met.

It should be noted that there is a strong interaction between radial concentration gradients, and radial heat transfer limitations, as is demonstrated by Wehinger, Eppinger & Kraume (2014). When radial heat transfer limitations are significant, radial concentration gradients may be significant, even in wide packed tubes ($d_t/d_p \gg 20$). This is because temperature, which would vary radially in this case, has a strong effect on the local reaction rate and thus concentrations of reactants and products. Slim tubes (small d_t/d_p) are beneficial in packed beds with known radial heat transfer limitations. Thus, the tube diameter must balance the effect of channelling (typical of small tube diameters) and radial heat transfer limitations (prominent with large tube diameters).

2.2.3.2 Bed dilution

It is common in laboratory practice to dilute a catalyst bed with inert particles, such as silicon carbide, with low surface area and good heat transfer properties to improve the heat transfer rate within the bed as well as to reduce axial dispersion (Berger et al., 2002). Berger et al. (2002) investigated the effects of the homogeneity of bed dilutions on kinetic parameter estimation. The following criterion has been derived by Berger et

al. (2002), using a discrete catalyst particle distribution model, to restrict the deviation in the conversion, between a diluted bed and an ideal undiluted bed, to less than 5% :

$$\Delta_{BedDil} = \frac{X_{ideal,undiluted} - X_{diluted}}{X_{ideal,undiluted}} \approx \frac{b}{1-b}\frac{Xd_p}{2L_{bed}} < 0.05 \qquad (27)$$

It should be noted that this criterion is valid for conversions below 80% and that first-order kinetics were assumed. Deviations in the conversion (Δ_X) of higher order reactions are expected to be larger (Berger et al., 2002).

Berger et al. (2002) showed that, when diluted catalyst beds are not well-mixed, deviation in conversions would result due to bypassing. Furthermore, it is recommended to avoid combination of high bed dilutions and high conversions (Berger et al., 2002).

2.3 Estimation of transport coefficients

Many of the expressions and criteria reviewed in section 2.2 require transport coefficients to be evaluated. In the absence of experimentally determined values these may be estimated by various models and correlations. These are reviewed briefly here. A more complete account as well as correlation coefficients and other necessary parameters can be found elsewhere (for example in Poling et al. (2008)).

2.3.1 Diffusion coefficients

An extensive discussion on diffusion in porous catalyst particles is given in Welty et al. (2009). Diffusion may be classified as molecular, Knudsen (see section 2.3.1.3) or configurational depending on pore sizes. Expected diffusivities for these regions are shown in figure 4.

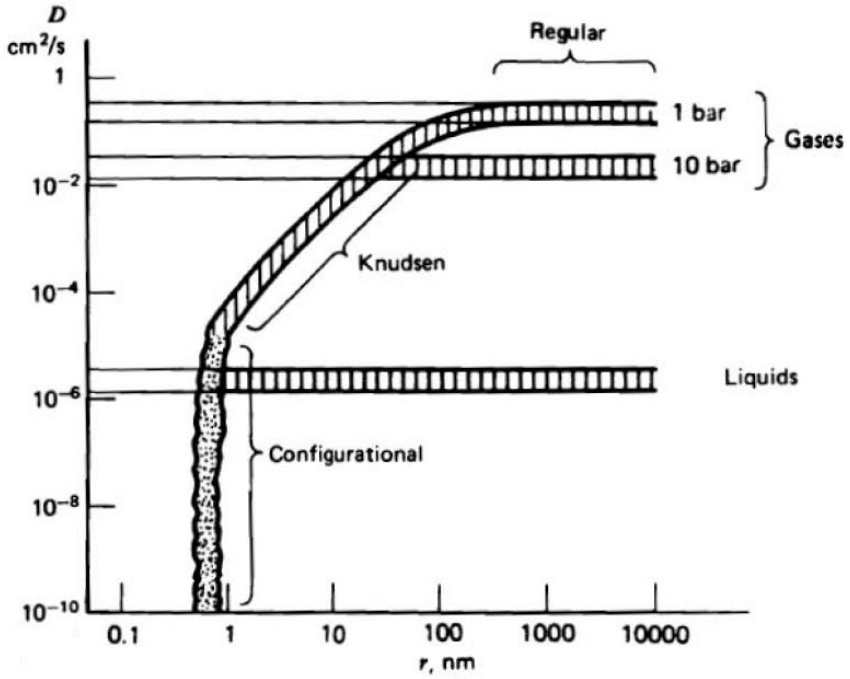

Figure 4 – Expected diffusivities in different pore sizes. [Adapted from Froment, Bischoff & DeWilde (2011)]

2.3.1.1 Binary diffusion coefficient

The diffusivity of a chemical species varies widely depending on parameters such as the state of aggregation (gas/liquid), temperature, molecular size and shape, and intermolecular interactions. Various correlations are available in literature for the prediction or extrapolation of binary diffusion coefficients (D_{ij}). A commonly used predictive, semi-empirical correlation, applicable for a wide variety of gas pairs, is given by Fuller, Schettler & Giddings (1966):

$$D_{ij} = \frac{3.2 \times 10^{-11}\, T^{1.75} \left[\frac{1}{M_i} + \frac{1}{M_j}\right]^{0.5}}{P\left((\sum \mathrm{v})_i^{1/3} + (\sum \mathrm{v})_j^{1/3}\right)^2} \tag{28}$$

Diffusion volumes (v) are available for a large variety of polyatomic gases. Additionally, the diffusion volume may be estimated from the additive contributions of the individual atoms of molecules (as is assumed in the form of equation 28).

2.3.1.2 Mixture diffusion coefficient

It is often necessary to deal with gaseous mixtures of more than two components. These systems may be treated with the Maxwell-Stefan method using binary diffusion coefficients, however, calculations by this method become complex when diffusion is coupled with reaction and more so when thermal effects are accounted for. A simpler treatment is found in estimating the effective diffusion coefficient of a species in the mixture. The following equation is based on the Maxwell-Stefan method:

$$D_{i,m} = \frac{1 - y_i \sum_{j=1}^{N_c} {N_j}/{N_i}}{\sum_{j=1}^{N_c} \frac{y_j - y_i {N_j}/{N_i}}{D_{ij}}} \tag{29}$$

In conventional reactive, steady state systems the ratio of the mass flux of two species is equal to the ratio of their stoichiometric coefficients $\left({N_j}/{N_i} = {\upsilon_j}/{\upsilon_i}\right)$.

2.3.1.3 Effective diffusivity in porous particles

Most catalyst supports are made from porous materials with high specific surface area. When the size of a pore is small compared to the mean free path length of a molecular species present therein, collisions between the molecules and the pore wall occur more frequently than collisions between molecules. In such a case transport occurs via 'Kudsen' diffusion. The Knudsen diffusivity, $D_{i,K}$, is given by:

$$D_{i,K} = 48.5\, d_p \sqrt{\frac{T}{M_i}} \tag{30}$$

Equation 30 gives the diffusivity of the open pore area. The particle voidage (ε_p) is needed to make it applicable to the cross-sectional area of the porous particle. Another factor that must be accounted for is the tortuosity of diffusion paths. For simple, ideal pore structures a tortuosity factor (τ) can be calculated from the ratio of the actual tortuous path length to the shortest distance to the same point. Tortuosity factors are often treated as an adjustable parameter that can be determined experimentally.

Values for a range of materials, calculated from experimental data, can be found in Satterfield (1970). They range in value from about 0.1-10. Values smaller than unity, calculated from experimental data, result from systems where a single pore size cannot accurately describe diffusion in a porous system (Satterfield, 1970).

Punčochář & Drahoš (1993) give a useful predictive relation for the tortuosity in a bed of particles which may be used in the absence of experimental data with the assumption that the porous particle can be represented as an agglomerate with a structure similar to a fixed bed of particles.

$$\tau = \frac{1}{\sqrt{\varepsilon}} \tag{31}$$

The effective mass diffusivity transitions from Knudsen to molecular diffusion with increasing pore size. For a system with a sufficiently narrow pore size distribution the effective diffusivity (be it in the transition region or not) may be calculated as follows (Welty et al., 2009) :

$$D_{i,e} = \frac{\varepsilon_p}{\tau_p}\left[\frac{1}{D_{i,m}} + \frac{1}{D_{i,K}}\right]^{-1} \tag{32}$$

Calculations using a single average pore size may give inaccurate results when pore sizes follow a distribution rather than taking narrow value.

A more generally applicable model was developed by Johnson & Stewart (1965). They consider a system of parallel cylindrical pores with an arbitrary size distribution, inclined at an angle to the effective direction of mass transport, where the concentration of a species is the same for any pore at a given coordinate. The question of what the effective angle of inclination is, is analogous to the concept of tortuosity (Satterfield, 1970). The total flux is given by the sum of contributions of pores of different sizes. The resulting expression for the effective diffusivity is:

$$D_{i,e} = \frac{D_{ij}}{\tau_p \left(1 + \frac{N_j}{N_i}\right)\left(y_{i,L} - y_{i,b}\right)} \int_0^\infty ln \left[\frac{1 - y_{i,b}\left(1 + \frac{N_j}{N_i}\right) + \frac{D_{ij}}{D_{i,K}(r_{pr})}}{1 - y_{i,L}\left(1 + \frac{N_j}{N_i}\right) + \frac{D_{ij}}{D_{i,K}(r_{pr})}} \right] f(r_{pr}) dr_{pr} \quad (33)$$

The ratio of mass flux may again be equated to the ratio of stoichiometric coefficients. Here the function $f(r_{pr})$ is related to the void volume distribution over pore sizes such that $f(r_{pr})dr_{pr}$ gives the void fraction of pores with sizes between r_{pr} and $r_{pr} + dr_{pr}$ (Johnson & Stewart, 1965). The integral may be evaluated numerically given pore size distribution data, such as may be measured by physisorption or mercury intrusion porosimetry (MIP). An iterative approach is needed to calculate the mole fraction for the species of interest at the unknown boundary ($y_{i,L}$) for reactive systems. For the case of equimolar counter diffusion ($N_i = -N_j$), the model reduces to:

$$D_{i,e} = \frac{1}{\tau_p} \int_0^\infty \left[\frac{1}{D_{ij}} + \frac{1}{D_{i,K}(r_{pr})} \right]^{-1} f(r_{pr}) dr_{pr} \quad (34)$$

Another model which makes use of pore size distribution data, was developed by Wakao & Smith (1962), termed the 'random pore' model. This model is applicable to materials having a bimodal pore size distribution and considers diffusion paths through macro- and micro-pores only and a series path.

$$D_{i,e} = \frac{{\varepsilon_{p,a}}^2}{\left[\frac{1 - \left(1 + \frac{N_j}{N_i}\right) y_i}{D_{ij}} + \frac{1}{D_{i,K}(r_{pr,a})} \right]} + \frac{\frac{{\varepsilon_{p,i}}^2 (1 + 3\varepsilon_{p,a})}{1 - \varepsilon_{p,a}}}{\left[\frac{1 - \left(1 + \frac{N_j}{N_i}\right) y_i}{D_{ij}} + \frac{1}{D_{i,K}(r_{pr,i})} \right]} \quad (35)$$

The Knudsen diffusion coefficients ($D_{i,K}$) and pore volume fractions (ε_p) are calculated using characteristic micro- and macro-pore sizes (subscripts i and a, respectively). These pore sizes are taken as the volume average, calculated by integration over the range of pore sizes up to ~100 Å for the micro-pore size and upwards thereof for the macro-pore size.

2.3.1.4 Axial dispersion coefficient

The effective axial dispersion coefficient for packed beds under reaction conditions was studied theoretically by Wakao, Kaguei & Nagai (1978). They consider molecular transport by static and turbulent contributions. The stagnant contribution was investigated theoretically by a cell model and found to be affected by the bulk fluid and intra-particle diffusivities, and the particle Thiele modulus. The prediction of the axial dispersion coefficient by their method requires the particle Thiele modulus.

The static contribution has been interpreted differently by Berger (2012) who considers it to be affected only by the bed porosity and tortuosity:

For $Re_p > 5$

$$\frac{1}{Bo} = \frac{\varepsilon_{bed} D_{i,m}}{\tau_{bed} d_P \bar{u}} + 0.5 \tag{36}$$

For $Re < 1$

$$D_{i,ax} = \frac{\varepsilon_{bed} D_{i,m}}{\tau_{bed}} \tag{37}$$

Both axial and radial dispersion in fixed beds was later investigated by Gunn (1987), who correlated a more complex theoretical equation for axial dispersion to experimental measurements over a wide range of Reynolds numbers and Schmidt numbers.

2.3.1.5 External mass transfer coefficient

The external mass transfer coefficient (k_c) has been studied theoretically and experimentally by many. A comprehensive account can be found in *Perry's Chemical Engineers' Handbook, section 5* (Hottel et al., 2008). Wakao & Funazkri (1978) note that most early studies neglect the effect of axial dispersion in the treatment of experimental measurements of the external mass transfer coefficient and have shown this to be significant at low Reynolds numbers (Re_p). Variations in bed voidage have also been neglected by many (Welty et al., 2009). Petrovic & Thodos (1968) have correlated data which accounts for bed voidage and which is corrected for axial dispersion. Later, Hsiung & Thodos (1977) performed a similar study extending to lower

Reynolds numbers, covering the range of Reynolds numbers common in laboratory scale, gas-phase reactors:

$$\text{For } 0.1 < Re_p < 100 \qquad Sh = \frac{0.499}{\varepsilon_{bed}} Re_p^{\,0.618} Sc^{\frac{1}{3}} \tag{38}$$

With: $Re_p = \frac{\rho_g \bar{u} d_p}{\mu_g}$; $Sh = \frac{k_c d_p}{D_{i,m}}$; $Sc = \frac{\mu_g}{\rho_g D_{i,m}}$

Their correlation corresponds reasonably well to that of Wakao & Funazkri (1978) and of Petrovic & Thodos (1968) (see figure 5).

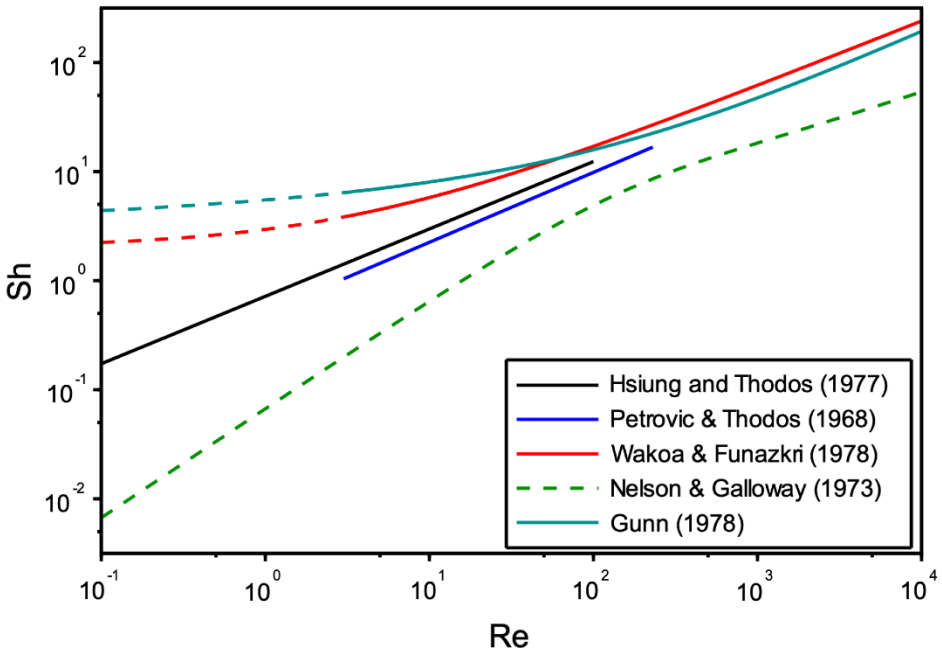

Figure 5 – Correlations and theoretical models of the Sherwood number vs. Reynolds number for packed beds with $\varepsilon_b = 0.39$ *and* $Sc = 0.64$*. Solid lines indicate regions where experimental data is correlated. Broken lines indicate extrapolations or theoretical plots.*

A well-known theoretical prediction gives a limiting value of 2 for the Sherwood number, as the Reynolds number tends to 0. This applies, by analogy to heat transfer, for the Nusselt number. The prediction is based on comparison of the film model to a conduction model (no convective heat transfer) with an infinite medium boundary condition. Nelson & Galloway (1975) question the validity of the infinite medium boundary condition and offer an alternate interpretation based on a finite radius boundary condition (zero concentration gradient at a finite radius). Their development

produces a semi-empirical equation for Nusselt and Sherwood numbers with zero lower limits for both.

Wakao, Kaguei & Funazkri (1979) have reviewed various theories regarding the anomalously low transfer coefficients of both external mass and heat transfer at low Reynolds number and argue for a non-zero limit of the Sherwood and Nusselt numbers. Their work, as well as that of Gunn (1978), suggests that axial thermal and mass dispersion (not explicitly treated by Nelson & Galloway (1975)) is the main reason for anomalous data and the observation of zero limits for the Nusselt and Sherwood groups at low Reynolds numbers. Correlations and models of the authors discussed are shown in figure 5.

2.3.2 Heat transfer coefficients

Energy is transported by one or more of three mechanisms, namely: conduction, convection and radiation. The relative contributions of these mechanisms depend on the properties of the reaction system. Notably, heat transport by radiation is often neglected or lumped into effective heat transport coefficients (Froment, Bischoff & DeWilde, 2011). Heat flux by radiation increases rapidly with increasing temperature. Its contribution may become important at temperatures as low as 200 °C (Gonzo, 2002) but may often be justifiably neglected at higher temperatures for beds with moderate thermal properties. Van Antwerpen, Du Toit & Rousseau (2010) provides an extensive review of correlations and models to estimate the radiative heat flux in packed beds.

2.3.2.1 Porous particle thermal conductivity

Thermal conductivities (λ_P) for some non-metallic porous particles are reported by Satterfield (1970). They fall mainly within one order of magnitude, from 0.075 – 0.47 W/m.K. Smith et al. (2013) provide an insightful comparison of predictive models for thermal conductivities of porous materials. They note that the key parameters affecting effective internal thermal conductivity are the thermal conductivities of the solid phase (λ_s) and the pore fluid (λ_g), and the pore volume fraction (ε_p).

Catalytic materials often contain different solid phases, making it difficult to estimate the thermal conductivity accurately without knowing the thermal conductivity of the

mixed solid phase. In this case, conservative estimates must be made depending on the properties of the various solid and fluid phases. Carson et al. (2005) provide useful recommendations in this regard.

For catalyst beds diluted with inert particles, Berger (2012) suggests estimating the solid conductivity via a volume average of the conductive resistances of the catalyst and diluent particles:

$$\frac{1}{\lambda_p} = \frac{1-b}{\lambda_{p,cat}} + \frac{1}{\lambda_{p,dil}} \tag{39}$$

2.3.2.2 External heat transfer coefficient

Cybulski et al. (1975) gives a correlation for the Nusselt number from the author's own data while Kunii & Suzuki (1967) develop a semi-empirical model with comparison to experimental data from various authors, all in the low Reynolds number range (Re < 3; as is often prevalent in laboratory fixed-bed reactors). However, as with external mass transfer, experimental measurements for the external heat transfer coefficient at low Reynolds number are prone to error and misinterpretation. Discussions on the difficulties in measurements of experimental data in the low Reynolds number range is given by Wakao, Kaguei & Funazkri (1979) and Gunn & De Souza (1974) who have criticized the interpretation of data by the former authors.

Wakao, Kaguei & Funazkri (1979) suggest that experimental data are prone to error and misinterpretation at low flow velocity due to invalid assumptions made in model equations. They suggest that, in this case, the use of centre symmetric equations and the disregard of axial heat transfer in the bed introduce large errors and yield anomalously low heat transfer coefficients.

Here the external heat transfer coefficient (h_f) as correlated by Wakao, Kaguei & Funazkri (1979) is used:

For $Re_p < 8500$ $$Nu = 2 + 1.1\, {Re_p}^{0.6} Pr^{\frac{1}{3}} \tag{40}$$

With: $Re_p = \frac{\rho_g \bar{u} d_p}{\mu_g}$; $Nu = \frac{h_f d_p}{\lambda_g}$; $Pr = \frac{\mu_g \hat{C}_p}{\lambda_g}$

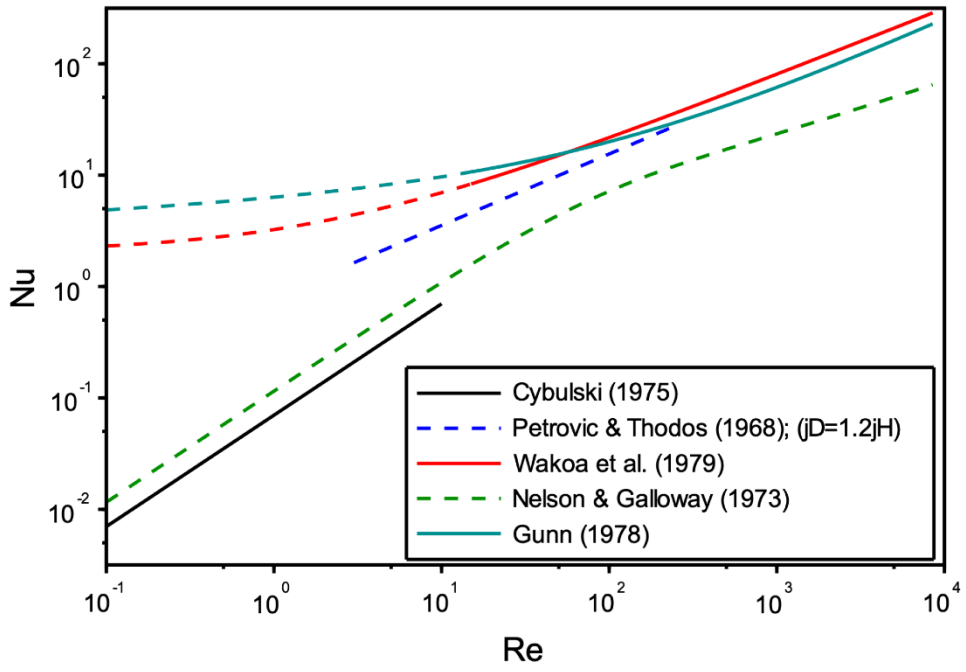

Figure 6 - Correlations and theoretical models of the Nusselt number vs. Reynolds number for packed beds with $\varepsilon_b = 0.39$ *and* $Pr = 1.46$. Solid lines indicate regions where experimental data is correlated. Broken lines indicate extrapolations or theoretical plots.

2.3.2.3 Effective radial thermal conductivity of a packed bed

Specchia, Baldi & Sicardi (1980) give a summary of preceding studies on the effective radial thermal conductivity ($\lambda_{e,rad}$). They present a correlation for $\lambda_{e,rad}$ using extensive data from preceding literature. It has been observed that $\lambda_{e,rad}$ increases linearly with flow velocity with a non-zero intercept (Specchia, Baldi & Sicardi, 1980). Hence, $\lambda_{e,rad}$ is widely correlated as a sum of stagnant ($\lambda_{e,0}$) and flow velocity dependant, turbulent ($\lambda_{e,tur}$) contributions:

$$\frac{\lambda_{e,rad}}{\lambda_g} = \frac{\lambda_{e,0}}{\lambda_g} + \frac{\lambda_{e,tur}}{\lambda_g} \tag{41}$$

The stagnant contribution is given by a semi-empirical model which considers conduction through the fluid in the void spaces, the solid particles and the gas near the contact points between particles (Specchia, Baldi & Sicardi, 1980):

$$\frac{\lambda_{e,0}}{\lambda_g} = \varepsilon_{bed} + \frac{1 - \varepsilon_{bed}}{0.22{\varepsilon_{bed}}^2 + \frac{2}{3}\frac{\lambda_g}{\lambda_p}} \tag{42}$$

A modified Peclet number ($Pe_{e,tur}$), introduced for the turbulent contribution, has been found to be constant, at about 8.65, except when the particle diameter is about a tenth of the tube diameter or larger (Specchia, Baldi & Sicardi, 1980). The turbulent contribution is hence correlated as:

$$\frac{\lambda_{e,tur}}{\lambda_g} = \frac{Pe_g}{Pe_{e,tur}} = \frac{Re_p Pr}{8.65\left(1 + 19.4\left(\frac{d_p}{d_t}\right)^2\right)} \tag{43}$$

2.3.3 Gas viscosity

Viscosity (μ_i) data and accurate empirical correlations for the viscosity of many pure gases and vapours are available from chemical databanks. Measured gas viscosities are often corelated with the equation:

$$\mu_i = \frac{AT^B}{1 + D/T + C/T^2} \tag{44}$$

Where A, B, C and D are empirical constants. Alternatively, or in the absence of such data, pure species viscosities may be estimated.

Early studies have given the viscosity of pure gases from the fundamental view of the kinetic theory of gases. Therewith, predictions of transport properties were found to be only qualitatively correct and the temperature dependence of gas viscosities was found to be weaker than experimental measurements indicate, due to the inadequacy of the constant-diameter rigid-sphere model (Bird, Stewart & Lightfoot, 2002).

A more realistic approach, which considers intermolecular forces in terms of the Lennard–Jones potential energy function, is found in Chapman-Enskog theory. For the viscosity of gases at low density the result is:

$$\mu_i = 2.6693 \times 10^{-6} \frac{\sqrt{M_i T}}{\sigma_i \, \Omega_{\mu,i}(T)} \tag{45}$$

Here, the Lennard-Jones collision diameter (σ_i) is a property of the molecular species, as is the Lennard-Jones collision integral ($\Omega_{\mu,i}$), which is also a function of temperature. Whilst a more accurate temperature dependency is given by equation 45, prediction of viscosities for polar molecules may be inaccurate (Welty et al., 2009). It should also be noted that a pressure dependency must be accounted for at higher pressures (>10 atm) (Welty et al., 2009).

It is often necessary to work with mixtures of various gases. Wilke (1950), by application of the kinetic theory of gases to preceding theoretical equations, has developed a semi-empirical equation for the viscosity of multicomponent gas mixtures in terms of molecular weights and pure gas viscosities:

$$\mu_m = \sum_{i=1}^{N_c} \frac{y_i \mu_i}{\sum_{i=1}^{n} y_i \phi_{ij}} \tag{46}$$

With:

$$\phi_{ij} = \frac{1}{\sqrt{8}} \left(1 + \frac{M_i}{M_j}\right)^{-1/2} \left[1 + \left(\frac{\mu_i}{\mu_j}\right)^{1/2} \left(\frac{M_j}{M_i}\right)^{1/4}\right]^2 \tag{47}$$

Rigorous comparisons of calculations with equation 46 and 47 to experimental data for binary mixtures of gases has shown this method to be very accurate, with an average deviation between theory and experimental values of less than 1% (Wilke, 1950).

2.3.4 Gas thermal conductivity

Heat transfer by conduction in gases occurs via molecular interaction in a similar way to momentum transfer. Thus, their proportionality constants, the thermal conductivity (λ_i) and the viscosity, are treated in an analogous way and measured conductivity data are correlated with the same equation as viscosity data (equation 44).

As was found with predictions of gas viscosities, the kinetic theory of gases produced unsatisfactory predictions for the thermal conductivity. Applications of Chapman-Enskog theory was found to yield accurate results for monatomic gases (Bird, Stewart & Lightfoot, 2002). To account for interactions between polyatomic gas molecules at low pressure, Eucken (1913) developed the following semi-empirical formula:

$$\lambda_i = \left(\hat{C}_p + \frac{5}{4}\frac{R}{M_i}\right)\mu_i \tag{48}$$

The thermal conductivity of a gas mixture can be calculated with (Bird, Stewart & Lightfoot, 2002):

$$\lambda_{mix} = \sum_{i=1}^{n} \frac{y_i \lambda_i}{\sum_{i=1}^{n} y_i \phi_{ij}} \tag{49}$$

Here, the interaction parameters (ϕ_{ij}) are still given by equation 47.

3 Scope and objectives of present study

Additional expressions and criteria are developed to quantify the requirements of achieving differential rate measurements, of establishing lower conversion limits (to achieve the desired precision in rate measurements) and of avoiding the effects of axial pressure drop on rate measurements.

The sensitivity and prevalence of these effects and of various transport limitations towards commonly controlled experimental parameters are investigated numerically for a theoretical case of the WGS reaction over $Cu/ZnO/Al_2O_3$. Suppression of the various effects by control of experimental parameters is investigated. The reaction-catalyst system is chosen for its moderate properties in various aspects, including the rate and heat of the (equimolar) reaction and operating temperatures and pressures, and for its prevalence in literature and industrial use, and its high selectivity.

Lastly, the use of the various criteria is demonstrated in an experimental performance test of a novel, proprietary medium-temperature (MT) WGS catalyst developed at the University of Cape Town. More importantly, by repeating tests with different catalyst particle sizes, this experiment serves as a platform to compare experimental internal mass transfer effectiveness factors (an effect which is widely discussed and expected to be prevalent) to those predicted from theory.

The objectives of this study are therefore to:

- Develop expressions and criteria to aid in (1) establishing differential reactor conditions, (2) establish upper and lower conversion limits and (3) avoid the effects of pressure drop in a fixed catalytic bed.
- Determine the prevalence and sensitivity of reviewed and developed criteria in a theoretical reaction system; WGS over $Cu/ZnO/Al_2O_3$.
- To compare experimental and model (predicted) internal mass transfer limitations for a novel catalyst.

4 Development of additional performance criteria for tubular laboratory fixed-bed reactors

Whilst the review in sections 2.1 and 2.2, on catalyst testing and transport limitation criteria, provides a guide to catalyst testing and a coverage of potentially important transport phenomena which may influence rate measurements of catalysts, some questions and uncertainties remain regarding testing practises. The first relates to the practical needs to establish 'differential' rate measurements, needed to enable the evaluation of some of the transport criteria. The second question considers what the lower limit for the measurement of reaction rate, through measurement of the chemical conversion, should be. Lastly, the issue of the effect of pressure drop across a catalytic, packed, flow reactor on the observed reaction rate is considered.

4.1 Conversion limits for the measurement of differential reaction rate

As noted in section 2.1.2.1, to measure the condition-specific activity of a catalyst in a tubular fixed-bed reactor, spatial variations of conditions in the reactor must be minimised. Under such differential conditions the reaction rate is effectively constant throughout the reactor and interpretation of experimental measurements is simple. However, the specific, quantitative requirements for operation under differential conditions have so far been unclear.

As was seen with criteria derived for mass and heat transfer phenomena, a criterion can be defined to limit the observed (integral) reaction rate across a catalyst bed to within 5% of the reaction rate at the reactor inlet conditions.

$$\Delta_{DiffR} = \left| 1 - \frac{\Re_{i,obs}{}'}{\Re_i{}'(C_0, T_0)} \right| < 0.05 \qquad (50)$$

To derive a useable criterion from equation 50, some simplifying assumptions are made: (1) the reaction kinetics are described by irreversible, first-order kinetics (taken to be in terms of an arbitrary chemical species 'A'), (2) the ideal-gas law applies, (3) the reactor exhibits perfect plug-flow and (4 & 5) the reactor is isothermal and isobaric. With these, the following criterion for differential conditions results:

$$\Delta_{DiffR} = \left|1 + \frac{X_A}{\xi X_A + (\xi + 1) ln(1 - X_A)}\right| < 0.05 \qquad (51)$$

The derivation of this criterion and the definition of ξ is given in appendix B. For an equimolar ($\xi = 0$), reaction the criterion will be met at conversions not exceeding 9.8%. The deviation of the observed/integral rate to the initial reaction rate, given by equation 51, is plotted in figure 7 for different values of ξ.

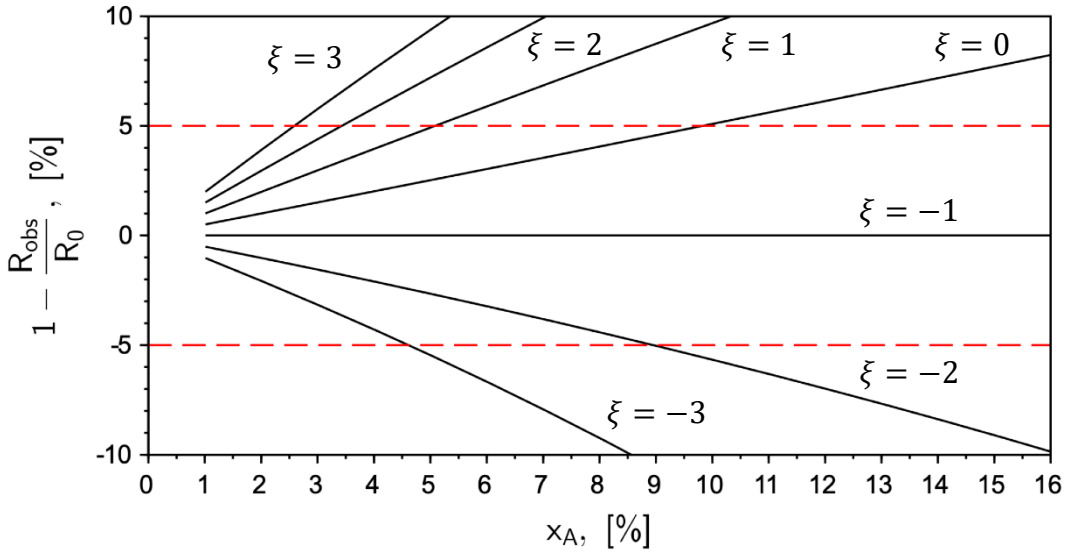

Figure 7 – Deviation between observed and initial rate for a first-order reaction in a packed bed reactor vs. conversion, plotted for different stoichiometric effects (ξ).

The criterion becomes very difficult to fail at ξ near -1. This is because there is an overall consumption of molecules which decreases the gas volume, keeping the concentration of species A nearly constant and thus the reaction rate.

4.2 Guidelines for lower limits of conversion

For qualitative experimental measurements of chemical conversion to be meaningful, the measurement must be, at least, statistically distinguishable from a negative result, i.e. from zero conversion. Similarly, in the case where catalysts are to be qualitatively ranked, conversions must be shown to be significantly different from each other. These tests of significance can be done using a t-test. Assuming equal variances ($\sigma^2(X)$) of a blank sample (no conversion) and a positive conversion measurement, the t-value is expressed in the same way for both tests:

$$t = \frac{\Delta x}{\sigma(X)\sqrt{\frac{2}{n}}} \tag{52}$$

Where n is the number of repeat measurements in the sample. When a single conversion is to be shown to be distinguishable from zero, Δx is equal to the conversion ($\Delta X = X - 0$). To reject the null hypothesis (that there is no difference in the conversions between two samples or that a single measurement is not different to zero), the calculated t-value must be greater than the critical t-value, given the desired probability level (termed the α-value) and degrees of freedom $(n - 1)$. Expressed in terms of conversion:

$$\Delta x > \sigma(X)\sqrt{\frac{2}{n}}\, t_{crit}(\alpha, n) \tag{53}$$

The value on the right-hand side gives the minimum conversion or difference in conversion (Δx_{min}) required to satisfy the criterion and can be calculated given the desired number of repeat measurements and the variance of the conversion. The variance of the conversion depends greatly on the precision of the chemical analytical methods used. The critical t-value decreases slowly with increasing n. Thus, an increase in the number of repeat measurements reduce ΔX_{min} faster than with the inverse root of n, $\left(\frac{1}{\sqrt{n}}\right)$.

A standard deviation of the conversion $\left(\sigma(x)\right)$ of 0.5% was calculated from in-house experimental data on a medium-temperature, WGS catalyst (see appendix G). Measurements were made by gas chromatography (GC) using a thermal conductivity detector. The variance in conversion was found to be relatively insensitive to the level of conversion in the range of 4-12%. The right-hand side of equation 53 is plotted in figure 8 as a function of the number of repeat measurements per sample, n, for different values of the standard deviation of conversion, $\sigma(X)$.

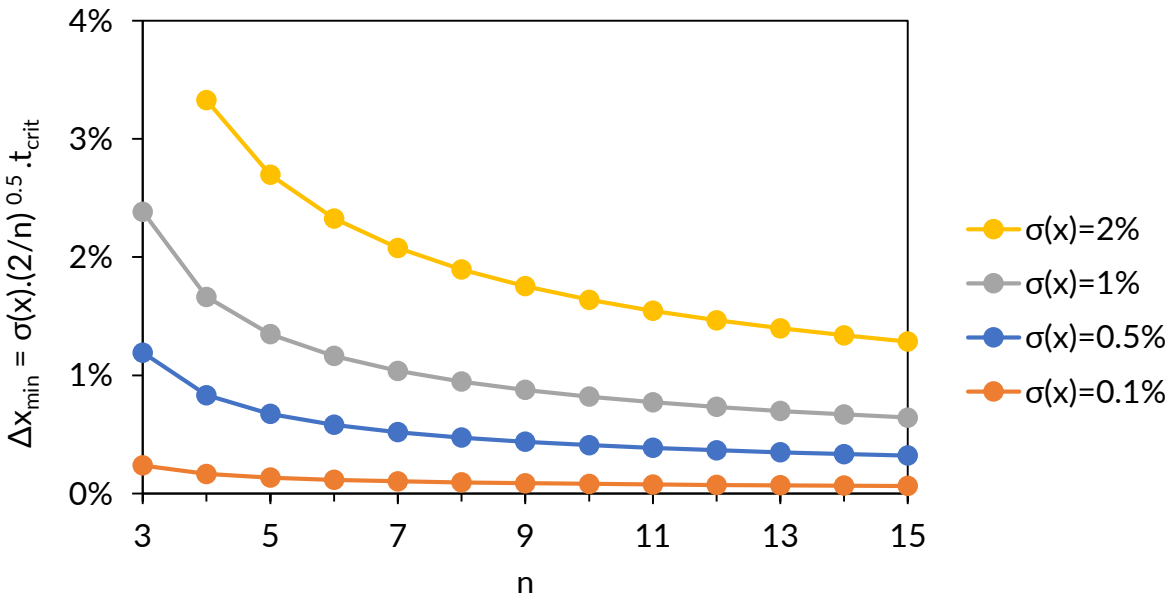

Figure 8 - Minimum conversion difference required for qualitative comparison of two conversion measurements as a function of the sample size for different values of the standard deviation of the conversion.

The requirement (ΔX_{min}) to fulfil the criterion is sensitive to the variance of conversion measurements and as expected to the number of repeat measurements when this value is relatively low. However, precision of contemporary analytical methods is generally high and thus make the typical, practical requirements for this criterion relatively low even with small numbers of repeat measurements.

A different criterion statement must be used when quantitative results for conversion are required. There is confidence in a quantity derived from measurement when it is made with high precision. To gauge the precision of the quantity of the measured conversion its relative error must be considered. Analogous to methods described in section 2.2, an expression can be defined to limit the relative error to 5%. Expressed in terms of the standard deviation of the mean:

$$\Delta_{XStat} = \frac{\left(\frac{\sigma(X)}{\sqrt{n}}\right)}{X} < 0.05$$

$$X > 20\left(\frac{\sigma(X)}{\sqrt{n}}\right) \tag{54}$$

The value on the right-hand side in equation 54 thus gives the minimum conversion (X_{min}) required to limit the relative error in conversion to less than 5%. This value is plotted in figure 9, as before. In addition, the upper conversion limit ($X = 9.8\%$) for the measurement of a differential rate for an equimolar reaction ($\xi = 0$; see figure 7) is plotted.

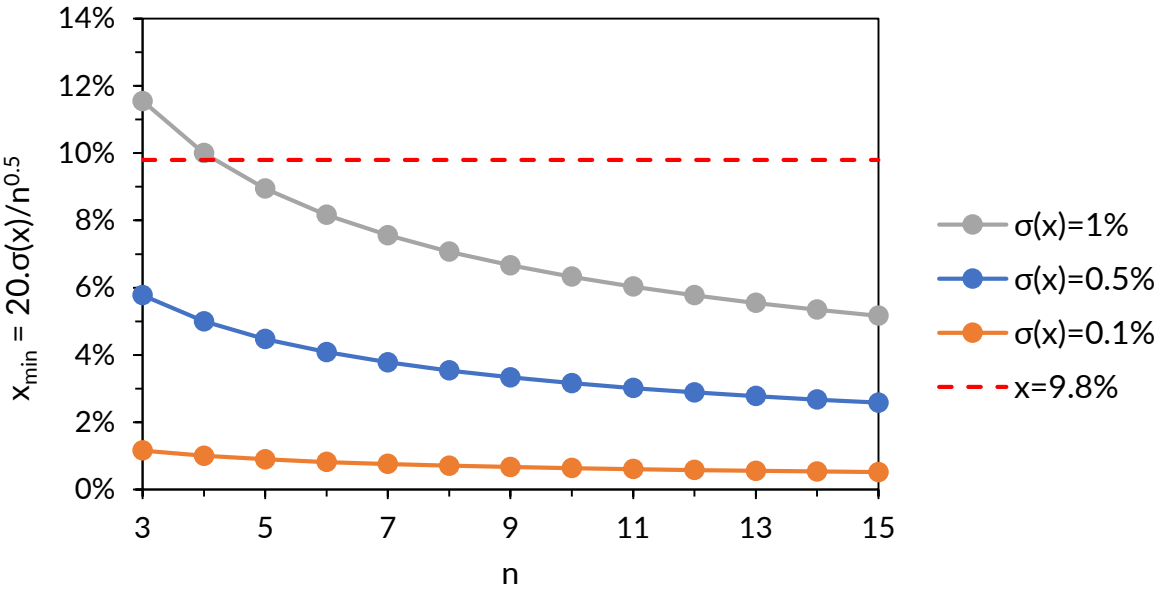

Figure 9 - Minimum conversion (x_{min}) required to limit the standard error of conversion ($\sigma(x)/\sqrt{n}$) to 5% of the conversion, as a function of the sample size for different values of the standard deviation of the conversion.

It is not surprising that the requirements for quantitative measurements should be harsher than for qualitative measurements as is seen from the comparison between figures 8 and 9. Here the variance of conversion measurements also has a much larger impact.

Since the level of conversion reached for new catalysts in catalyst performance testing may not be known prior to chemical analysis, it is useful to plan experiments such that the difference between the upper and lower bounds of conversion, as set by the criteria derived here, is as large as practically realisable. In other words, given a precision of conversion measurements ($\sigma(X)$), the number of repeat measurements (n) must be chosen to balance the time required to perform the measurements and the need to maximise the target window (where both criteria are met) for measured conversions.

4.3 Effect of axial pressure drop on observed reaction rate

When a fluid flows through a bed of particles there is a loss of pressure across the bed. This is commonly described by the Ergun equation. Allen, Von Backström & Kröger (2013) review the subject of pressure drop across packed beds and correlations from various authors and discuss challenges in predicting pressure drop and the limitations of the Ergun equation.

The local total pressure and partial pressures of chemical species influence catalytic reaction rates. In experiments where there is significant pressure drop, and thus, a non-uniform reaction rate across the bed, interpretation of data becomes complex. Pressure is commonly measured and controlled upstream and/or downstream of the reactor. A criterion can be stated to restrict the integral reaction rate to within 5% of the reaction rate evaluated at reactor inlet conditions:

$$\Delta_{PD} = \left| 1 - \frac{\Re_{i,obs}{}'}{\Re_i{}'(z = L_b)} \right| < 0.05 \tag{55}$$

Some simplifying assumptions are again needed to derive a simple, useable criterion from equation 55: (1) the reaction kinetics are described by irreversible, first-order kinetics, (2) concentrations of molecular species are constant (differential conditions apply), (3) the reactor exhibits perfect plug-flow, (4) the reactor is isothermal and (5) the pressure decreases linearly along the reactor axis. With these, the following criterion results:

$$\Delta_{PD} = \frac{\Delta P_T}{2P_{T,0}} < 0.05 \tag{56}$$

The derivation of this criterion is given in appendix C.

5 Sensitivity analysis of performance testing criteria in varying conditions

The transport limitation phenomena discussed in section 2.2 along with the introduction of additional considerations introduced in section 4 forms a set of potentially important effects which should be considered in performance tests of heterogenous catalysts in packed bed reactors. For convenience, this group is listed in table 1 and table 2.

Table 1 – Summary of theoretical deviations from ideality due to transport effects in tubular, packed bed reactors.

Nr.	Effect	Theoretical deviation values
1	Intraparticle mass transfer	$\Delta_{IntMT} = f(\eta_{int}\varphi^2)$
2	Interfacial mass transfer	$\Delta_{ExMT} = \frac{\Re_{p,obs}}{a_m k_c C_{i,b}}$
3	Axial dispersion	$\Delta_{AxDisp} = \frac{n}{Pe} ln\left(\frac{1}{1-X}\right)$
4	Intraparticle heat transfer	$\Delta_{IntHT} = \beta_{Int}\gamma_S(\eta\varphi^2)$
5	Interfacial heat transfer	$\Delta_{ExHT} = \bar{\beta}\gamma Ca$
6	Radial heat transfer	$\Delta_{RadHT} = \frac{\lvert-\Delta H_r\rvert(1-\varepsilon_{bed})(1-b)\Re_p {d_t}^2 E_a}{32\lambda_{rad} R {T_w}^2}$
7	Radial dispersion	$\Delta_{RadDisp} = \frac{d_p}{2d_t}$
8	Bed dilution	$\Delta_{BedDil} = \frac{b}{1-b}\frac{X d_p}{2L}$

Table 2 – Additional criteria developed by this study to address practical concerns of catalyst testing.

	Additional criteria	
9	Differential reaction rate (see section 4.1)	$\Delta_{DiffR} = \left\lvert 1 + \frac{X}{\xi X + (\xi + 1) ln(1 - X)} \right\rvert$
10	Statistically significant/distinguishable conversion(s) (see section 4.2)	$\Delta X > \sigma(X) \sqrt{\frac{2}{n}}\, t_{crit}(\alpha, n)$
11	Relative error in conversion (see section 4.2)	$\Delta_{XStat} = \frac{\left(\frac{\sigma(X)}{\sqrt{n}}\right)}{X}$
12	Axial pressure drop (see section 4.3)	$\Delta_{PD} = \frac{\Delta P_T}{2P_{T,0}}$

It can be difficult to say with certainty which effects will be important to control during a given catalyst performance test, especially of newly formulated catalysts. Conversely, it is unclear which changeable experimental variables (operating temperature, particle size, reactor tube diameter etc.) will be sensitive to different effects and what their values should be to avoid these confounding effects.

This question is perhaps impossible to answer for general gas phase heterogeneous reaction systems, due to the large variety of fluid and catalyst properties and the complexity of accurately describing transport phenomena and their cross-interactions. However, a critical theoretical comparison of pairs of transport criteria is given by Kapteijn & Moulijn (2008), which partially addresses the question. In short, their analysis suggests, generally, that:

$$\Delta_{RadHT} > \Delta_{ExHT} > \Delta_{IntMT} > \Delta_{IntHT} > \Delta_{ExMT}$$

Placement of these phenomena in this hierarchy depends on what the range of variables needed for the evaluation of deviation values in table 1 are assumed to be. The placement of the remaining transport effects are not addressed by Kapteijn & Moulijn (2008). The converse question, of what values the changeable experimental variables must be, remains unclear.

Here, these questions/uncertainties are explored by applying the expressions in table 1 and table 2 to different theoretical reaction-reactor systems.

5.1 Case specifications: low-temperature water-gas shift reaction over $Cu/ZnO/Al_2O_3$

As a first case study, the WGS reaction over a 'low-temperature' (LT-WGS) catalyst, $Cu/ZnO/Al_2O_2$, is chosen.

$$CO + H_2O \leftrightarrow CO_2 + H_2$$

This system has moderate properties in various aspects, namely, catalyst activity, heat of reaction, pore sizes and nominal operating temperatures and pressures.

Evaluation of the various deviation values requires specification of the properties of the reaction system. The following properties are fixed for the reaction system:

Table 3 – Estimated bed, particle and reaction properties of the WGS-$Cu/ZnO/Al_2O_3$ catalytic reaction system.

Catalyst bed properties	Value	Reference
Bed voidage, ε_{bed}	0.43	This work
Bed density, ρ_{bed}	1020 kg/m^3	This work
Thermal conductivity of SiC diluent, λ_{dil}	$6.11 \times 10^4/(T - 115)$ W/m.K	Nilsson et al. (1997)
Catalyst particle properties		
Particle voidage, ε_p	0.59	This work
Particle density, ρ_p	1790 kg/m^3	This work
BET average pore size, d_{pore} $(4V/A)$	14.5 nm	This work
Thermal conductivity, λ_p	0.1 W/m.K	Satterfield (1970)
Reaction properties	$CO + H_2O \leftrightarrow CO_2 + H_2$	
Heat of reaction, $\Delta {H_r}^o$	-41.1 kJ/mol	Choi & Stenger (2003)
Activation energy, E_a	47.4 kJ/mol	Choi & Stenger (2003)
Reaction rate, $\Re'_p$	$8.22 \times 10^4\ exp\left(-\frac{E_a}{RT}\right)\left(P_{CO}P_{H_2O} - \frac{P_{CO_2}P_{H_2}}{K_{eq}}\right)$ mol/s.kg	Choi & Stenger (2003)
Equilibrium constant, K_{eq}	$exp\left(\frac{4577.8}{T} - 4.33\right)$	Choi & Stenger (2003)

For the investigations to follow, it is assumed that the diluent material is silicon carbide and that its particle size and bed voidage is equal to that of the catalyst.

Among the required variables are independent variables, which, to some extent, may be manipulated by researchers to favour the quality of performance measurements (activity, selectivity and stability). These are identified in the table 4 with ranges given for their expected values in a laboratory scale performance test.

Table 4 – Common experimental independent variables with expected ranges for a LT-WGS-Cu/Zno/Al_2O_3 catalytic reaction system.

Independent variable	Value range	Units
Total volumetric feed rate, F_T	200 – 2000	SCCM
Feed temperature, T	180 – 220	°C
Catalyst particle size, d_p	50 – 750	µm
Catalyst mass. W	0.1 – 1.0	g
Bed dilution fraction, b	0.35 – 0.95	-
Reactor tube ID, d_t	6 – 16	mm

The total pressure and feed gas composition were kept constant. These were specified at 1 atm total pressure and a dry feed gas composition of 5% CO, 18% CO_2, 60% H_2 and 17% N_2, with a steam-to-dry gas molar ratio of 0.4.

Although many of the criteria in table 1 are specified only for first-order reactions, it can be shown that the reaction rate, as given by the expression developed by Choi & Stenger (2003), can be approximated reasonably well (±5%) by a first-order reaction rate form (in the partial pressure of CO; see appendix A), given the specified feed composition and a CO conversion of less than 9.8% (to which we limit ourselves for a first-order, equimolar reaction, as discussed in section 4.1). Hence, such criteria that require first-order kinetics, are applicable to this reaction system within the limit of 10% CO conversion.

Furthermore, the original correlation of the reaction was done free from the influence of limitation (Choi & Stenger, 2003) Here, however, it is assumed to be representative of the observed reaction rate, as required by the various criteria. This assumption becomes invalid when the observed reaction rate deviates significantly, for whatever reason, from the intrinsic. Hence, the 'boundary' of limitation-free performance testing may be found by this method with reasonable confidence, but values for the various

deviations may not be accurate when significant deviations from intrinsic behaviour are expected.

5.2 Mid-level study

The independent variables listed in table 4 were specified at the mid-points of their respective given ranges and the remaining required properties were estimated with the methods outlined in section 2.3 and with the ideal gas-law.

Subsequently, deviation values were calculated for the resulting LT-WGS system. Criterion 10 in table 2 is neglected for now in favour of the more severe criterion 11 (Δ_{XStat}), both of which impose an upper limit on the conversion of CO. For the evaluation of criterion 11 in table 2, it is assumed that $n = 7$ and $\sigma(X) = 0.5\%$. The CO conversion was calculated numerically using equation 1. Results of the evaluation of the deviation values for this reaction system are summarised in figure 10.

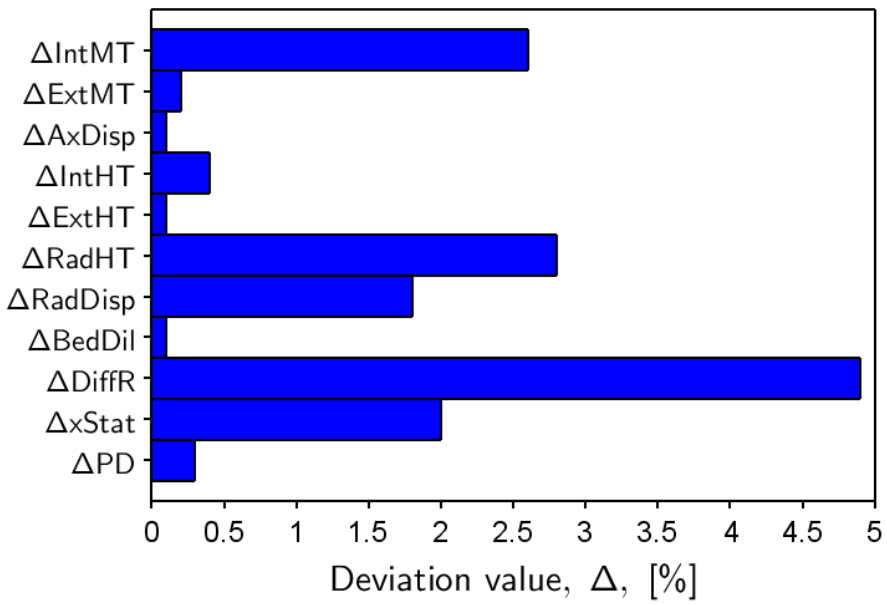

Figure 10 – Deviations from ideality from various effects for a typical a LT-WGS-Cu/Zno/Al_2O_3 catalytic reaction system

For this theoretical system, all calculated deviation values are smaller than the specified limit of 5%. Hence, measured rates in a real system with these properties would be expected to be representative of intrinsic kinetic behaviour and free from confounding effects.

5.3 Factorial study

A broader investigation of the prevalence of different limiting effects in the LT-WGS system can be done by calculating deviation values for the whole range of values of the independent variables in table 4 (as opposed to a single value for each independent variable as in section 5.2). In other words, a wide range of theoretical reaction systems may be specified by simultaneously varying the independent variables (within their respective ranges) and calculating deviation values for each (as done in section 5.2).

One way to achieve this is to define a factorial grid for the specification of the independent variables and to calculate deviation values for every combination of the different levels in the range of the independent variables.

Each set of values for each independent variable is defined to include the upper and lower bounds of the given range with intermediate values at equal spacing. The desired number of values in a set is specified by the 'grid density' (n_{grid}). In mathematical terms:

$$\{\vartheta\} = \vartheta_{LL} + \left(\frac{\vartheta_{UL} - \vartheta_{LL}}{n_{grid} - 1}\right) k_{grid} \tag{57}$$

With $$\left\{k_{grid} | k_{grid} \in \mathbb{N}_0, k_{grid} \leq n_{grid} - 1\right\} \tag{58}$$

If the grid density is kept equal for all six independent variables, the number of unique combinations of independent variables, all of which create a unique reaction system, is then given by:

$$N_{Calc} = {n_{grid}}^6 \tag{59}$$

Since the number of unique systems to be evaluated increase rapidly with the grid density, all calculations (specification of the factorial grid, evaluation of system properties and evaluation of deviation values) and interpretation of results are performed with the aid of the open-source, numerical computational package Scilab.

The results of such a factorial calculation can be interpreted in different ways. For instance, the number of combinations of independent variables that resulted in all criteria being met, relative to the total number of combinations/calculations made, can give an indication of the 'total success rate' of the system for the given ranges of independent variables.

$$\overline{N}_{All\ met} = \frac{N_{All\ met}}{N_{Calc}} \tag{60}$$

Where $N_{All\ met}$ is the number of combinations in the factorial grid resulting in all criteria being met. Similarly, a failure rate can be found for individual criteria by comparing the number of times the criteria is met to the total number of calculations.

$$\overline{N}_{\Delta,Fail} = 1 - \frac{N_{\Delta\ met}}{N_{Calc}} \tag{61}$$

Where $N_{\Delta\ met}$ is the number of combinations resulting in a given criterion (Δ) being met.

It should be noted that the prevalence of the failure of different criteria are each influenced by different combinations of the independent variables as well as the ranges of values that these are allowed to take (here chosen to be relevant to laboratory-scale performance testing of heterogenous catalysts). For example, the failure rate of the internal mass transfer limitation criterion (Δ_{IntMT}) is theoretically only influenced by the temperature and catalyst particle size in the context of this factorial study.

5.3.1 Criteria failure rates: results and discussion

Results of a factorial calculation must be independent of the grid density chosen for the independent variable sets. This convergence requirement has been investigated, the results of which indicate that a grid density of 6 or more is required. Further detail on this is given in appendix D.

The total success rate for the factorial LT-WGS system was calculated to be 11% with a grid density of 8. This indicates that 11% of all possible combinations of the independent variables (within a given practical range; as identified in table 4), result in a performance test of a LT-WGS catalyst (as described by section 5.1) which is

theoretically free from the confounding effects listed in table 1 and table 2. In other words, 11% of all possible choices of test conditions (within a practically realisable range) for this system would, theoretically, be expected to produce intrinsic rate measurements.

Additionally, individual criteria failure rates were calculated. The results thereof are summarised in figure 11.

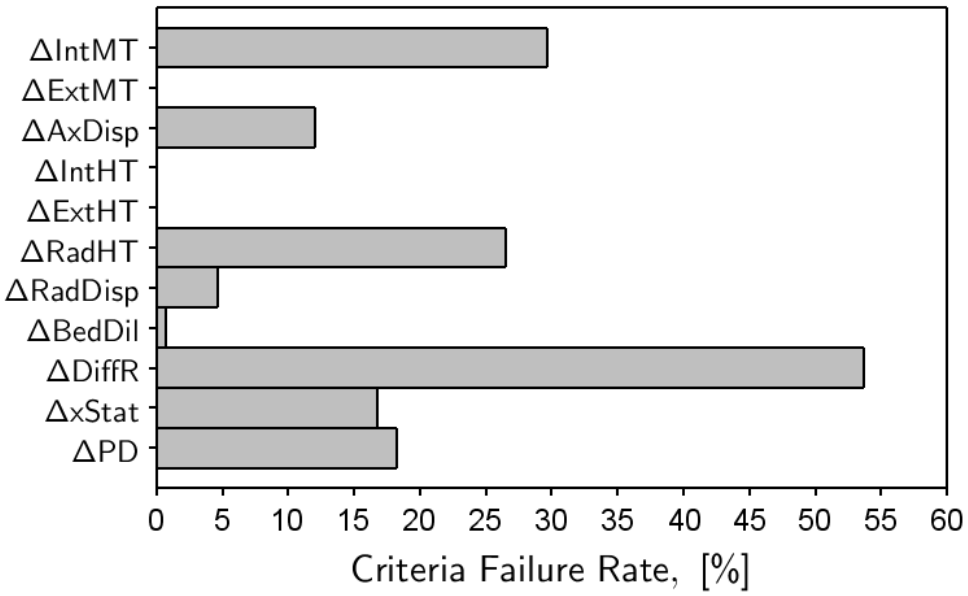

Figure 11 – Failure rates of deviation-free criteria in a factorial space of independent variables (typical operating conditions) for a typical a LT-WGS -Cu/Zno/Al_2O_3 catalytic reaction system.

In terms of transport limitations, a high prevalence of internal mass transfer (~30%), and radial heat transfer (~27%) limitations are expected for performance tests of Cu/ZnO/Al_2O_3 under LT-WGS conditions. Limitations due to axial dispersion (~12%) and radial dispersion (5%) are suggested to be lesser, yet significant factors.

It is somewhat surprising that no influence of external mass transfer, external heat transfer and internal heat transfer is expected for the whole range of independent variables. It is especially surprising of external heat transfer in comparison to the analysis performed by Kapteijn & Moulijn (2008) on comparing transport limitations. This is perhaps explained by the difficulties and differing views on correlating external heat transfer coefficients at low Reynolds number, as discussed in section 2.3.2.2.

Here, the correlation of Wakao, Kaguei & Funazkri (1979) is used which gives a higher external heat transfer coefficient at low Reynolds number compared to other authors.

In terms of the additional criteria developed in section 4, the influence on the observed reaction rate due to the pressure drop across a flow reactor is also expected to be significant (~18% of the factorial grid) while the limits imposed on the conversion (Δ_{DiffR} and Δ_{xStat}) is rather severe. The results shown in figure 11, indicate that ~54% of the factorial grid of independent variables results in a reaction system which produces a conversion of CO larger than 9.8%, the limit imposed by criterion 9 (Δ_{DiffR}). In contrast, a significant portion (~17%) of the factorial grid results in a conversion smaller than 3.8%, the limit imposed by criterion 11 (Δ_{xStat}).

5.3.2 Effect of operating conditions (independent variables) on performance testing criteria

The results of section 5.3.1 give an indication of the overall prevalence of the different confounding effects for a $Cu/ZnO/Al_2O_3$ LT-WGS system under an expected range of experimental conditions (independent variables) without yielding information on how to avoid such effects. Here, the effects of the independent variables on the overall success rate and the failure rate of individual criteria in the factorial system is investigated.

The effects of the independent variables on the overall success rate can be gauged as follows:

$$\overline{N}_{All\ met}(\vartheta) = \frac{N_{All\ met}(\vartheta)}{N_{Calc}(\vartheta)} \tag{62}$$

Where $N_{Calc}(\vartheta)$ is the number of combinations in the factorial grid which has a given independent variable at a specified value (in its set). This is equal to N_{Calc}/n_{grid} when the grid density is the same for all independent variables. The value $N_{All\ met}(\vartheta)$ is the number of combinations in the factorial grid which has a given independent variable at a specified value (in its set) and which results in all criteria being met. Thus, $\overline{N}_{All\ met}(\vartheta)$ gives an overall success rate when one given independent variable is at a certain value.

For example, as seen in figure 12, the value of $\bar{N}_{All\ met}(d_p = 450\ \mu m)$ is 19%, indicating that 19% of the combinations in the factorial grid, which have the particle size specified at 450 µm, result in all criteria being met. This is a significantly higher success rate than the average over all particle sizes (and over all independent variables) which is 11%.

In a similar way, the effect of independent variables on the failure rates for specific criteria can be calculated:

$$\bar{N}_{\Delta,Fail}(\vartheta) = 1 - \frac{N_{\Delta\ met}(\vartheta)}{N_{Calc}(\vartheta)} \tag{63}$$

Where $N_{\Delta\ met}(\vartheta)$ is the number of combinations in the factorial grid which has a given independent variable at a specified value (in its set) and which results in a given criterion (Δ) being met. For example, as seen in figure 13 the value of $\bar{N}_{\Delta IntMT,Fail}(d_p = 550\ \mu m)$ is 50%, indicating that 50% of the combinations in the factorial grid, which have the particle size specified at 550 µm, result in the failure of the internal mass transfer criterion.

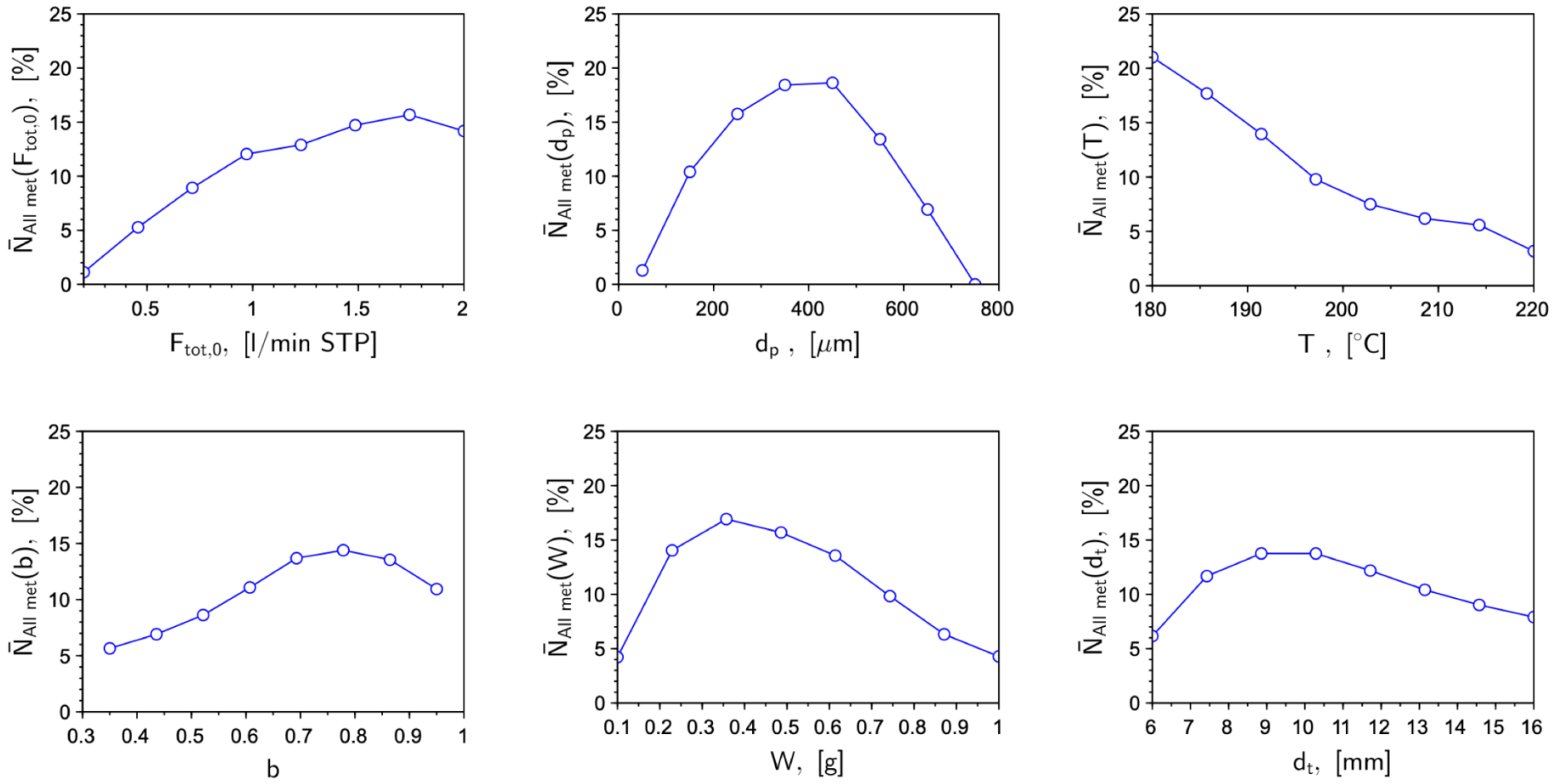

Figure 12 – Overall success rate (all criteria met) of a factorial study of the LT-WGS-Cu/Zno/Al_2O_3 catalytic reaction system as functions of the six common independent variables.

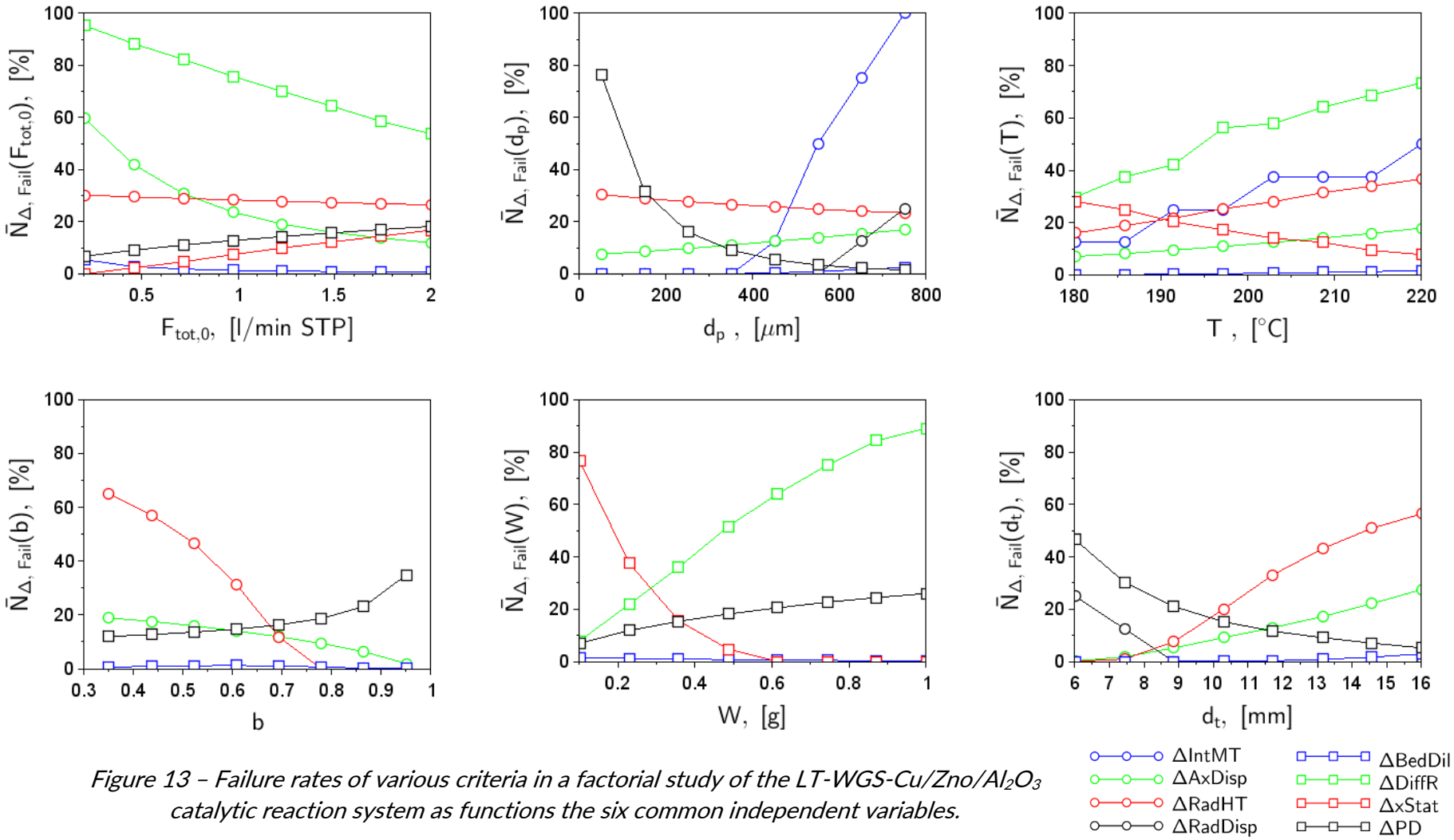

Figure 13 – Failure rates of various criteria in a factorial study of the LT-WGS-Cu/Zno/Al_2O_3 catalytic reaction system as functions the six common independent variables.

While the individual trends in figure 13 are not particularly surprising (these trends could be inferred directly from the theories and descriptions that make up the various criteria) their combined effects on the total success rates in figure 12 provide useful insights for choosing experimental conditions for catalyst performance testing.

With the exception of the operating temperature (T), figure 12 exhibits optima for the independent variables, where the total success rate is maximised. These optima are formed by different failure rates of the criteria under variation of the independent variables, as seen in figure 13. In general, for an independent variable, failure rates of one or more criteria will increase with the increasing value of the independent variable while failure rates of one or more other criteria increase with a decrease in its value, creating a minimum total failure rate (maximum success rate) at an intermediate value. Although no optimum value is seen for the operating temperature, an optimum is likely to exist at a lower temperature where the failure rate of Δ_{xStat} (the restriction on the relative error in the measured conversion) increases. Selection of experimental conditions are thus important in balancing overlapping deviations from ideality such that confounding effects may simultaneously be suppressed.

The strength of the responses, or the slope of the trends, in figure 13 for the independent variables give an indication of the sensitivity of a criterion to different independent variables. Such knowledge can aid experimenters in deciding which variables are important to control for the control of different potentially confounding effects. For instance, the failure rate of the internal mass transfer criterion increases rapidly with an increase in the catalyst particle size, while the response due to increasing temperature is low in comparison. Thus, when internal mass transfer limitations need to be eliminated, control of the catalyst particle size is likely to be more important than the temperature.

In the same sense, radial heat transfer limitations are most effectively addressed by the dilution ratio and the reactor tube diameter; excessive pressure drop by the particle size, reactor tube diameter and the dilution ratio (if at high dilution); axial dispersion by the molar feed rate; and the conversion by the catalyst loading/mass and the molar feed rate.

6 Experimental performance test of a medium temperature WGS catalyst

As demonstration of the theories reviewed and discussed hereto on catalyst performance testing, a proprietary catalyst, developed at the University of Cape Town, was evaluated for its WGS activity under medium-temperature shift (MT-WGS) conditions. Henceforth, this catalyst is referred to as the UMW catalyst.

Furthermore, the robustness of the theoretical evaluation of internal mass transfer limitations from a single measurement of catalyst activity is of interest, since, from the analysis conducted in section 5, this effect is expected to be particularly important to characterise if intrinsic catalyst activity is to be measured. Hence, as part of the experimental study, catalyst samples having different mean particle sizes were tested.

6.1 Experimental methodology

The UMW catalyst was characterised in terms of its specific surface area, pore size distribution, bed and particle properties, and WGS activity, stability and selectivity in order to evaluate the various catalyst testing criteria given in table 1 and table 2. Some measurements that were required for section 5 were also performed for a $CuO/ZnO/Al_2O_3$ LT-WGS catalyst precursor.

6.1.1 Specific surface area and pore size distribution

The UMW catalyst and a $CuO/ZnO/Al_2O_3$ catalyst precursor was submitted for nitrogen physisorption analysis conducted in a Micromeritics TriStar II 3020. Catalyst samples (approximately 0.5 g each) were degassed at 120 °C under vacuum. Equilibrium nitrogen adsorption isotherms were then measured at -195.8 °C. Specific surface areas and pore volumes were calculated by the Brunauer-Emmett-Teller (BET) method. The pore size distribution of the UMW catalyst was calculated by the Barrett-Joyner-Halenda (BJH) method. For the $CuO/ZnO/Al_2O_3$ sample, only an average pore size from the surface area and pore volume was estimated for use in section 5.

Additionally, the UMW catalyst was submitted for mercury intrusion porosimetry (MIP) analysis in a Micromeritics AutoPore IV 9500. A sample of ~1 g was evacuated at 4 Pa

for 20 min. Volumetric measurements were taken at pressures from 0.040 to 4060 bar(a). By application of the Washburn equation, this corresponds to pore widths of 317 μm and 3 nm, respectively, assuming a mercury contact angle of 130° and surface tension of 485 mN/m. Data were corrected to exclude interstitial volumes (between particles) by excluding measurements taken below the threshold pressure (Webb, 2001). The sample surface area was calculated by the method reported by Rootare & Prenzlow (1967).

6.1.2 Catalyst grinding and sieving

Samples of UMW catalyst of different size fractions were prepared by crushing and grinding down larger catalyst particles (as synthesised; from the same batch) in a ceramic mortar and pestle and sieving the contents into three size classes, namely, 75-100 μm, 500-600 μm and 850-1000 μm. Different particle size fractions were also prepared for the dilution of catalyst samples with inert silicon carbide. This was done to avoid separation of catalyst and diluent particles in the mixed bed. To this end silicon carbide sized into the following fractions: 75-300 μm, 300-710 μm and 1000-1400 μm.

Sieving was aided by mechanical shaking in a Retsch AS200 analytical sieve shaker. A stack consisting of the sieves were arranged large apertures at the top to decreasing apertures going down, with a collector plate at the bottom and clamped in the shaker. Fines were collected, and sieving allowed to continue until no further production of fines was observed.

6.1.3 Particle size distribution

Particle size distributions were determined by microscopic and photographic observation for each of the three different size fractions of UMW catalyst. The smallest size fraction (sieved to 75-100 μm) was photographed under 50x magnification with the use of a light microscope. The two larger fractions were photographed without magnification. Since particle shapes were observed to be irregular, a mounting resin was used to effect random orientation of particles on slides. To achieve this a thin film of mounting resin was spread on a glass slide and allowed to cure until scratches in the

resin remained (instead of closing by resin flow). Image analysis software, ImageJ, was used to analyse the photo- and micrographs of individual projections of randomly oriented particles. Particle sizes were interpreted as the diameter of a circle having the same area as the area of the particle projection ($d_p = 2\sqrt{A_{p,proj}/\pi}$). Additionally, particle aspect ratios (AR), roundness and 'MinFeret' diameter (minimum calliper diameter; the shortest distance between two points on the edge of a particle projection) were measured.

6.1.4 Bulk and particle density

Bulk and particle densities were measured for the silicon carbide diluent, the UMW catalyst and the $CuO/ZnO/Al_2O_3$ catalyst precursor. Bulk densities were measured by simple measurements of the packing volume (in 10 ml volumetric flask) and mass (by digital balance) of catalyst particles. The volumetric flask was tapped on a hard surface until no further change in the packing volume was observed before recording the volume.

$$\rho_{b,cat} = \frac{m_{cat}}{V_{bed,cat}} \tag{64}$$

Particle densities were measured by a method adapted from Buczek, Bronislaw (1991), where a fine powder is used as a pycnometric fluid. A fine silica powder (<75 µm) was used for this purpose. The bulk density of the pycnometric powder ($\rho_{b,pf}$) was first determined$\rho_{b,pf}$. A 10 ml volumetric flask was again used to measure bed volumes. Catalyst samples of approximately 2.5 g were added to the volumetric flask and weighed. The pycnometric powder was then added, ensuring encapsulation of the catalyst particles by the powder, and compacted by tapping, as with the bulk density determination. Lastly, the flask containing the catalyst sample and pycnometric powder was weighed and the volume recorded. The density of catalyst particles could then be determined with:

$$\rho_{p,cat} = \frac{m_{cat}}{V_{bed,T} - m_{pf}/\rho_{bed,pf}} \tag{65}$$

6.1.5 Catalyst testing apparatus

Measurement of the activity of the UMW catalyst was performed in the apparatus shown in figure 14. The apparatus allows for the mixing of an artificial, dry syngas stream by individual control via mass flow controllers (MFC) of up to 5 gases into a common gas line. Similarly, the flow of the dry, mixed gas to three parallel reactors may be controlled individually. A bypass line channels excess gas from the mixing section to a 6-port selector valve downstream of the reactor assemblage which allows one incoming gas flow to be directed to a GC, sending the other gas streams to be vented. This aids in stability of flow control, allows control of the pressure between the mixing section and the dry gas feed (to the reactors) flow controllers and allows the dry feed gas to be analysed in the GC.

Three Scientific Systems, Inc. (SSI) Series 1 pumps independently supplied de-ionised liquid water to each reactor at a controlled rate. Pump rates were monitored by recording the mass loss from water feed pots.

The three tubular reactors are seated in a brass furnace block which was heated electrically in four separately controlled axial zones. Axial temperature profiles in the reactor tubes could be measured by a moveable thermocouple in a central, axial thermowell. Measurements were made at different temperature settings under liquid water and inert gas flow to determine where isothermal conditions could be achieved during catalyst performance tests. Differences in axial temperature profiles between reactors in different positions in the furnace block were found to be negligible. Operating temperatures were confirmed to be within 1 °C of the intended temperature during catalyst performance tests.

Each reactor effluent gas stream was cooled in a coiled line around which coolant was circulated. The ethylene glycol/water coolant mixture was cooled and pumped by a LAUDA LCKD1907 refrigeration bath. The cooled product gas streams each were fed to a gas/liquid separator which was cooled by circulating coolant in coils. The separators are designed to minimize dead gas volumes therein. The three cooled, dry reactor effluent streams were fed to the selector valve, allowing a selected stream to be directed to a GC whilst the other are vented.

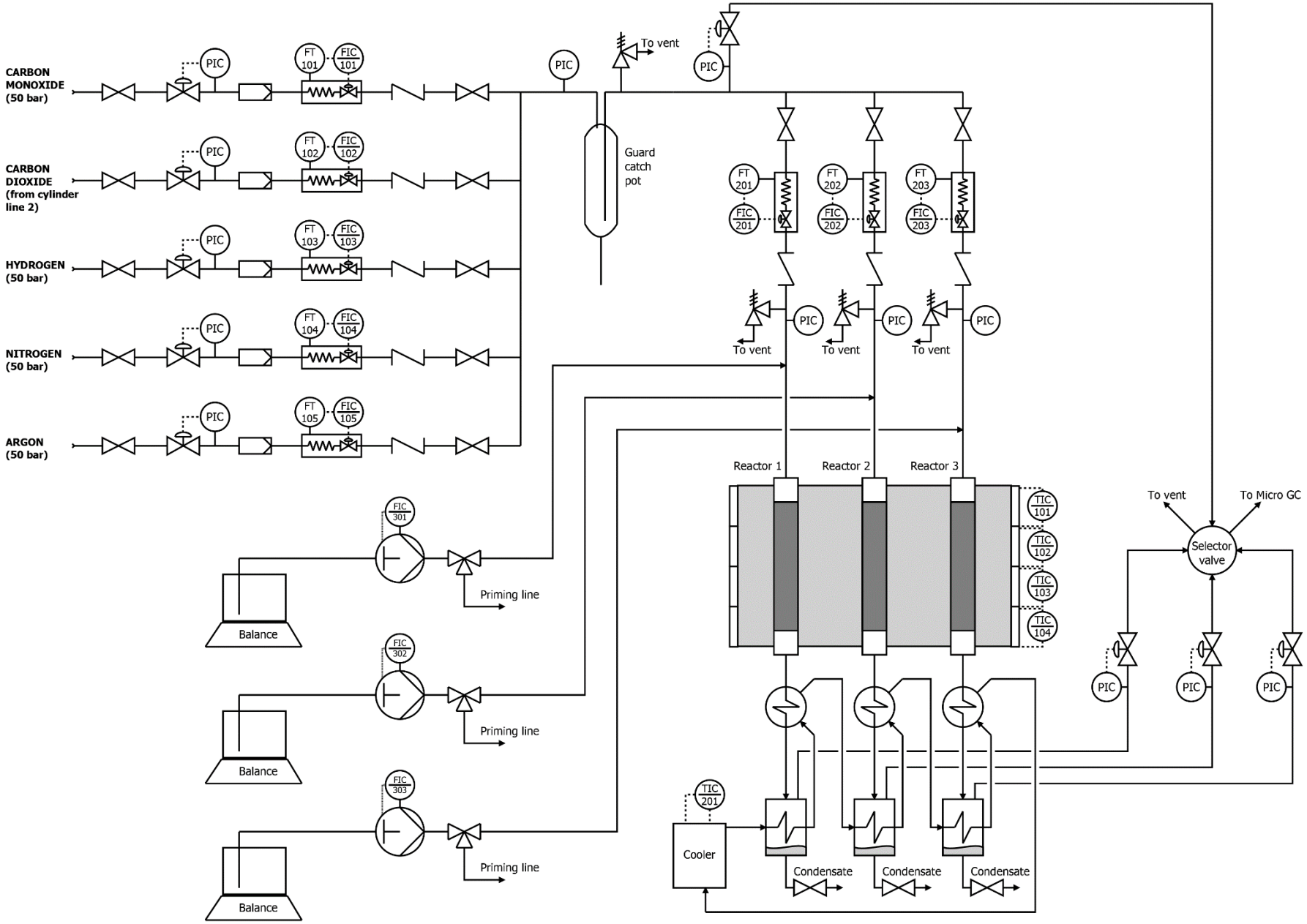

Figure 14 – Flow sheet of catalyst testing apparatus

6.1.6 Gas compositions by gas chromatography (GC)

The dry feed gas and dry reactor effluent gas streams were analysed by gas chromatography in an Agilent Technologies 490 Micro gas chromatograph. Two columns were used to resolve H_2, N_2, CO and CO_2 from the mixed gas sample. A thermal conductivity detector was used to quantify the concentrations of these species in gas samples.

A 10 m Molecular Sieve 5A (MS5A) column was operated at a temperature of 80 °C and 300 kPa, using Ar as carrier gas. This column was used to separate H_2, N_2 and CO from the gas mixture, with retention times of 0.31, 0.39 and 0.52 min, respectively.

A 10 m PoraPLOT Q (PPQ) column was operated at a temperature of 60 °C and 150 kPa, using H_2 as carrier gas. This column was used to separate CO_2 from the gas mixture, with a retention time 0.41 min. Small amounts of residual water vapour in reactor effluent samples were observed in this column with a retention time of 0.85 min. This was not quantified since the water vapour content of gas samples was found to be very small, due to the low temperature of the condensers (4 °C), and the complexity of calibrating the GC for accurate analysis of water vapour. The balance of species compositions indeed indicated that the residual water vapour corresponded well to the vapor pressure of water at 4 °C.

An example of typical chromatograms for these two columns and calibrations of signal responses to different analyte concentrations are given in appendix E.

6.1.7 Reactor specifications and loading

The three UMW catalyst samples with different size distributions were loaded as fixed beds in tubular reactors. The mass of catalyst loaded in each reactor was 150 mg. This sample mass was chosen with a guessed/approximated expected catalyst activity in mind, informed from the activity of a similar catalyst developed by Brown (2018).

One catalyst sample was loaded into a reactor with an ID of 14.8 mm which has an internal, central, axial thermowell. The remaining two catalyst samples were loaded into reactors without axial thermowells, which have a narrower section in the isothermal

zone, with an ID of 10.2 mm. Tight fitting and contact with the furnace block in the narrower section was ensured by metal jacketing to the furnace seating size. The axial thermowell allows a thermocouple to measure temperatures at any axial position, enabling confirmation of isothermal zones under different experimental reaction conditions and control of the isothermal zone temperature. The catalyst sample with the smallest average particle size was preferred for the reactor with the larger ID since the radial dispersion effects would be expected otherwise.

Table 5 – Reactor loading specifications

	Units	Reactor 1	Reactor 2	Reactor 3
Reactor specifications				
Tube ID	mm	10.2	10.2	14.8
Thermowell OD	mm	-	-	3.2
Catalyst bed specifications				
UMW catalyst	g	0.150	0.150	0.150
SiC[1]	g	0.71	0.71	0.71
Dilution ratio, b	-	0.9	0.9	0.9
UMW catalyst particle size[2]	µm	500-600	850-1000	75-100

[1] Calculated from the measured bulk density of three size fractions of SiC used
[2] Given by the mesh sizes of sieves used

A dilution fraction, b, of 0.9 was chosen. This value is high considering the results shown in figure 12, however, pressure drop effects were expected to be less important due to a much lower maximum total feed gas flow, and radial heat transfer effects were expected to be more significant by comparison.

A simplified drawing of the reactors used in experiments is shown in figure 15 illustrating the loading procedure and packing zones.

Loading was done as follows: (1) glass wool was inserted to contain particles which may otherwise wash out of the reactor, (2) a bed of coarse silicon carbide (~1 mm) was packed to aid in axial heat transfer and to place the catalyst/silicon carbide mixed bed in the desired isothermal zone, (3) glass wool separated the inert silicon carbide bed from the mixed catalyst/silicon carbide bed, (4) the catalyst sample was packed after thorough mixing with inert silicon carbide of a similar particle size, (5) a glass wool layer separated the different packings and aided in redistribution of gas flow from the adjacent, coarser packing of SiC (6), which provided thermal mass and surface area for

heat transfer for evaporation of the liquid water feed as well as preheating of the resultant gas mixture to the desired reaction temperature.

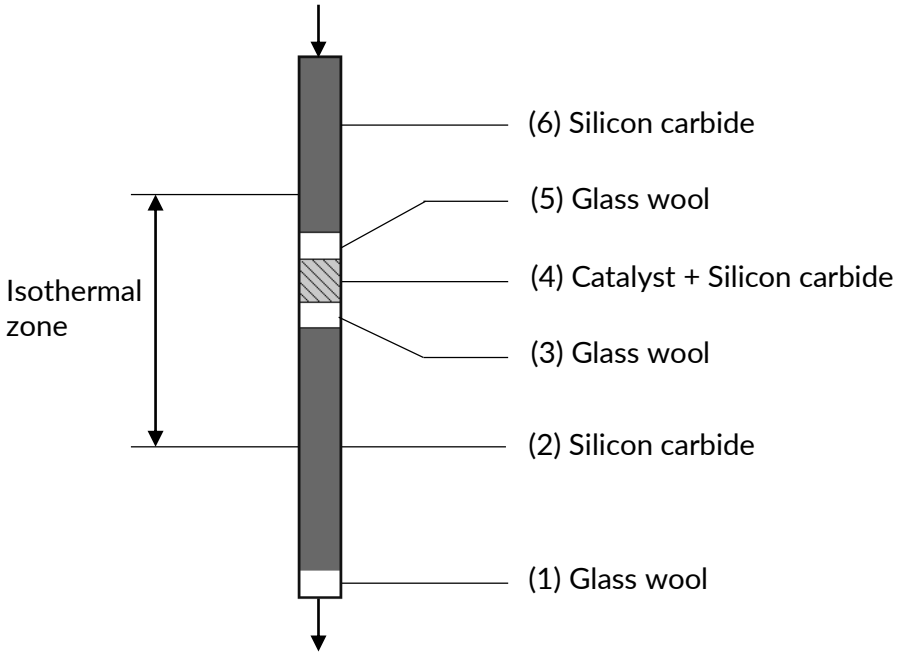

Figure 15 – Loading of fixed-bed reactors

6.1.8 Operating conditions for performance tests

The composition of the experimental reactor feed gas was chosen to approximate the product gas composition expected from an LPG steam reformer, operating close to atmospheric pressure at 700 °C, with a steam-to-carbon molar ratio of 4. This was done to be applicable to research conducted in-house on fuel processing of an LPG feedstock and for ease of comparison to a similar catalyst previously synthesised in-house and characterised by Brown (2018). The gas composition used in the feed to the three experimental reactors was thus 6.6% CO, 6.6% CO_2, 46.6% H_2, 33.3% H_2O and 6.6% N_2. This corresponds to a dry-gas composition of 10% CO, 10% CO_2, 70% H_2, and 10% N_2 with a steam-to-dry-gas molar ratio of 0.5. A total operating pressure of 1 atm(a) pressure was used throughout.

As previously noted, the total gas flow rate to each reactor is controllable during testing. However, due to the dry-gas composition, the need for a small amount of gas flow through the bypass (87 SCCM) and the limitations of the gas mixing section MFCs (particularly the hydrogen MFC at 1000 SCCM maximum flow), a maximum total dry-

gas flow to each reactor of 433 SCCM could be achieved with the existing MFCs. This corresponds to a total (wet) WHSV of 158 h^{-1}.

Table 6 – Reactor feed composition and flow rates

	Units	CO	CO_2	H_2	N_2	H_2O	Total
Gas composition							
Feed gas (dry)	mol%	10	10	70	10	-	100
Feed gas	mol%	6.7	6.7	46.7	6.7	33.3	100
Flow rates (per reactor)							
Mass flow rate	g/min	0.054	0.085	0.027	0.054	0.174	0.395
Volumetric flow rate (vapor)	SCCM	43.3	43.3	303.3	43.3	216.7	650

The operating temperature was chosen to be appropriate to the 'medium temperature' WGS conditions, to enable comparison to the catalyst formulation tested by Brown (2018) and to experimentally characterise internal mass transfer limitations. Hence, all three prepared size fractions of the UMW catalyst were tested at three temperatures in the 'medium temperature' range, at 275 °C, 300 °C and at 325 °C. The UMW catalyst sample with the smallest average particle size, was expected to have negligible internal mass transfer limitations, allowing for measurement of the catalytic activation energy.

6.1.9 Operation of catalyst testing apparatus

Prior to measurement of catalyst activity, the UMW catalyst was conditioned under a reducing environment. To achieve this, a mixture of 5 mol% H_2 in N_2 was fed to each reactor at a rate of 200 SCCM. The temperature of the reactors was then increased at a rate of 1 °C/min from ambient to 275 °C and held at his temperature for 10 hours. The gas flow was then switched to pure hydrogen (analytical grade) for one hour to ensure full reduction of the catalyst's active metal sites.

Reaction conditions were subsequently introduced incrementally. The desired nitrogen and hydrogen flows were set first. This was followed by the introduction of the desired liquid water flow, ensuring that the temperature of the circulating coolant was in the range of 3-5 °C. Lastly, the CO and CO_2 flows were set. Water flow rates were monitored throughout the experiment and analysis of reactor product gases performed only while the water flow rate to that reactor was within 5% of the desired flow (0.174 g/min).

Analysis of the dry feed gas and reactor product gases (by GC) were performed such that a minimum of 10 repeat measurements were taken with each GC column, ensuring that the measurements had stabilised to the set reactor conditions. Measurements were performed in the sequence: (1) dry feed gas; (2,3,4) reactor product gases in random order; (5) dry feed gas. This sequence of analysis was repeated for reactor isothermal zone temperatures of 275 °C, 300 °C and 325 °C where reactor temperatures were cycled from low to high 3 times, such that 3 sets of gas composition measurements were acquired for each reactor at each specified temperature. In this way the dry feed gas was analysed periodically to ensure that the feed gas composition remained the same during analysis of reactor product gases and a preliminary, qualitative investigation of the catalyst stability (over 8 days) could be performed.

6.2 Results and discussion

6.2.1 Specific surface area and pore size distribution

Results of analysis of the largest particle size fractions of the LT-WGS catalyst precursor ($CuO/ZnO/Al_2O_3$) and the UMW catalyst by N_2 physisorption and of the UMW catalyst by MIP is given in table 7. The results of these measurements were assumed to be independent of particle size since these samples were found to be hard (non-compactible) and since they have a negligible external surface area compared to the internal surface area. Fitting of the BET equation to N_2 isotherm data was done in the relative pressure range of 0.049-0.174 for $CuO/ZnO/Al_2O_3$ and 0.011-0.174 for the UMW catalyst, resulting in R^2 values larger than 0.999 for both materials.

Table 7 – N_2 physisorption and MIP results

Sample	Surface area, [m^2/g]	Pore volume, [cm^3/g]	Pore size, $(4V/A)_{pore}$, [Å]
$CuO/ZnO/Al_2O_3$ (BET)	90.1	0.33	145
UMW catalyst (BET)	28.3	0.045	64
UMW catalyst (MIP)	26.7	0.065	133

Surface areas of the UMW catalyst, measured by MIP and BET, correspond well, differing by only 6%. The BET specific surface area of $CuO/ZnO/Al_2O_3$ was found to be roughly 3 times more and the specific pore volume 5 times more than of the UMW catalyst. This is somewhat misleading considering the difference in particle densities (see section 6.2.3). On a volume basis the surface areas are comparable, at 161 and 121 m^2/cm^3 for $CuO/ZnO/Al_2O_3$ and the UMW catalyst respectively, and the pore fractions differ by a factor of two, at 0.59 and 0.27. A large relative difference in the pore volume of the UMW catalyst is observed between the two methods (table 7). This is in part due to the difference in the range of these methods where MIP can quantify volumes of pores up to ~500 µm (Giesche, 2006) while physisorption is typically ill-suited for characterisation of macro-porosity (De Lange et al., 2014) and is typically used for pores smaller than a few hundred nano-metres. The lower bound of application of these methods is similar at 35 Å (De Lange et al., 2014, Giesche, 2006).

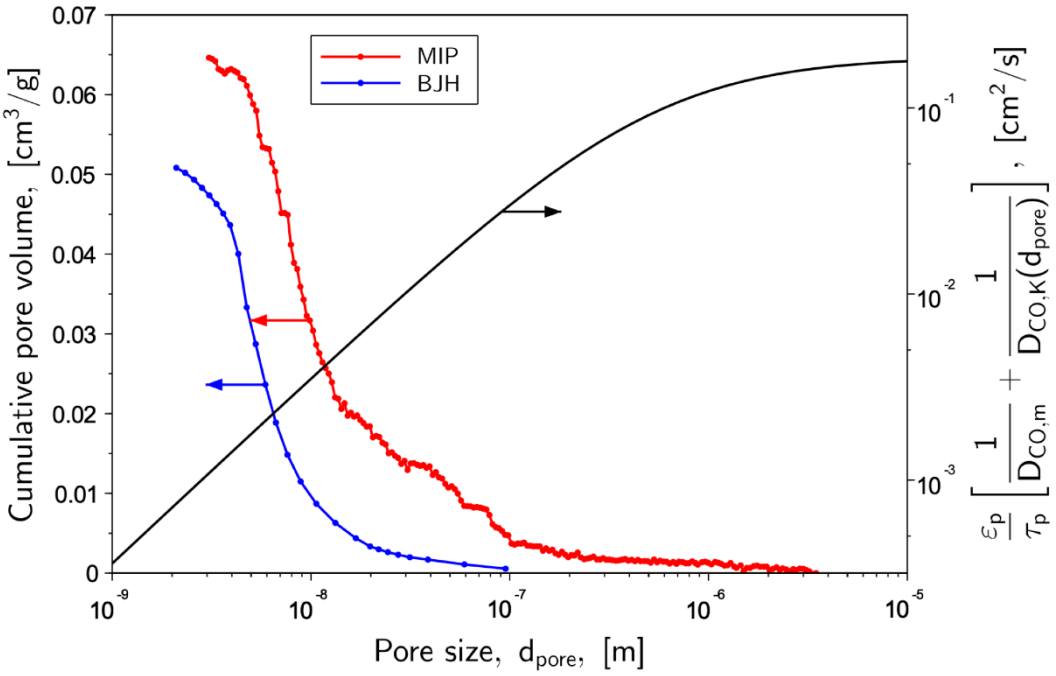

Figure 16 – Cumulative pore size distribution of the (proprietary) UMW catalyst and transition of CO diffusivity at 325 °C from Knudsen to molecular diffusion.

Thus, there remains a degree of uncertainty in the total pore volume due to the limited range of these methods, especially with physisorption where macro-pores are excluded.

Both methods resulted in pore volume measurements for pores between 30 – 130 Å of 0.041 cm^3/g, a large fraction of the porosity by either method. A large difference in pore volumes of pores in the 130 – 1000 Å range is seen however. One possible explanation for this discrepancy is that some of the macro-pores, which are not filled during N_2 physisorption, may only be accessed from the exterior by smaller pores. In addition to being excluded by physisorption, these pore volumes may appear as smaller pores in the MIP analysis due to the intrusion of mercury therein occurring at a higher pressure. Giesche (2006), among others, warns against this phenomenon.

Since the pore size distribution is used to estimate the effective diffusivities of gas species within the catalyst particle (see section 2.3.1.3), the transition of Knudsen to molecular diffusion with increasing pore size, for CO at 325 °C, is plotted in figure 16, along with the cumulative pore size distribution. This comparison suggests that intraparticle diffusion occurs mostly by Knudsen diffusion, with only a small number of pores measured by MIP in the transition region.

It should be noted that, with the BJH method, the pore volume becomes increasingly uncertain as the pore width decreases (De Lange et al., 2014, Thommes et al., 2015) and the pore width becomes increasingly uncertain as the pore width increases (De Lange et al., 2014). Furthermore, the size of narrow mesopores is underestimated due to limitations of the Kelvin equation in describing curvature and surface forces in narrow mesopores (Thommes et al., 2015). In fact, De Lange et al. (2014), argues that the pore size distribution as calculated by the BJH method typically is unsuitable for drawing quantitative conclusions.

6.2.2 Catalyst particle size distribution

The particle sizes obtained from photographic analysis all approximately follow gaussian distributions. Samples of particles having undergone the same sieving process were found to yield significantly different ($p < 5\%$) mean sizes depending on whether mounting resin was used or not. This is indicative of irregular particle shapes, producing non-random orientations on glass slides. Indeed, particles were observed to be irregularly shaped by visual and microscopic inspection. An example of a processed micrograph is shown in figure 18.

The measurement of particle sizes that are larger than the aperture size of its upper sieve (see table 8 and table 9) is a seemingly contradictory result. However, this result can be explained by the irregular, elongated shapes of the UMW catalyst particles and the square geometry of the apertures of the sieves used. Square sieve apertures of 100 µm (the lengths of the square sides are 100 µm) have diagonal dimensions of ~140 µm.

Table 8 - Particle size and aspect ratio data for UMW catalyst samples (no mounting media).

Number of particles in sample	Lower sieve size, [µm]	Upper sieve size, [µm]	Average particle size, $d_p = 2\sqrt{A_{proj}/\pi}$, [µm]	Standard deviation of size, σ(d_p), [µm]	Average aspect ratio (AR)	Standard deviation of aspect ratio, σ(AR)
395	75	100	125	26	1.5	0.4
704	500	600	910	108	1.5	0.3
499	850	1000	1269	159	1.4	0.3

Table 9 - Particle size and aspect ratio data for randomly oriented (with mounting media) UMW catalyst samples.

Number of particles in sample	Lower sieve size, [µm]	Upper sieve size, [µm]	Average particle size, $d_p = 2\sqrt{A_{proj}/\pi}$, [µm]	Standard deviation of size, σ(d_p), [µm]	MinFeret diameter, [µm]	Standard deviation of MinFeret diameter, [µm]
522	75	100	129	26	112	23
585	500	600	738	106	652	104
431	850	1000	1206	159	1098	151

Interpretation of particle 'size' by the diameter of a circle having the area as the particle projection introduces an assumption that particles are spherical and produce a circular projection. In reality, given a large enough aspect ratio, the dimensions of an irregularly shaped particle may produce a projection with an area equivalent to a circle with diameter larger than the reported aperture size of the sieve whilst still allowing the

particle to fall through a sieve aperture, lengthwise. Thus, non-circular apertures and non-spherical particles allow dimensions larger than the aperture size to be observed after sieving. A more quantitative indication that particles are irregularly shaped is found in the particle aspect ratio and similarly, the minimum calliper diameter (MinFeret diameter).

Characterisation of particle sizes of the three size fractions of UMW catalyst particles, prepared by sieving, is summarised in figure 17. Frequency histograms are normalised such that frequency distribution sum to 1.

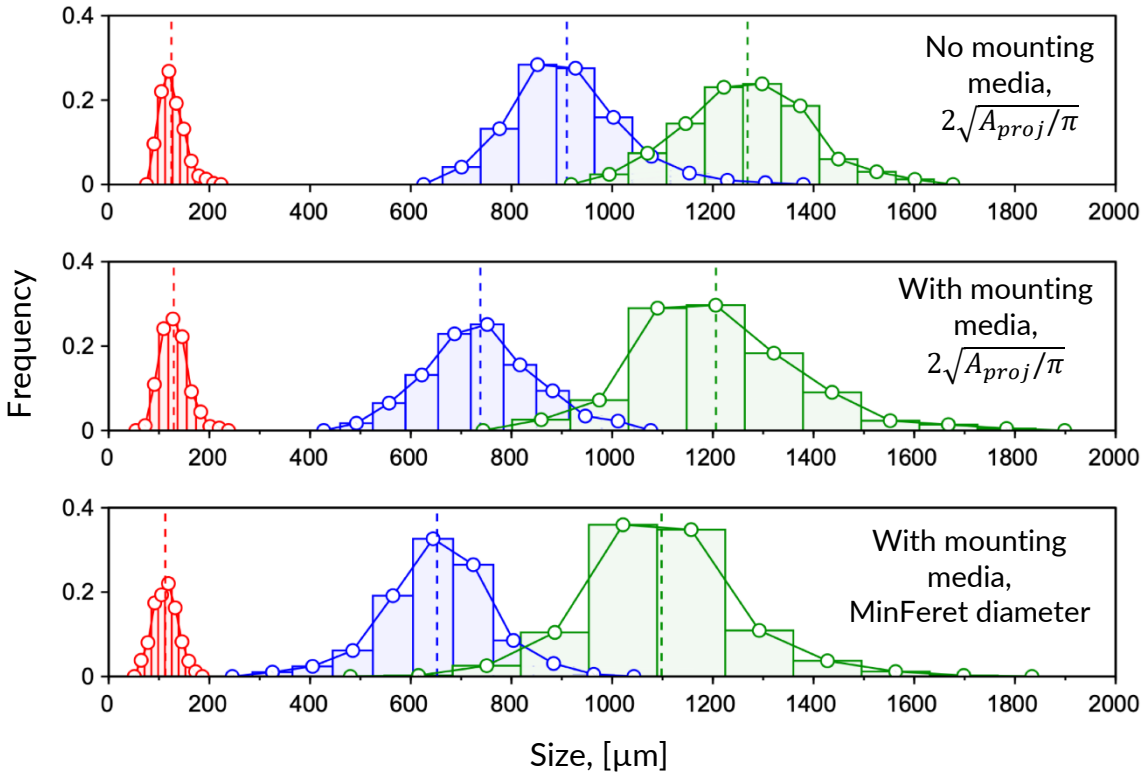

Figure 17 – Particle size distributions of ground and sieved particles of the UMW catalyst.
Sieve sizes: 75-100 µm; 500-600 µm; 850-1000 µm

For irregularly shaped particles much of the information is lost when particles are characterised by a single size descriptor, as is often called for in the various expressions in section 2.

Figure 18 – Example of a processed micrograph of UMW catalyst particles for digital analysis.

6.2.3 Bed and particle characteristics

Both bulk and particle densities were measured using large particles of the LT-WGS precursor and UMW catalyst (850-1000 µm) as is recommended by Buczek, B & Geldart (1986) for the measurement of particle densities. Different sized particles of the UMW catalyst were found to be similar in terms of shape (as observed visually and indicated by similar aspect ratios). Hence, different size fractions were assumed to pack similarly resulting in similar bed densities. Bed and particle void fractions were subsequently calculated from bulk and particle densities.

Table 10 – Catalyst bed and particle densities

Sample	Units	$CuO/ZnO/Al_2O_3$	UMW catalyst
Bulk/bed density, ρ_b	g/cm^3	1.02	3.25
Bed voidage, $e_b = 1 - \rho_b/\rho_p$	-	0.43	0.28
Particle density, ρ_p	g/cm^3	1.79	4.54
Particle voidage, $e_p = V_{pore} \cdot \rho_p$	-	0.59	0.27

The bulk densities of the bed diluent, SiC, and the fine pycnometric powder, SiO_2, were measured at 1.72 and 0.59 g/cm^3, respectively.

6.2.4 Selectivity

The average sum of mole fractions of CO, CO_2, H_2 and N_2 for all dry gas samples was 98.9%. This value increases to 99.7% assuming the presence of residual water vapour (not directly quantified by GC) in the concentration of 0.8 mol%, an amount corresponding to the equilibrium vapour pressure of water at 4 °C (the temperature of the coolant in the condensers). No analytes other than those expected for the WGS reaction and N_2 as inert diluent were observed. This indicates an exceptionally high, practically total selectivity of the UMW catalyst to the WGS reaction.

6.2.5 Conversion and observed rate

The conversion of CO is here defined as:

$$X_{CO} = 1 - \frac{F_{CO}}{F_{CO}^0} \tag{66}$$

The molar flow rate of CO leaving the reactor is not measured directly and is inferred from the composition analysis of the dry reactor effluent gas. With a total selectivity towards the WGS reaction, the CO conversion could be expressed in terms of the CO fraction of the dry reactor feed gas and the dry reactor effluent:

$$X_{CO} = \frac{1 - \frac{y_{CO,D}}{y_{D,CO}^0}}{1 + y_{CO,D}} \tag{67}$$

The derivation of equation 67 is given in appendix F. The observed (integral) rate of reaction was then calculated from the CO conversion by equation 2. The results of these calculations are summarised in figure 19, figure 20 and figure 21. These data are also tabulated in appendix G. Error bars for conversions and particle sizes indicate one standard deviation on each side.

Regarding the repeatability of the measured conversions, a previous experiment reproduced the conversion of the largest UMW catalyst size fraction at 300 °C (all other conditions being the same throughout) within an error of 2%. Another indicator for the repeatability of the experiments can be inferred from the initial activities (TOS ~ 0 h) measured for the three catalyst samples of different size fractions at low temperature (275 °C; figure 19). These measured activities were found to have very little influence from confounding effects (see figure 1H and 1I) and yielded very similar activities (11.0±0.6 µmol/s.g_{cat}). Thus, catalyst activities measured subsequently were assumed to be reproducible within a maximum relative error of 5%.

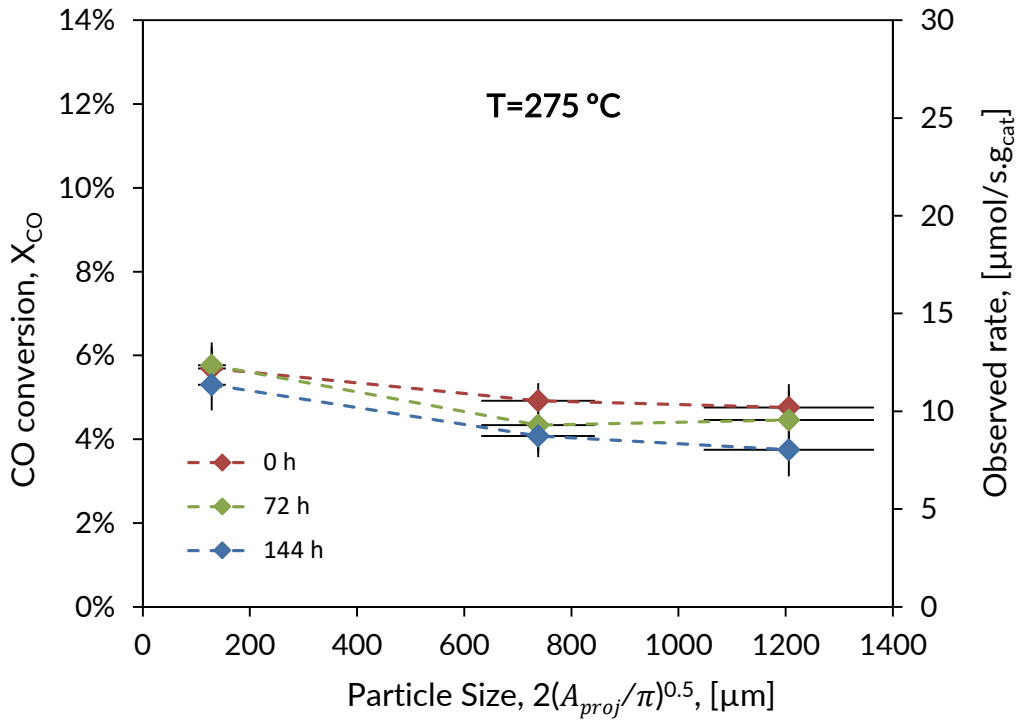

Figure 19 – CO conversion and observed rate of different particle sizes of the UMW catalyst at 275 °C, 1 atm total pressure, dry feed composition of 10% CO, 10% CO_2, 70% H_2, 10% N_2, steam-to-dry gas ratio of 0.5 and 4333 SCCM/g_{cat} total feed flow.

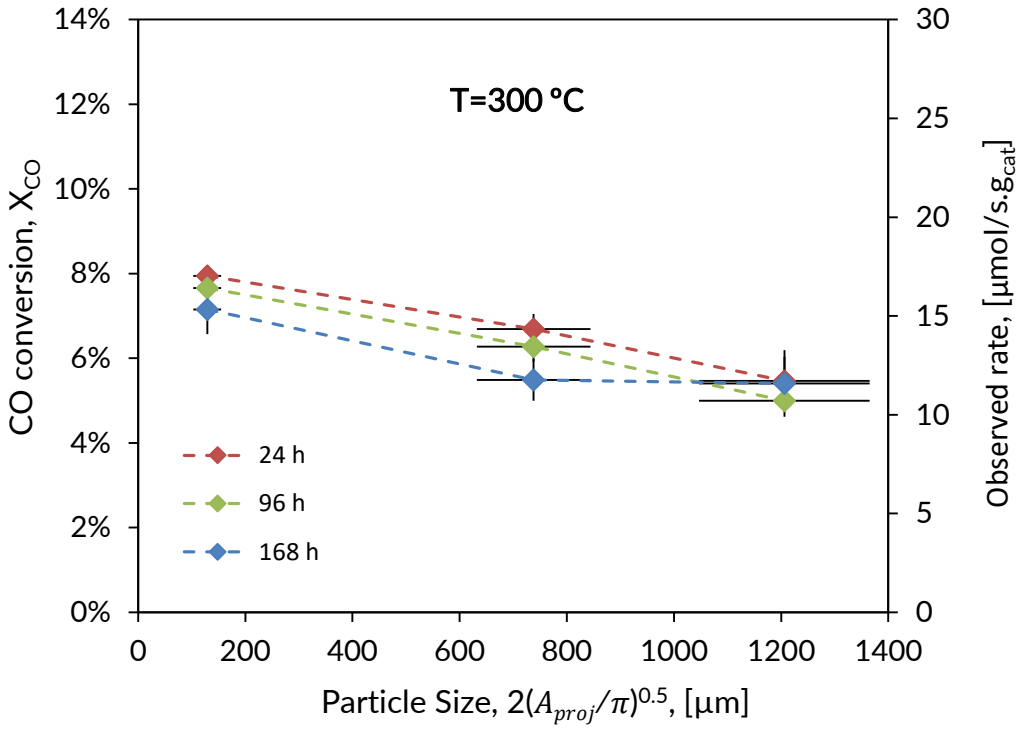

Figure 20 - CO conversion and observed rate of different particle sizes of the UMW catalyst at 300 °C, 1 atm total pressure, dry feed composition of 10% CO, 10% CO_2, 70% H_2, 10% N_2, steam-to-dry gas ratio of 0.5 and 4333 SCCM/g_{cat} total feed flow.

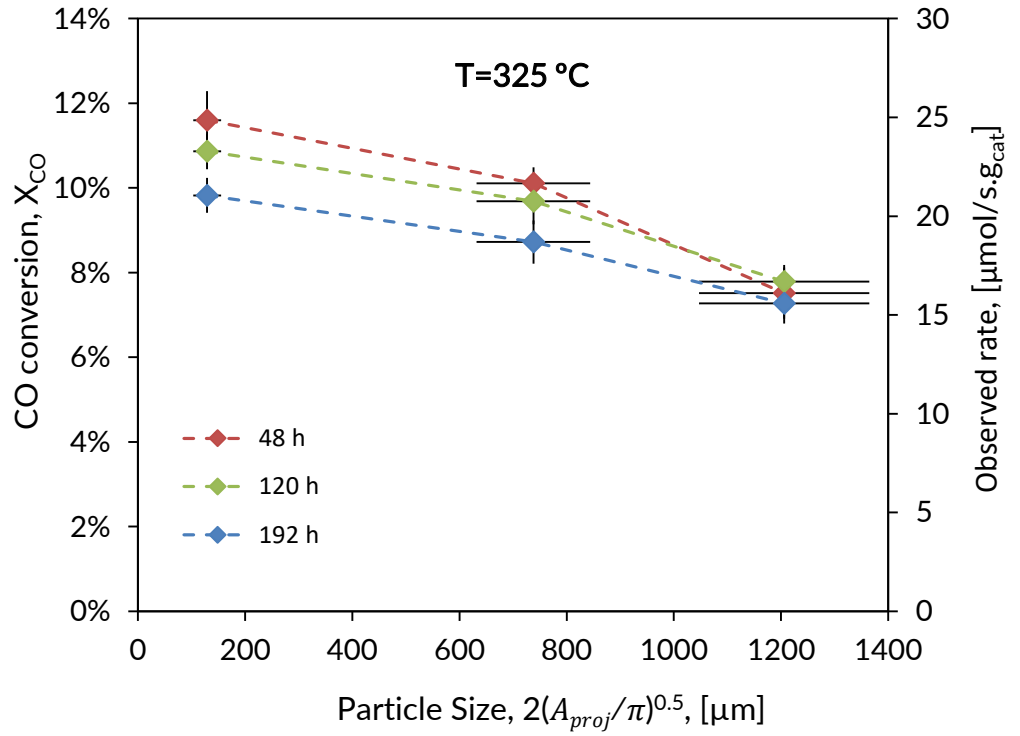

Figure 21 - CO conversion and observed rate of different particle sizes of the UMW catalyst at 325 °C, 1 atm total pressure, dry feed composition of 10% CO, 10% CO_2, 70% H_2, 10% N_2, steam-to-dry gas ratio of 0.5 and 4333 SCCM/g_{cat} total feed flow.

At all three test temperatures a decrease in the CO conversion is observed with an increase in the average catalyst particle size. These trends suggests that internal mass transfer limitations are experienced by the samples of mid-sized and large particle sizes. This is not necessarily true of sample of the smallest particle size. An argument that there are negligible internal mass transfer limitations for the smallest sized particles is given in section 7.2.

Catalyst activities from this study are comparable to other catalysts developed for MT-WGS conditions. Among many more, activities are reported by Azzam et al. (2008) for Pt-Re supported on TiO_2 and by Brown (2018) for Pt supported on CeO_2. Kinetic data from these two authors have been extrapolated to the conditions used in this study using their reported kinetic equations (Azzam et al., 2008, Brown, 2018). Their data are compared to measurements from this study at a time on-stream (TOS) of ~48 h or less (first temperature cycle) in table 11.

Table 11 – Comparison of MT-WGS catalyst activities

Temperature, [°C]	Activity, [µmol/g_{cat}.s]		
	This work, UMW	Azzam et al. (2008) Pt-Re/TiO_2	Brown (2018) Pt/CeO_2
275	12.2 ± 0.3	39.0	1.4
300	17.1 ± 0.1	52.5	4.0
325	24.9 ± 0.4	68.9	10.5

It should be noted that these comparisons are made based only on catalyst mass. Additional factors such as the loading and dispersion of the active material/metal should be considered for a more rigorous comparison,

6.2.6 Stability

Assessment of the stability of the UMW catalyst over time is confounded for the samples of mid-sized and large particle sizes since conversion measurements for these samples are not representative of intrinsic catalytic activity. Hence, only comparisons of activities of the smallest catalyst particles are considered in the context of stability, since only this sample is expected to yield near-intrinsic rate measurements.

The significance of the difference between CO conversions, measured at the same temperature after a different TOS, was tested by the T-test method (95% confidence level).

After one temperature cycle (corresponding to a difference in TOS of approximately 72 h or 3 days), a decrease in activity (from the initial measurements) of 6±2% and was observed between measurements taken at 325 °C. No significant difference could be resolved at 275 °C or 300 °C after one temperature cycle.

After two temperature cycles (corresponding to a difference in TOS of approximately 144 h or 6 days), a decrease in activity of 10±2% was observed between measurements taken at 300 °C and a decrease of 15±2% was observed for measurements at 325 °C. No significant difference could be resolved at 275 °C after two temperature.

6.2.7 Activation energy

As was done for the assessment of the catalyst stability, the reaction activation energy was calculated from rate measurements of the sample with the smallest average particle size to minimise the effect of transport limitations. The activation energy was calculated for the first temperature cycle to avoid the effect of catalyst deactivation. The influence of catalyst deactivation on this calculation is expected to be small since, as noted in section 6.2.6, no significant deactivation (from the first measurement) was observed after one temperature cycle at 275 °C and at 300 °C. Furthermore, a decrease in activity of only 6±5% was observed over ~72 h at 325 °C while the first measurements at 325 °C were taken at a TOS of ~48 h.

Results of fitting of the Arrhenius equation to the observed rate at different temperatures are summarised in the figure 22.

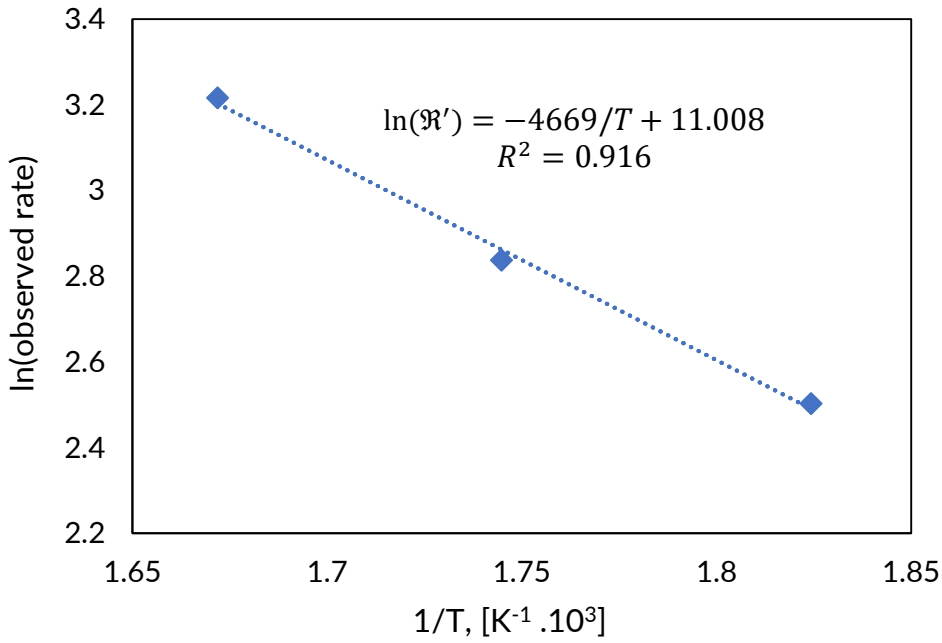

Figure 22 – Temperature dependence of the observed rate on temperature for the WGS reaction over the UMW catalyst with fitted Arrhenius equation ($E_{a,obs}$ = 39 ± 2 kJ/mol).

It should be noted that the activation energy was calculated from 60 measurements of the CO conversion (at TOS ≤ 48 h), consisting of three data sets (one for each temperature), condensed in figure 22 as the mean at each temperature. The calculated activation energy of 39±2 kJ/mol is within the expected range considering values reported by other authors for similar catalysts. A lower value of 31 kJ/mol is reported by Azzam et al. (2008) for Pt-Re supported on TiO_2 while higher values of 71 and 110 kJ/mol are reported by Radhakrishnan et al. (2006), for Pt-Re supported on CeO_2/ZrO_2, and by Brown (2018), for Pt supported on CeO_2, respectively.

6.2.8 Evaluation of catalyst testing criteria

Experimental parameters and results of the catalyst characterisation techniques reported in section 6.2 were used for the theoretical evaluation of potential transport limitations and of the additional criteria developed in section 4 for the experimental activity measurements reported in section 6.2.5. Additional parameters needed for calculations were estimated by the methods described in section 2.3.

Except for characterisation of internal mass transfer limitations, which is discussed in section 7, results of these calculations are shown in figure 23 for 325 °C for the first temperature cycle (TOS ≤ 48 h).

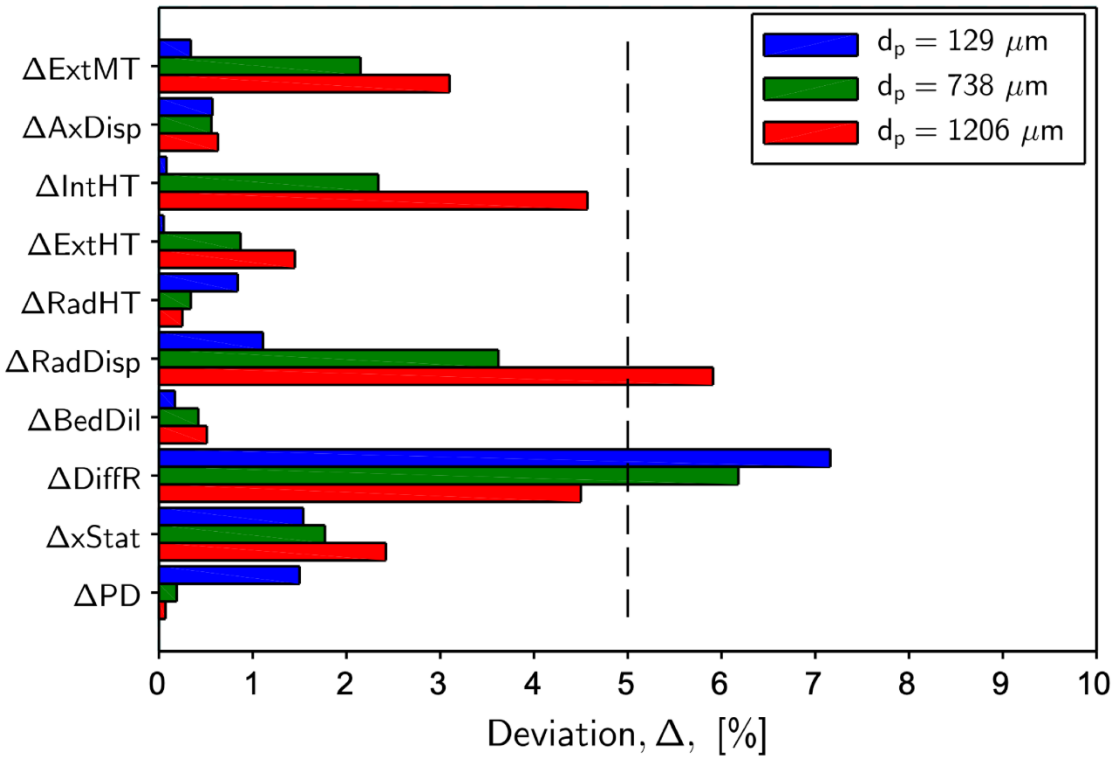

Figure 23 – Evaluation of performance criteria for a performance test of the WGS reaction over the UMW catalyst at 325 °C and TOS ≤ 48 h

Results of the evaluation of the various criteria suggests that very little influence (<5%) on the observed rate is expected from external mass and heat transfer, internal heat transfer, axial dispersion, radial heat transfer, bed dilution and pressure drop for all three catalyst size fractions. Precision in the measured CO conversion was good, as indicated by a low standard deviation of the mean conversion (Δ xStat).

Excluding internal mass transfer, only three instances of calculations of deviation values yielded values above the targeted 5%, namely radial dispersion for the large particle size fraction and the deviation from a differential rate for the small- and mid-sized particle size fractions. Although these criteria are transgressed at a 5% level, the influence of their effects on the observed rate measurements are expected to be small, being only slightly above this arbitrarily chosen limit. Hence, the only potentially

limiting effect on the measurements reported in section 6.2.5 are assumed to be from internal mass transfer limitations.

With this conclusion along with the observation that mass transfer limitations could be neglected for the smallest particle size fraction tested in section 6.2.5, the activation energy calculated in section 6.2.7 is taken to be representative of the intrinsic behaviour of the catalyst.

Evaluation of criteria for measurements taken at 300 °C and 275 °C produced similar results, however ΔDiffR was below 5% for all particle sizes (at both temperatures). The values of ΔRadDisp, being a function of tube and particle sizes only, is the same as shown for 325 °C. The results of performance criteria evaluations for all temperatures are given in appendix H.

7 Comparison of experimental and model effective diffusivities and internal mass transfer effectiveness factors

As previously noted, the results of measurements of the catalytic WGS reaction rate given in section 6.2.5 show a clear decrease in the observed rate with increasing particle size. This is an indication that internal mass transfer limitations were experienced for at least some catalyst samples. Theoretical analysis of the experimental data suggests that the smallest size fraction of catalyst particles did not experience internal mass transfer limitations in the temperature range of 275-325 °C. Support for this observation is discussed further in section 7.2.

These observed rate data were evaluated in section 6.2.8 in terms of various expressions for the estimation of the influence of the various transport effects, reviewed in section 2.2, and the additional expressions developed in section 4. This indicated that, theoretically, influences from the various confounding effects, other than internal mass transfer limitations, could be neglected.

Rate measurements from the catalyst sample with the smallest mean particle size were assumed to be, experimentally, free of transport limitations and representative of intrinsic, differential reaction rates. Subsequently, experimental effectiveness factors of the catalyst samples having larger mean particle sizes could be calculated directly by the ratio of the observed rate of the larger particles to that of the smallest particles (Satterfield, 1970).

As with other transport effects, the effect of internal mass transfer on the observed rates were estimated theoretically for all three particle size fractions using the observed rate data. Here, a comparison between experimental and model effectiveness factors is given. Effective diffusivities were calculated by using the different models given in section 2.3.1.3 and, subsequently effectiveness factors (for first-order reaction in a spherical catalyst particle) were estimated using equation 9.

7.1 Effective diffusivities

The predictive effective diffusivity models include the single pore (SP) model (equation 32), the parallel-path pore (PPP) model (equation 34) and the random pore (RP) model (equation 35). For the use of the latter two models, pore size distribution data from both MIP and BJH analysis was considered.

These predictive models are also compared to the case where diffusion is assumed to occur via molecular diffusion, regardless of pore size (no Knudsen effect), through the tortuous, porous structure. In this case the effective diffusivity is given by $(\varepsilon_p/\tau_p)D_{CO,m}$ (where τ_p is estimated with equation 31 and ε_p taken from table 1). This corresponds to a catalyst particle having enough macro-porosity throughout to negate the restrictive effect of Knudsen diffusion.

The effective diffusivity could also be estimated independently from the experimental effectiveness factors (given in section 7.2) by fitting this data to equation 9. The various effective diffusivities are given in table 12.

Table 12 – Comparison of experimental and model CO effective diffusivities

Diffusivity model	Effective diffusivity, $D_{CO,e}$, [mm^2/s]		
	275 °C	300 °C	325 °C
SP (BET)	0.15	0.15	0.16
SP (MIP)	0.31	0.32	0.32
PPP (BJH)	0.19	0.20	0.20
PPP (MIP)	0.99	1.0	1.1
RP (MIP)	0.56	0.58	0.60
$(\varepsilon_p/\tau_p)D_{CO,m}$	16	17	19
Experimental/regression	3.9	2.6	3.4

Comparison of the experimental diffusivities to the values given by $(\varepsilon_p/\tau_p)D_{CO,m}$ indicates that the diffusive flux in the catalyst particle is restricted, in part, by Knudsen diffusion in narrow pores.

However, all predictive models (PPP, RP and SP) underestimated the effective diffusivity in the UMW catalyst when using either MIP or physisorption based pore size distributions. Predictions fell within factors of about 3 to 20 below the experimental values. The SP model greatly underestimated diffusivities regardless of the average pore size being measured by BET or MIP. The PPP model with BJH data produced similar predictions. Values produced by the RP model with MIP data fell within a factor of about 6 to the experimental values. No calculation was attempted with the RP model with BJH data since the macro-porosity could not be quantified with N_2 physisorption. The use of the PPP model with MIP pore size data produced the most accurate diffusivities at about a third of the experimental values. This corresponds well with what is noted by Satterfield (1970).

It should be noted that, except for the RP model, these model predictions depend on the tortuosity factor, which is expected to fall in the range of about 1-10 Satterfield (1970). Here it is estimated with equation 31 for particle agglomerates, which yields a tortuosity factor of 1.9. Direct measurement of the tortuosity is complex and not typically done in catalyst activity studies; a situation which does introduce uncertainty in the evaluation of potential internal mass transfer limitations. The tortuosity can also be inferred from the measured effective diffusivity and the PPP model. In this case, would lead to a tortuosity factor below 1. This not physically possible and suggests that the prediction using the model combinations leads to description of diffusion in the complex porous system which is limited in accuracy.

The models used to predict the effective diffusivities make several simplifying assumptions which limits the accuracy of prediction. The simplest, SP, model is characterised by a single, effective pore size. Such a value is not easily estimated and leaves much of the complexity of porous materials unaddressed. The structure, connectivity and spatial distribution of pores of different sizes are considered in broad terms by the PPP and RP models. Here these models are found to yield more accurate predictions, however, the method of simplification of porous materials yields varying results, as indicated by the differences in their predictions for the same systems. Moreover, the methods of characterisation of pore size distributions by MIP and BJH/physisorption analysis are known to be prone to inaccuracies as discussed in

section 6.1.3. The lack of characterisation of the macro-porosity by the N_2 physisorption/BJH method is found here to have a large impact on the accuracy (under estimation) of the effective diffusivity.

7.2 Effectiveness factors

Strong indications have been found that the smallest size fraction of catalyst particles did not experience internal mass transfer limitations in the temperature range of 275-325 °C.

Predicted effectiveness factors for reaction at 325 °C for the small catalyst particles ranged from 0.86 to 0.98. This suggests that the effective diffusivity would have to be very low (<0.15 mm^2/s), occurring well within the Knudsen regime, for the system to experience significant internal diffusion limitations for the smallest catalyst particles. This is unlikely to be the case since we know from the MIP analysis (shown in figure 16) that a significant portion of the pore volume are of pores large enough to facilitate local effective diffusivities on the order of 1 mm^2/s, as well as some pore volume of larger pores still.

The trend of the relatively small decrease in the observed activity with increasing particle size is characteristic of a larger effective diffusivity than what is suggested by the model predictions (see figure 24 and appendix I). The Arrhenius plot (figure 22) does not deviate significantly from linearity. This indicates that measurements were made in the same regime. The measured activation energy was also shown to be well within the range of what was measured by others (Azzam et al., 2008, Brown, 2018, Radhakrishnan et al., 2006), for similar catalysts, who claim to have eliminated intra-particle diffusion limitations.

Thus, negligible internal mass transfer limitations were assumed for the smallest size fraction of catalyst particles. This assumption suggests that catalyst particles of this size will only fail the internal mass transfer criterion (at a 5% level) when the observed rate is more than 7 times greater (7 x 25 $\mu mol/s.g_{cat}$), given the same experimental diffusivity (3.4 mm^2/s), or similarly when the diffusivity is one seventh given the same observed rate.

The trend of the accuracies of the predictions of effectiveness factors follows that of the effective diffusivities. It should be noted however that the accuracies of predictions are not equal since the effectiveness factor is non-linear in the effective diffusivity and the particle size. Here, the results at 325 °C are given and discussed since internal mass transfer limitations are the most pronounced at this higher temperature. The observed trends, however, are the same at lower temperatures. Results at all temperatures are tabulated and graphed in appendix I.

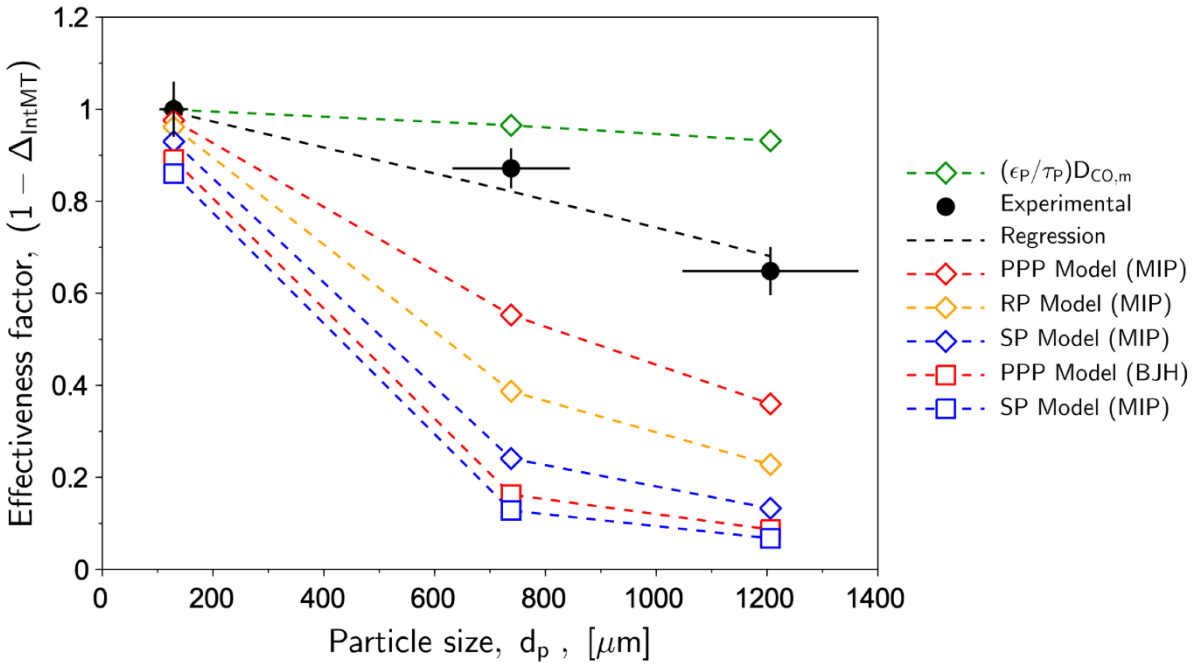

Figure 24 – Comparison of experimental and model effectiveness factors for the WGS reaction over the UMW catalyst at 325 °C and TOS ≤ 48 h. Error bars indicate one standard deviation (per side).

The accuracy of predicted effectiveness factors is much lower for the larger catalyst particles. Here the effectiveness factor is much more sensitive to the effective diffusivity. However, there are several sources of uncertainty, besides those associated with the effective diffusivity models and pore size distributions, which influence the accuracy of prediction of the effectiveness factor. Among these are the assumptions made about the catalyst particle size and shape.

The sensitivity of the effectiveness factor to the particle size was found to be small compared to the uncertainty of the measured particle sizes. This was also found to be

true considering the differences in interpretation of particle sizes from micrographs (equivalent circle diameter of the projected area vs. minimum Feret diameter).

The effect of catalyst particle shape on the effectiveness factor is reviewed by Satterfield (1970). It is noted by Satterfield (1970) that the shape of the particle can have a significant influence at intermediate values of $\eta_{int}\varphi^2$ and that the spherical geometry yields the most conservative predictions for a given characteristic length, which is given by the particle volume to exterior surface area. As noted in section 6.1.3, analysis of particle size and shape for ground and sieved UMW catalyst particles showed that particle shapes were highly irregular and that particle dimensions could exceed aperture sizes of sieves that they fell through. This is not likely to be an uncommon situation in laboratories. This makes measurement of the exterior particle surface area complex.

8 Conclusions

Various authors have provided useful, general guidelines and discussions on the measurement of catalyst performance, including subjects such as experiment design, selection of test equipment, process conditions and transport limitations. However, the quantitative requirements of some aspects of catalyst testing seemed to remain unclear. This is addressed, in part, in section 4. In this section an upper limit is derived for the chemical conversion in a first-order reaction such that differential rate conditions are established (4.1), a lower limit on the chemical conversion is applied to limit the loss of precision in conversion measurements (4.2) and an expression is derived to limit the effect of pressure drop across a catalyst bed on the observed rate of a first-order reaction (4.3).

The derived criteria, along with various criteria for the absence of transport limitations (reviewed in section 2.2) were investigated, by application to a theoretical reaction system. Herein was gauged, their sensitivities to commonly controlled experimental parameters and their overall prevalence when these experimental parameters were varied factorially within practical limits in a laboratory scale experiment. The WGS reaction over $Cu/ZnO/Al_2O_3$ was chosen for this purpose for its moderate properties in various aspects and its prevalence in industry and literature.

The upper limit for conversion (of CO in this case) was found to be particularly severe within the parameter limits. Internal mass transfer and radial heat transfer limitations were also prevalent, occurring in about 25% of the factorial combinations of the experimental parameters. This value was about 15% for the axial dispersion, pressure drop and lower conversion limit criteria with the remaining criteria failing in less than 5% of the factorial combinations.

The analysis of the sensitivity of criteria to experimental parameters provided insights in terms of the control of the different criteria and interactions that should be considered in selecting values for experimental parameters. It was found that optimum values could be found for most of these parameters, within the factorial system, such that the overall success rate (where all criteria are met) is maximised. Notably, the optima for the catalyst particle size was ~400 μm, the dilution fraction was ~0.8, the catalyst mass was ~0.3 g and the tube inner diameter was ~10 mm. It should be noted that these values are specific to the limits imposed on the experimental parameters and the reaction system.

Application of the various criteria was demonstrated in an experimental test of activity, selectivity and short-term stability of a novel medium-temperature WGS catalyst developed in-house. More importantly, this experiment served to measure experimental effectiveness factors for catalyst samples with different mean particle sizes. Evaluation of criteria required characterisation of the catalyst pore size distribution, particle size distribution and bed and particle densities.

Evaluation of the observed rate data in terms of the set of criteria indicated that, theoretically, only a very small influence on the observed rate was expected from any of the considered confounding effects other than internal mass transfer limitations. Results also indicated that internal mass transfer limitations could be neglected only for the catalyst sample having the smallest mean particle size. This agreed with observations of the trend of the observed rate with catalyst particle size.

Analysis of product compositions, by gas chromatography, of the catalyst sample with the smallest mean particle size showed near complete selectivity towards the WGS reaction. A decrease of catalyst activity of ~15% was observed over 144 h on stream

at 325 °C. It should be noted that the operating temperature was cycled between 275 °C, 300 ° and 325 °C during this time. Activities at 325 °C were found to be comparable to other MT-WGS catalysts reported elsewhere on a total catalyst mass basis. However, no comparison is made in terms of turn-over frequency since the formulation of the catalyst of interest in this study is proprietary.

Effective diffusivities could be estimated from the experimentally measured effectiveness factors by regression of the diffusion model for a first-order reaction in a spherical particle. Effective diffusivities were also predicted by the 'random pore', 'parallel-path pore' and 'single pore' models using both N_2 physisorption and MIP data. These models all underestimated the effective diffusivities by factors of about 3 to 20. The most accurate model was found to be by the parallel-path pore model when MIP data was used. When pore size distributions from BJH analysis of physisorption data was used, predictions were off by a factor of 16 or more regardless of the model used. It is noted that various simplifications in these models of the generally exceedingly complex reality of porous materials contribute to the error in predictions.

As expected, the accuracy of predicted effectiveness factors followed the trend of the accuracies of predictions of effective diffusivities. Here, additional sources of error contribute to the uncertainty in predictions. Among the factors are the uncertainty and distribution of the catalyst particle sizes, the effect of the irregular particle shapes and the uncertainty in the pore size distributions. Nonetheless and due to the non-linear and asymptotic nature of the diffusion model, relative accuracies of predictions of effectiveness factors were higher than those of the effective diffusivities.

9 Recommendations

- The work of Chu & Ng (1989) has been interpreted by others as a criterion for the absence of radial dispersion effects. However, the effect of radial dispersion has yet to be linked back to the effect it has on rate measurements as has been done for other criteria. More recent contributions to this field of study allow for further development of the criterion.
- The evaluation of criteria over factorially varied experimental parameters may be extended to other systems to investigate the prevalence of different transport limitations more broadly. The effect of differences in fixed variables (heat of reaction, activation energy, pore size distribution, etc.) between different reaction systems may hence be gauged.
- In a way similar to the method used in section 5.3, reactor tube diameters may be optimised for testing different types of reaction. For example, reactions with a larger heat of reaction will be expected to shift the optimal reactor tube size to a lower value due to the higher prevalence of radial heat transfer.
- Use of the PPP model with MIP data is recommended over the other methods since this was found to give the most accurate predictions of effective diffusivity. However, when there is doubt about internal mass transfer limitations, these are best characterised experimentally.
- Numerical methods exist for modelling the effectiveness factor of irregular shaped particles, however, these methods are complicated and not necessarily readily applied by most researchers. It is possible to develop an algorithm to calculate an effectiveness factor for an arbitrary 2-dimensional or 3-dimensional particle geometry. This can potentially be made to work with processed micrographs of particles or 3-dimensional representations of particles. Such an algorithm may be compiled into software as a tool for researchers
- Predictions of effectiveness factors were found to be conservative, however, this may not be the case for other transport limitation criteria. The accuracy of predictions thereof must be questioned by researchers and experiments must be performed outside of the uncertainty of their predictions.

References

Allen, K., Von Backström, T. & Kröger, D. 2013. Packed bed pressure drop dependence on particle shape, size distribution, packing arrangement and roughness. *Powder technology.* 246:590-600.

Azzam, K., Babich, I., Seshan, K. & Lefferts, L. 2008. Role of Re in Pt–Re/TiO2 catalyst for water gas shift reaction: A mechanistic and kinetic study. *Applied catalysis B: environmental.* 80(1-2):129-140.

Berger, R. 2012. EUROKIN spreadsheet on requirements for measurement of intrinsic kinetics in the gas-solid fixed-bed reactor.

Berger, R., Pérez-Ramírez, J., Kapteijn, F. & Moulijn, J.A. 2002. Catalyst performance testing: bed dilution revisited. *Chemical Engineering Science.* 57(22):4921-4932.

Bird, R.B., Stewart, W.E. & Lightfoot, E.N. 2002. *Transport phenomena.* 2nd. John Wiley & Sons, Inc. .

Brown, D.E. 2018. Kinetic models for the Pt/CeO_2 catalysed water-gas shift reaction. University of Cape Town.

Buczek, B. 1991. Measurement of the apparent density of porous particles by a powder characteristics tester. *Advanced Powder Technology.* 2(4):315-319.

Buczek, B. & Geldart, D. 1986. Determination of the density of porous particles using very fine dense powders. *Powder technology.* 45(2):173-176.

Burghardt, A. & Zaleski, T. 1968. Longitudinal dispersion at small and large Peclet numbers in chemical flow reactors. *Chemical Engineering Science.* 23(6):575-591.

Carson, J.K., Lovatt, S.J., Tanner, D.J. & Cleland, A.C. 2005. Thermal conductivity bounds for isotropic, porous materials. *International Journal of Heat and Mass Transfer.* 48(11):2150-2158.

Choi, Y. & Stenger, H.G. 2003. Water gas shift reaction kinetics and reactor modeling for fuel cell grade hydrogen. *Journal of Power Sources.* 124(2):432-439.

Chu, C. & Ng, K. 1989. Flow in packed tubes with a small tube to particle diameter ratio. *AIChE journal.* 35(1):148-158.

Cybulski, A., Van Dalen, M., Verkerk, J. & Van Den Berg, P. 1975. Gas-particle heat transfer coefficients in packed beds at low Reynolds numbers. *Chemical Engineering Science.* 30(9):1015-1018.

Dautzenberg, F.M. 1989. Ten guidelines for catalyst testing. In *Characterization and catalyst development, an interactive approach.* S.A. Bradley, M.J. Gattuso and R.J. Bertolacini, Eds. United States of America: American Chemical Society. 99-119.

De Lange, M.F., Vlugt, T.J., Gascon, J. & Kapteijn, F. 2014. Adsorptive characterization of porous solids: Error analysis guides the way. *Microporous and Mesoporous Materials.* 200:199-215.

Derouane, E.G. 2002. Challenges and Strategies for the Implementation of Combinatorial Methods and High Throughput Testing in Heterogeneous Catalysis. In *Principles and Methods for Accelerated Catalyst Design and Testing.* E.G. Derouane, V. Parmon, F. Lemos and F.R. Ribeiro, Eds.: Kluwer Academic Publishers. 3-12.

Dumesic, J.A., Huber, G.W. & Boudart, M. 2008. Principles of Heterogeneous Catalysis. *Handbook of heterogeneous catalysis: 8 volumes.* 1:1-15.

Eucken, A. 1913. Über das Wärmeleitvermögen, die spezifische Wärme und die innere Reibung der Gase. *Physik. Z.* 14(8):324-332.

Finlayson, B.A. & Biegler, L.T. 2008. Mathematics. In *Perry's chemical engineers' handbook.* 8th ed. D.W. Green and R.H. Perry, Eds. United States of America: McGraw-Hill.

Flank, W.H. 1989. A Philosophy for Testing. In *Characterization and catalyst development, an interactive approach.* S.A. Bradley, M.J. Gattuso and R.J. Bertolacini, Eds. United States of America: American Chemical Society. 90-98.

Fogler, S.H. 2006. *Elements Of Chemical Reaction Engineering.* 4th. USA: Prentice Hall International.

Froment, G.F., Bischoff, K.B. & DeWilde, J. 2011. *Chemical reactor analysis and design.* 3rd. United States of America: Wiley.

Fuller, E.N., Schettler, P.D. & Giddings, J.C. 1966. New method for prediction of binary gas-phase diffusion coefficients. *Industrial & Engineering Chemistry.* 58(5):18-27.

Gierman, H. 1988. Design of laboratory hydrotreating reactors: scaling down of trickle-flow reactors. *Applied Catalysis.* 43(2):277-286.

Giesche, H. 2006. Mercury porosimetry: a general (practical) overview. *Particle & particle systems characterization.* 23(1):9-19.

Gonzo, E.E. 2002. Estimating correlations for the effective thermal conductivity of granular materials. *Chemical Engineering Journal.* 90(3):299-302.

Gunn, D. 1978. Transfer of heat or mass to particles in fixed and fluidised beds. *International Journal of Heat and Mass Transfer.* 21(4):467-476.

Gunn, D. 1987. Axial and radial dispersion in fixed beds. *Chemical Engineering Science.* 42(2):363-373.

Gunn, D. & De Souza, J. 1974. Heat transfer and axial dispersion in packed beds. *Chemical Engineering Science.* 29(6):1363-1371.

Hottel, H.C., Noble, J.J., Sarofim, A.F., Silcox, G.D., Wankat, P.C. & Knaebel, K., S. 2008. Heat and Mass Transfer. In *Perry's chemical engineers' handbook.* 8th ed. D.W. Green and R.H. Perry, Eds. United States of America: McGraw-Hill.

Hsiung, T.H. & Thodos, G. 1977. Mass-transfer factors from actual driving forces for the flow of gases through packed beds (0.1< Re< 100). *International Journal of Heat and Mass Transfer.* 20(4):331-340.

Johnson, M.F. & Stewart, W.E. 1965. Pore structure and gaseous diffusion in solid catalysts. *Journal of Catalysis.* 4(2):248-252.

Kapteijn, F. & Moulijn, J.A. 2008. Laboratory catalytic reactors: aspects of catalyst testing. In *Handbook of heterogeneous catalysis.* 2 ed. G. Ertl, H. Knözinger, F. Schüth and J. Weitkamp, Eds. Germany: Wiley-VCH Verlag GmbH& Co. KGaA.

Kunii, D. & Suzuki, M. 1967. Particle-to-fluid heat and mass transfer in packed beds of fine particles. *International Journal of Heat and Mass Transfer.* 10(7):845-852.

Mears, D.E. 1971a. Tests for transport limitations in experimental catalytic reactors. *Industrial & Engineering Chemistry Process Design and Development.* 10(4):541-547.

Mears, D.E. 1971b. The role of axial dispersion in trickle-flow laboratory reactors. *Chemical Engineering Science.* 26(9):1361-1366.

Mears, D.E. 1971c. Diagnostic criteria for heat transport limitations in fixed bed reactors. *Journal of Catalysis.* 20(2):127-131.

Moulijn, J., Tarfaoui, A. & Kapteijn, F. 1991. General aspects of catalyst testing. *Catalysis Today.* 11(1):1-12.

Nelson, P.A. & Galloway, T.R. 1975. Particle-to-fluid heat and mass transfer in dense systems of fine particles. *Chemical Engineering Science.* 30(1):1-6.

Nilsson, O., Mehling, H., Horn, R., Fricke, J., Hofmann, R., Müller, S.G., Eckstein, R. & Hofmann, D. 1997. Determination of the thermal diffusivity and conductivity of monocrystalline silicon carbide (300-2300 K). *High Temperatures. High Pressures.* 29(1):73-79.

Petersen, E.E. 1965. *Chemical reaction analysis.* Prentice Hall.

Petrov, L. 2002. Problems and challenges about accelerated testing of the catalytic activity of catalysts. In *Principles and Methods for Accelerated Catalyst Design and Testing.* Kluwer Academic Publishers. 13-69.

Petrovic, L.J. & Thodos, G. 1968. Mass transfer in flow of gases through packed beds. Low Reynolds number region. *Industrial & Engineering Chemistry Fundamentals.* 7(2):274-280.

Poling, B.E., Thomson, G.H., Friend, D.G., Rowley, R.L. & Wilding, W.V. 2008. Physical and Chemical Data. In *Perry's Chemical Engineers' Handbook.* 8th ed. D.W. Green and R.H. Perry, Eds. United States of America: McGraw-Hill.

Punčochář, M. & Drahoš, J. 1993. The tortuosity concept in fixed and fluidized bed *Chemical Engineering Science.* 48(11):2173-2175.

Radhakrishnan, R., Willigan, R., Dardas, Z. & Vanderspurt, T. 2006. Water gas shift activity and kinetics of Pt/Re catalysts supported on ceria-zirconia oxides. *Applied catalysis B: environmental.* 66(1):23-28.

Rootare, H.M. & Prenzlow, C.F. 1967. Surface areas from mercury porosimeter measurements. *The Journal of physical chemistry.* 71(8):2733-2736.

Satterfield, C.N. 1970. *Mass transfer in heterogeneous catalysis.* The MIT Press.

Smith, D.S., Alzina, A., Bourret, J., Nait-Ali, B., Pennec, F., Tessier-Doyen, N., Otsu, K., Matsubara, H. et al. 2013. Thermal conductivity of porous materials. *Journal of Materials Research.* 28(17):2260-2272.

Specchia, V., Baldi, G. & Sicardi, S. 1980. Heat transfer in packed bed reactors with one phase flow. *Chemical Engineering Communications.* 4(1-3):361-380.

Thommes, M., Kaneko, K., Neimark, A.V., Olivier, J.P., Rodriguez-Reinoso, F., Rouquerol, J. & Sing, K.S. 2015. Physisorption of gases, with special reference to

the evaluation of surface area and pore size distribution (IUPAC Technical Report). *Pure and Applied Chemistry.* 87(9-10):1051-1069.

Van Antwerpen, W., Du Toit, C. & Rousseau, P. 2010. A review of correlations to model the packing structure and effective thermal conductivity in packed beds of mono-sized spherical particles. *Nuclear Engineering and design.* 240(7):1803-1818.

Wakao, N. & Smith, J. 1962. Diffusion in catalyst pellets. *Chemical Engineering Science.* 17(11):825-834.

Wakao, N. & Funazkri, T. 1978. Effect of fluid dispersion coefficients on particle-to-fluid mass transfer coefficients in packed beds: correlation of Sherwood numbers. *Chemical Engineering Science.* 33(10):1375-1384.

Wakao, N. & Kaguei, S. 1982. *Heat and mass transfer in packed beds.* Taylor & Francis.

Wakao, N., Kaguei, S. & Nagai, H. 1978. Effective diffusion coefficients for fluid species reacting with first order kinetics in packed bed reactors and discussion on evaluation of catalyst effectiveness factors. *Chemical Engineering Science.* 33(2):183-187.

Wakao, N., Kaguei, S. & Funazkri, T. 1979. Effect of fluid dispersion coefficients on particle-to-fluid heat transfer coefficients in packed beds: correlation of Nusselt numbers. *Chemical Engineering Science.* 34(3):325-336.

Webb, P.A. 2001. An introduction to the physical characterization of materials by mercury intrusion porosimetry with emphasis on reduction and presentation of experimental data. *Micromeritics Instrument Corp, Norcross, Georgia.*

Wehinger, G.D., Eppinger, T. & Kraume, M. 2014. Fluidic effects on kinetic parameter estimation in lab-scale catalysis testing–A critical evaluation based on computational fluid dynamics. *Chemical Engineering Science.* 111:220-230.

Weitkamp, J. & Gläser, R. 2008. Ancillary Techniques in Laboratory Units for Testing Solid Catalysts. In *Handbook of heterogeneous catalysis.* 2 ed. G. Ertl, H. Knözinger, F. Schüth and J. Weitkamp, Eds. Germany: Wiley-VCH Verlag GmbH& Co. KGaA.

Welty, J.R., Wicks, C.E., Rorrer, G. & Wilson, R.E. 2009. *Fundamentals of momentum, heat, and mass transfer.* John Wiley & Sons.

Wilke, C. 1950. A viscosity equation for gas mixtures. *The journal of chemical physics.* 18(4):517-519.

Appendix A: Approximations of kinetic equations by first-order kinetics

Here are shown first-order approximations of the empirically fitted power-law kinetic expressions given by Brown (2018) and Choi & Stenger (2003). Reaction rates were calculated from the power-law expressions and the first-order rate form (equation 2A) in terms of the CO partial pressure was fitted thereto. First-order approximations were well within 5% of the values given by the original expressions.

$$\Re(P_{CO}, T) = kP_{CO} \tag{1A}$$

$$\Re(C_A, T) = kP_{tot}y_{CO}^0(1 - X_{CO}) \tag{2A}$$

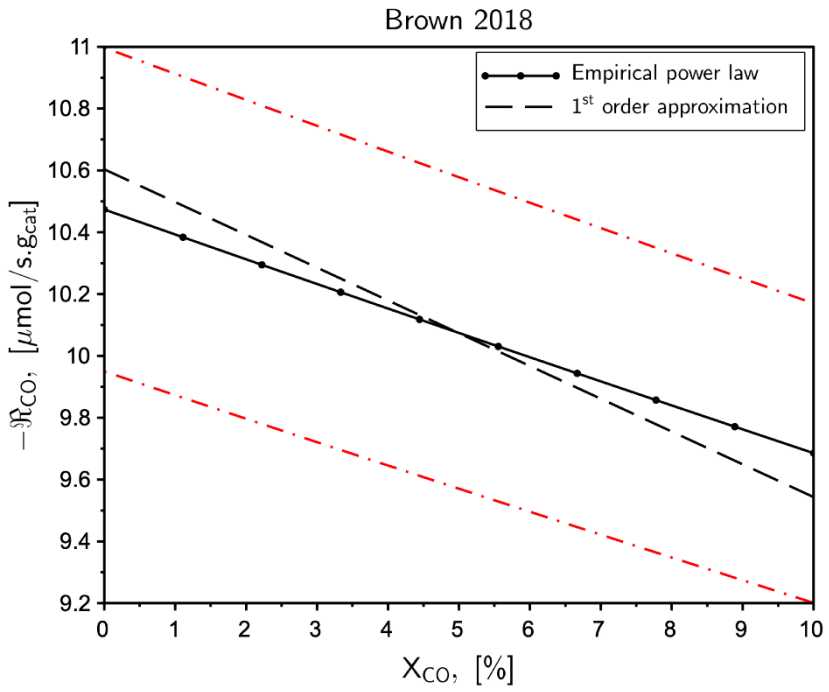

Figure 2A - First-order approximation of power-law kinetics from Brown (2018) at 325 °C, 1 atm total pressure, dry feed composition of 10% CO, 10% CO_2, 70% H_2, 10% N_2, steam-to-dry gas ratio of 0.5.

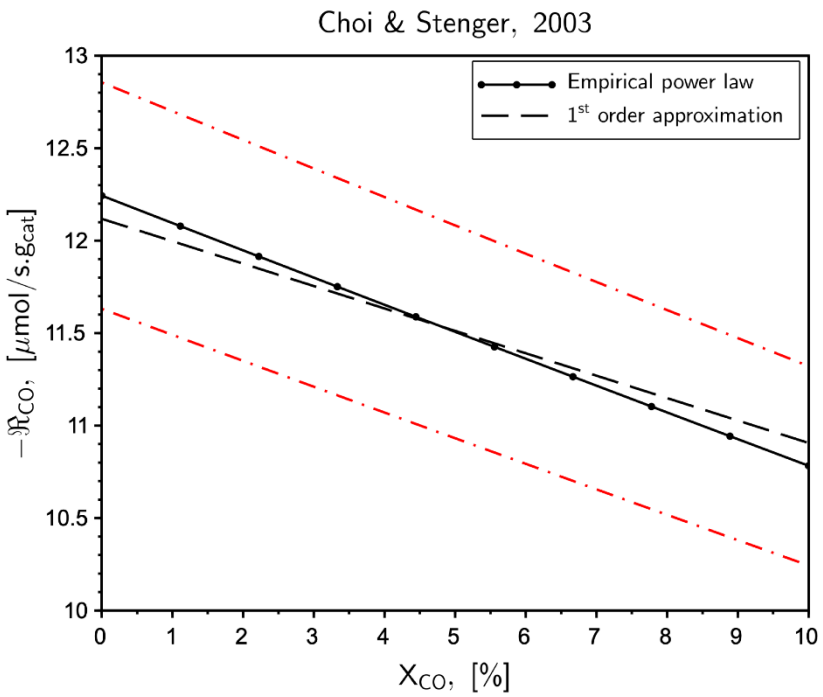

Figure 3A - First-order approximation of power-law kinetics from Choi & Stenger (2003) at 200 °C, 1 atm total pressure, dry feed composition of 10% CO, 10% CO_2, 70% H_2, 10% N_2, steam-to-dry gas ratio of 0.5.

Appendix B: Derivation of a criterion for differential reaction conditions.

As noted in section 4.1 we want to limit the observed (integral) reaction rate across a catalyst bed to within 5% of the reaction rate at the reactor inlet conditions:

$$\left|1 - \frac{\Re_{i,obs}{}'}{\Re_i{}'(C_0, T_0)}\right| < 0.05 \qquad (1B)$$

For the criterion to be useful it must be expressed in terms of experimentally observable quantities. It is clear that differential conditions will be approached at low conversions, however, a quantitative description for this is needed. Here will be shown that for a simple system, neglecting other phenomena, the criterion (equation 1B) can be expressed in terms of the chemical conversion.

The conversion is defined here in terms of an arbitrary chemical species A:

$$X_A = 1 - \frac{F_A}{F_{A,0}} \tag{2B}$$

The observed reaction rate $\Re_{i,obs}{}'$ is given by:

$$\Re_{i,obs}{}' = \frac{X_A F_{A,0}}{W} \tag{3B}$$

First-order kinetics in species A is assumed:

$$\Re'(C_A, T) = k' P_A \tag{4B}$$

Under plug-flow conditions:

$$\frac{dX_A}{dW} = \frac{\Re'}{F_{A,0}} \tag{5B}$$

Introducing the reaction rate relative to inlet conditions:

$$\frac{\Re'}{\Re_i{}'(C_0, T_0)} = \frac{P_A}{P_{A,0}} \tag{6B}$$

Using the ideal-gas law, the conversion definition and reaction stoichiometry (see Fogler (2006) pg.110) :

$$\frac{\Re'}{\Re_i{}'(C_0, T_0)} = \left(\frac{F_A(X_A)}{F_{A,0}}\right) \Big/ \left(\frac{\dot{V}(x_A)}{\dot{V}_0}\right) = \frac{1 - X_A}{1 + \xi X_A} \tag{7B}$$

With $$\xi = y_{A,0}\delta$$

$$\delta = Increase\ in\ number\ of\ \ moles\ per\ mole\ A\ reacted$$

Inserting this result into equation 5B:

$$\frac{dX_A}{dW} = \frac{\Re_i{}'(C_0, T_0)}{F_{A,0}} \frac{(1 - X_A)}{(1 + \xi X_A)} \tag{8B}$$

We now integrate to express $\Re_0{}'$ in terms of observable quantities:

$$\frac{W\Re_i{}'(C_0,T_0)}{F_{A,0}} = \int_0^{X_A} \frac{(1-X_A)}{(1+\xi X_A)}\,dx = -\xi X_A - (\xi+1)\ln(1-X_A) \qquad (9B)$$

Combining equations 1B, 3B and 9B expresses the criterion in terms of conversion:

$$\left|1 + \frac{X_A}{\xi X_A + (\xi+1)ln(1-X_A)}\right| < 0.05 \qquad (10B)$$

Appendix C: Derivation of a criterion for the absence of pressure drop effects on reaction rate.

As noted in section 4.3 a criterion to restrict the integral reaction rate across a catalytic flow reactor to within 5% of the reaction rate evaluated at reactor inlet conditions can be stated as:

$$\left|1 - \frac{\Re_{i,obs}{}'}{\Re_i{}'(z=L_{bed})}\right| < 0.05 \qquad (1C)$$

The observed/overall rate, $\Re_{i,obs}{}'$, can be calculated by averaging over the bed:

$$\Re_{i,obs}{}' = \frac{1}{L_{bed}}\int_0^{L_{bed}} \Re_i'(z)\,dz \qquad (2C)$$

The local reaction rate is a function of temperature, the total pressure and the partial pressures of chemical species:

$$\Re_i{}'(P_i,T) = k'(T).f(P_i,T) \qquad (3C)$$

$$P_i = y_i P_T \qquad (4C)$$

A first-order reaction in species A can thus be written:

$$\Re_i{}'(P_i,T) = k' y_A P_T \qquad (5C)$$

The total pressure decreases along the flow direction of the reactor. The pressure drop is commonly given by the equation:

$$\Delta P = P_{T,0} - P_{T,out} = \alpha_P L_{bed} = \left(\frac{f_b \rho_g \bar{u}^2}{d_p}\right) L_{bed} \tag{6C}$$

The friction factor, f_b, is usually correlated in terms of the Ergun Reynolds number:

$$Re_{Erg} = \frac{\rho_g \bar{u} d_p}{\mu_g (1 - e_{bed})} \tag{7C}$$

Correlations of the friction factor have been given by various authors. A recent review of previous correlations can be found in Allen, Von Backström & Kröger (2013).

Under reaction conditions the value of α_P in equation 6C changes depending on the extent of change in superficial flow velocity and the changing physical conditions in the reactor. However, the change can be expected to be negligible when the reactor is isothermal, the level of conversion is low (limiting the change in the superficial velocity) and the pressure drop is relatively small (limiting the change in gas density). In such a case, the coefficient, α_P, is assumed to stay constant and thus, the total pressure, P_{tot}, is assumed to decrease linearly in the axial direction (z) of the reactor:

$$P_{tot} = P_{T,0} - \alpha_P z \tag{8C}$$

Combining equations 2C, 5C and 8C we have:

$$\Re_{i,obs}{}' = \frac{1}{L_{bed}} \int_0^{L_{bed}} k' y_A \left(P_{T,0} - \alpha_P z\right) dz \tag{9C}$$

Under low conversions there is little change in the key species' mole fraction (y_A). Evaluating the integral in equation 9C and combining the result with equations 1C, 5C and 6C produces a usable criterion:

$$\frac{\Delta P_T}{2P_{T,0}} < 0.05 \tag{10C}$$

Appendix D: Convergence study for the density of sets of independent variables in factorial studies.

Results of a factorial calculation must be independent of the grid density chosen for the independent variable sets. The convergence in terms of the grid density has been investigated for the LT-WGS factorial system. Since the prevalence of the failure rate of different criteria (as given by equation 61), within the ranges of the independent variables, is of particular interest, convergence in this measure is required. The results of the convergence study are summarised in figure 1D.

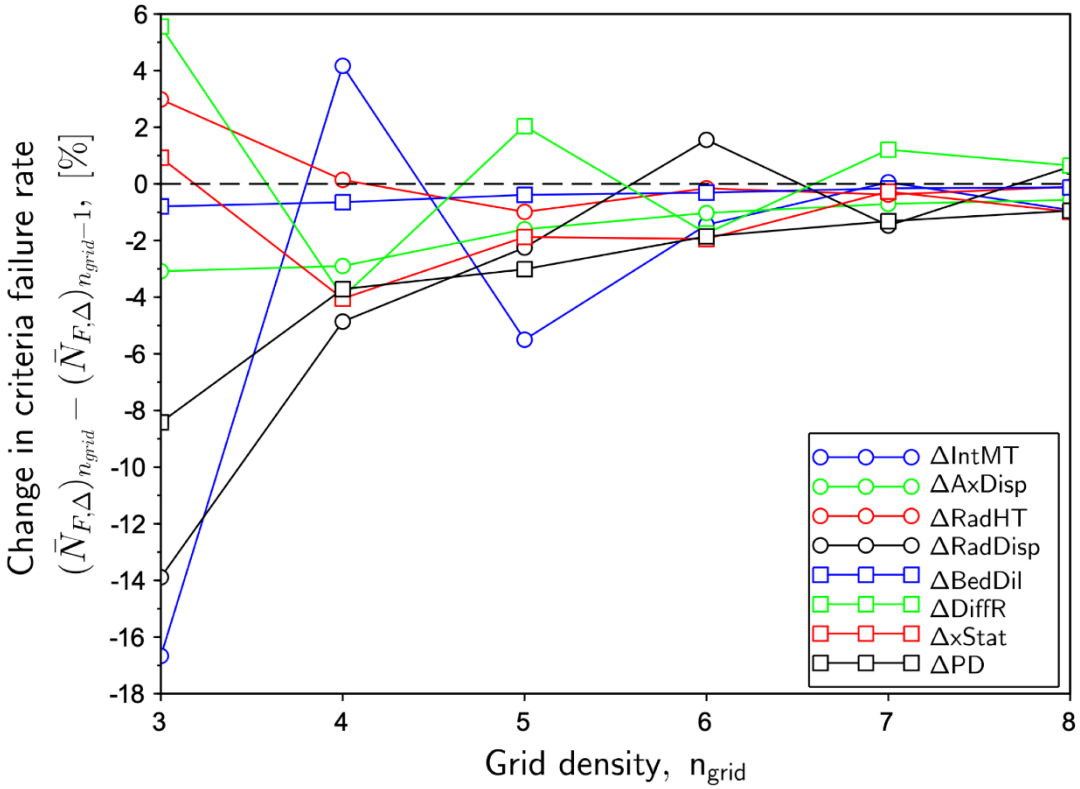

Figure 1D – Convergence of individual criteria rates to the factorial grid density

For clarity, criteria which had zero failure rates regardless of grid density in the factorial system have been omitted. The results suggest that a grid density of 6 is sufficient, given a maximum change in any criteria failure rate of 5%.

Appendix E: GC example chromatogram and calibration factors

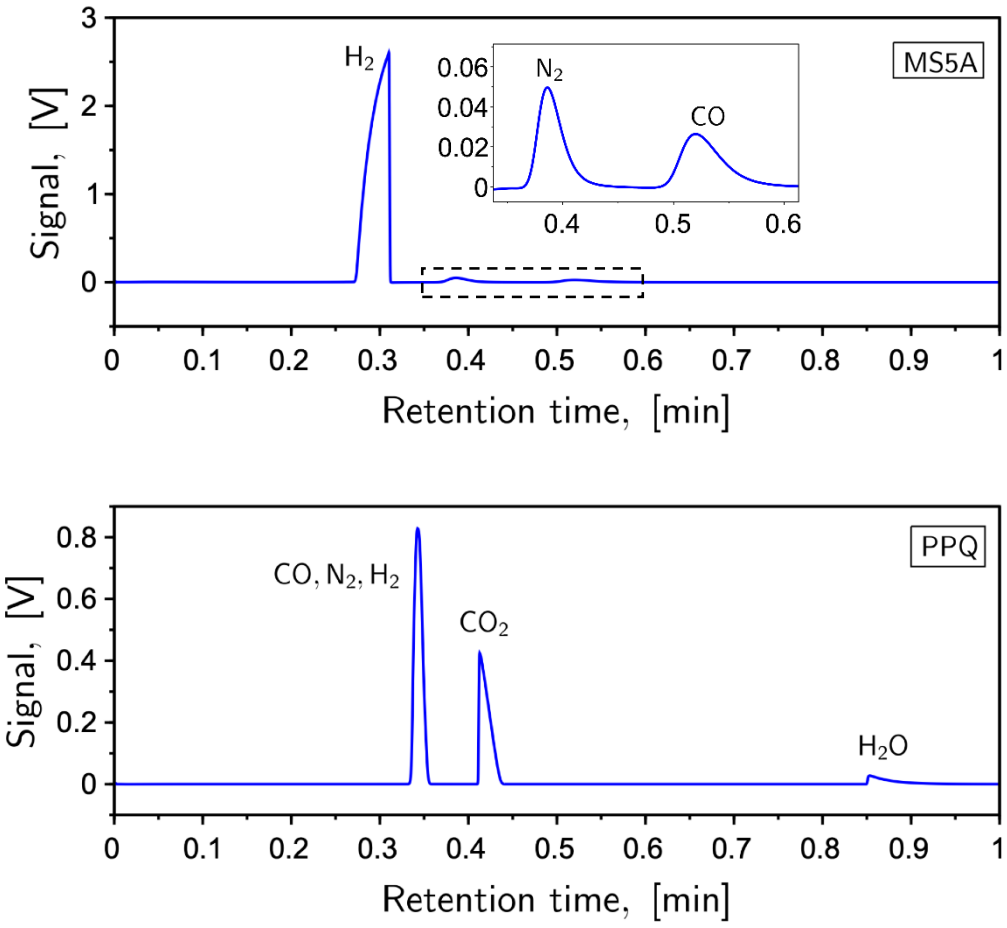

Figure 1E – Typical chromatograms of dry reactor product gas

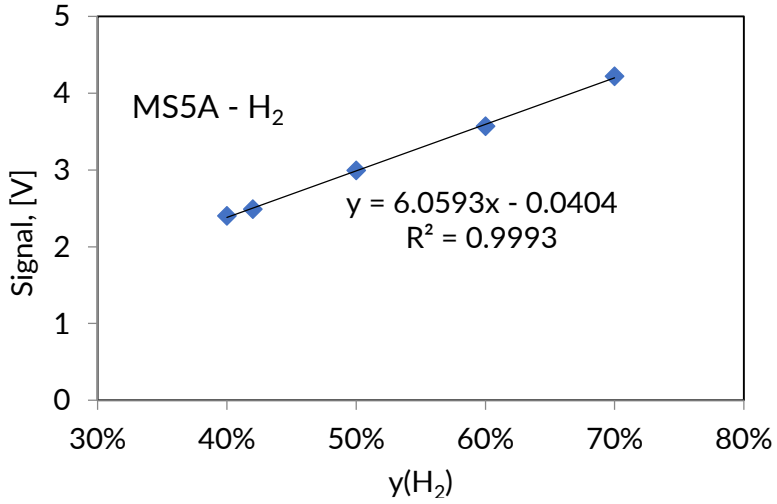

Figure 2E – Calibration of GC MS5A column response to H_2

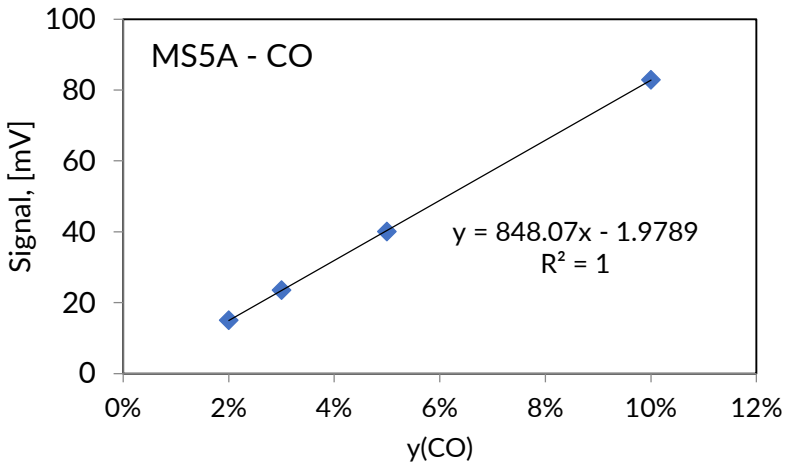

Figure 3E - Calibration of GC MS5A column response to CO

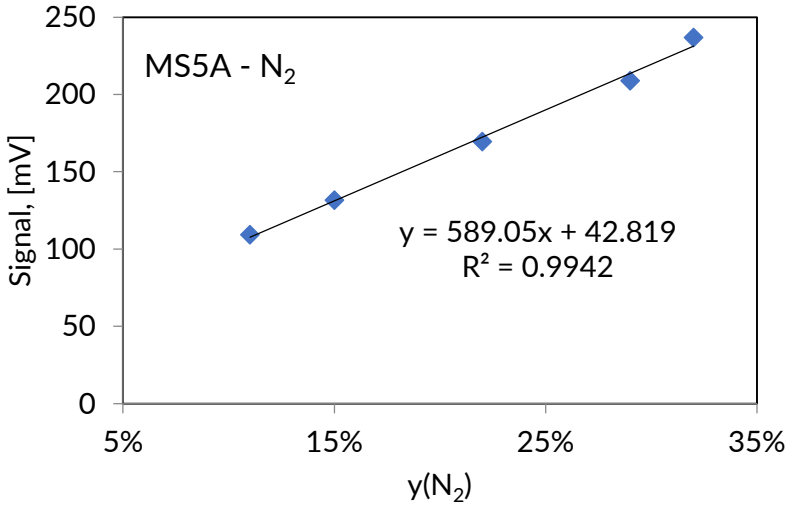

Figure 4E - Calibration of GC MS5A column response to N_2

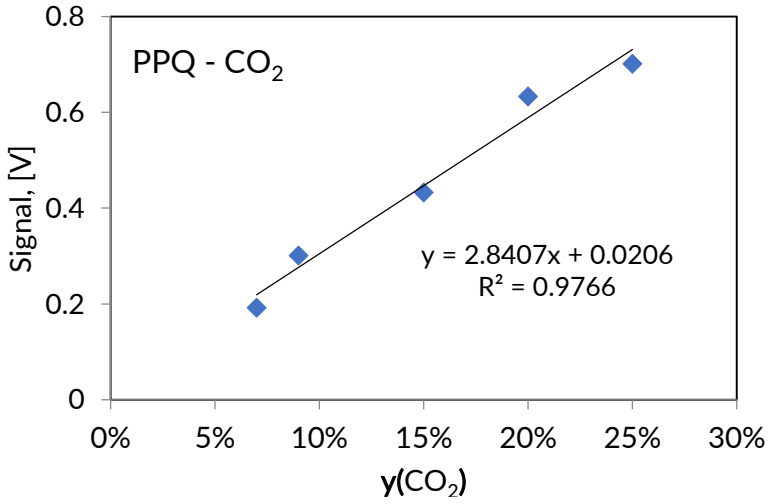

Figure 5E - Calibration of GC PPQ column response to CO_2

Appendix F: Conversion of CO from dry-gas compositions

The conversion of CO is defined as:

$$X_{CO} = 1 - \frac{F_{CO}}{F_{CO}^0} \tag{1F}$$

The flow of CO can be given in terms of the dry-gas composition and flow:

$$X_{CO} = 1 - \frac{y_{CO,D} F_{T,D}}{y_{CO,D}^0 F_{T,D}^0} \tag{2F}$$

The CO content of the dry-gas feed ($y_{CO,D}^0$) and dry reactor product ($y_{CO,D}$) are measured by GC analysis. For a WGS reaction system with complete selectivity, the flow-rate of the dry-gas is given by:

$$F_{T,D} = \sum_{i \neq H_2O} F_i = F_{CO} + F_{CO_2} + F_{H_2} + F_{inert} \tag{3F}$$

The component flow can be given in terms of the CO conversion:

$$F_i = F_i^0 + \upsilon_i X_{CO} F_{CO}^0 \tag{4F}$$

Combination of equations 3F and 4F leads to:

$$F_{T,D} = F_{T,D}^0 + X_{CO} F_{CO}^0 \tag{5F}$$

$$\frac{F_{T,D}}{F_{T,D}^0} = 1 + X_{CO} y_{D,CO}^0 \tag{6F}$$

Combining this result with equation 2F gives the CO conversion in terms of the dry-gas CO compositions only:

$$X_{CO} = \frac{1 - \frac{y_{CO,D}}{y_{D,CO}^0}}{1 + y_{CO,D}} \tag{7F}$$

Appendix G: Observed rate and conversion data

Table 1G - Observed rate and conversion data of UMW catalyst ,at 1 atm total pressure, dry feed composition of 10% CO, 10% CO_2, 70% H_2, 10% N_2, steam-to-dry gas ratio of 0.5 and 4333 SCCM/g_{cat} total feed flow.

n	X_{CO}	$\sigma(X_{CO})$	Observed rate, [μmol/s.g(cat)]	Particle size, $2\sqrt{(A_{proj}/\pi)}$, [μm]	Temperature, [°C]	TOS, [hr]	TOS, [days]
15	6%	0.5%	12.2	129		4	
19	5%	0.4%	10.6	738	275	2	0
16	5%	0.6%	10.2	1206		3	
12	8%	0.2%	17.1	129		26	
13	7%	0.4%	14.4	738	300	28	1
12	5%	0.7%	11.7	1206		25	
13	12%	0.7%	24.9	129		51	
14	10%	0.4%	21.7	738	325	52	2
16	8%	0.6%	16.1	1206		53	
30	6%	0.5%	12.4	129		74	
15	4%	0.6%	9.3	738	275	76	3
12	4%	0.7%	9.6	1206		75	
17	8%	0.4%	16.4	129		98	
12	6%	0.4%	13.5	738	300	99	4
13	5%	0.4%	10.7	1206		97	
28	11%	0.4%	23.3	129		124	
13	10%	0.5%	20.8	738	325	126	5
15	8%	0.4%	16.7	1206		126	
15	5%	0.6%	11.4	129		145	
10	4%	0.5%	8.8	738	275	147	6
11	4%	0.6%	8.0	1206		146	
15	7%	0.6%	15.4	129		169	
11	5%	0.5%	11.8	738	300	170	7
14	5%	0.6%	11.6	1206		169	
23	10%	0.4%	21.1	129		195	
13	9%	0.5%	18.7	738	325	194	8
14	7%	0.5%	15.6	1206		195	

Appendix H: Results of evaluations of performance test criteria

*Table 1H - Evaluation of performance criteria for a performance test of the WGS reaction over the UMW catalyst at **275 °C** and TOS ≤ 48 h*

	Deviation, Δ		
	d_p=129 µm	d_p=738 µm	d_p=1206 µm
ΔExtMT	0.2%	1.0%	2.0%
ΔAxDisp	0.3%	0.3%	0.4%
ΔIntHT	0.1%	1.3%	3.4%
ΔExtHT	0.0%	0.5%	1.1%
ΔRadHT	0.5%	0.2%	0.2%
ΔRadDisp	1.1%	3.6%	5.9%
ΔBedDil	0.1%	0.2%	0.3%
ΔDiffR	3.1%	2.6%	2.6%
ΔXStat	3.3%	3.9%	3.9%
ΔPD	1.2%	0.2%	0.1%

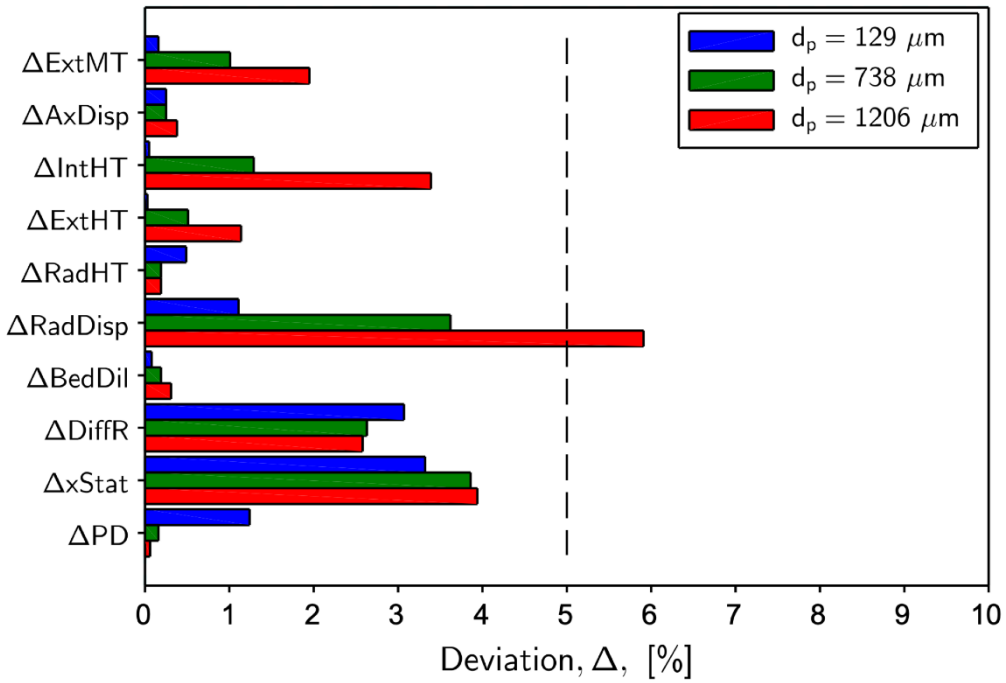

*Figure 1H - Evaluation of performance criteria for a performance test of the WGS reaction over the UMW catalyst at **275 °C** and TOS ≤ 48 h*

*Table 2H - Evaluation of performance criteria for a performance test of the WGS reaction over the UMW catalyst at **300 °C** and TOS ≤ 48 h*

	Deviation, Δ		
	d_p=129 µm	d_p=738 µm	d_p=1206 µm
ΔExtMT	0.2%	1.4%	2.2%
ΔAxDisp	0.4%	0.3%	0.4%
ΔIntHT	0.1%	1.6%	3.5%
ΔExtHT	0.0%	0.6%	1.2%
ΔRadHT	0.6%	0.2%	0.2%
ΔRadDisp	1.1%	3.6%	5.9%
ΔBedDil	0.1%	0.3%	0.4%
ΔDiffR	4.4%	3.7%	3.0%
ΔXStat	2.4%	2.8%	3.4%
ΔPD	1.4%	0.2%	0.1%

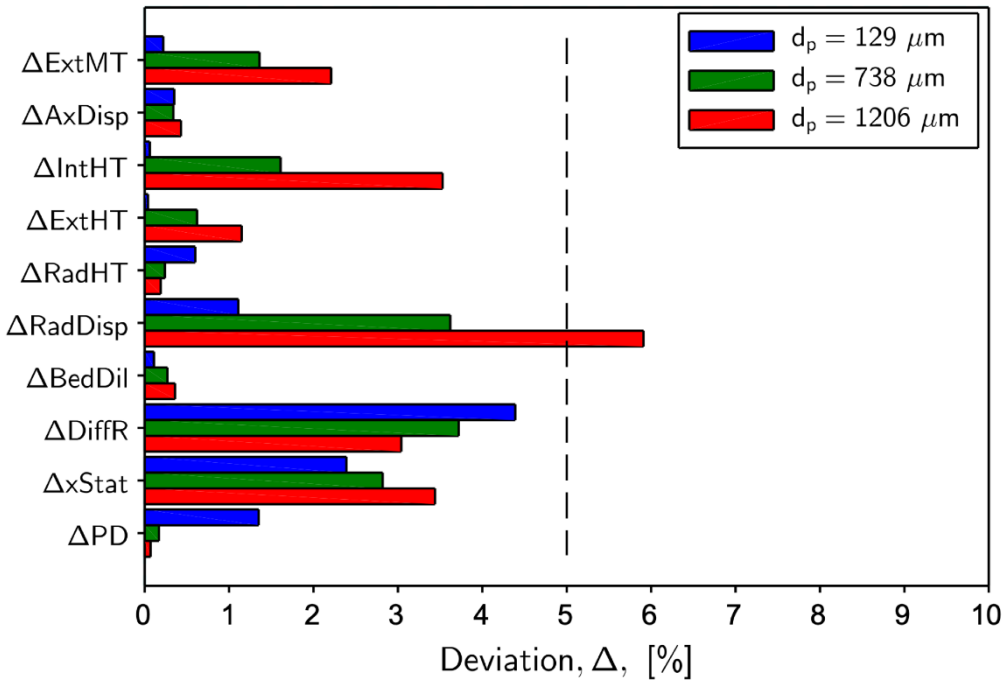

*Figure 2H - Evaluation of performance criteria for a performance test of the WGS reaction over the UMW catalyst at **300 °C** and TOS ≤ 48 h*

*Table 3H - Evaluation of performance criteria for a performance test of the WGS reaction over the UMW catalyst at **325 °C** and TOS ≤ 48 h*

	Deviation, Δ		
	d_p=129 µm	d_p=738 µm	d_p=1206 µm
ΔExtMT	0.3%	2.0%	3.0%
ΔAxDisp	0.5%	0.5%	0.6%
ΔIntHT	0.1%	2.2%	4.4%
ΔExtHT	0.1%	0.8%	1.4%
ΔRadHT	0.8%	0.3%	0.2%
ΔRadDisp	1.1%	3.6%	5.9%
ΔBedDil	0.2%	0.4%	0.5%
ΔDiffR	6.7%	5.9%	4.3%
ΔXStat	1.6%	1.9%	2.5%
ΔPD	1.5%	0.2%	0.1%

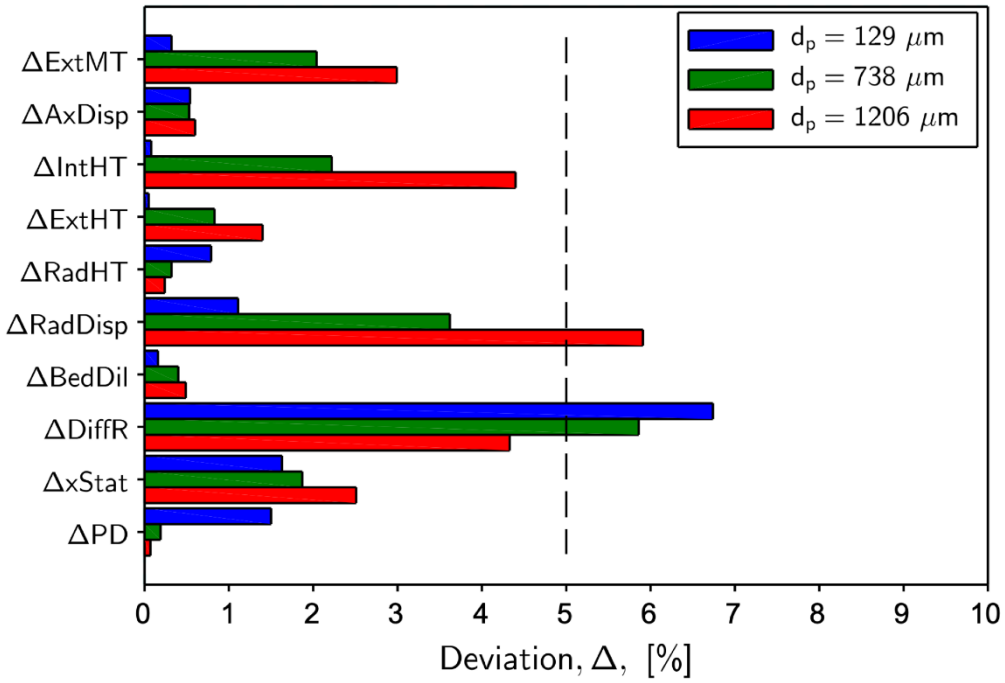

*Figure 3H - Evaluation of performance criteria for a performance test of the WGS reaction over the UMW catalyst at **325 °C** and TOS ≤ 48 h*

Appendix I: Experimental and model effectiveness factors

Model effectiveness factors for the UMW catalyst performance tests are tabulated (table 1I) in order (high to low) of their mean absolute relative residuals (MARR) given by:

$$MARR = \frac{1}{n_p}\sum_{1}^{n_p}\left|\frac{\eta_{i,p}^{exp} - \eta_{i,p}^{pred}}{\eta_{i,p}^{exp}}\right| \qquad (1I)$$

Where n_p is the number of measurements at different particle sizes (3) and $\eta_{i,p}$ refers to the effectiveness factor of the ith particle size.

*Table 1I – Comparison of experimental and model effectiveness factors of the WGS reaction over the UMW catalyst at **275 °C** and TOS ≤ 48 h*

Model	Internal mass transfer effectiveness factor, η_{IntMT}, [%]			MARR
	d_p=129 µm	d_p=738 µm	d_p=1206 µm	
SP(BJH)	93%	25%	11%	55%
PPPM(BJH)	95%	31%	14%	51%
SP(MIP)	97%	43%	21%	43%
RPM	98%	60%	33%	31%
PPPM(MIP)	99%	74%	49%	19%
MD	100%	98%	95%	9%
SP(fitted)	100%	93%	82%	4%
Experiment	100%	86%	84%	-

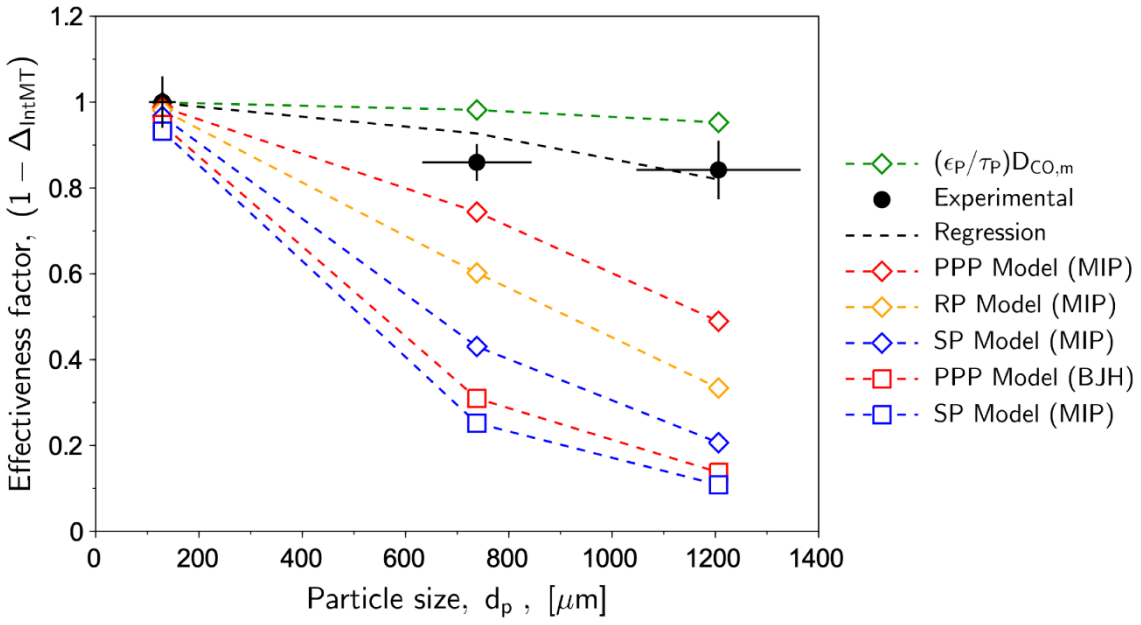

*Figure 1I – Comparison of experimental and model effectiveness factors of the WGS reaction over the UMW catalyst at **275 °C** and TOS ≤ 48 h*

Table 2I – Comparison of experimental and model effectiveness factors of the WGS reaction over the UMW catalyst at **300 °C** and TOS ≤ 48 h

Model	Internal mass transfer effectiveness factor, η_{IntMT}, [%]			MARR
	d_p=129 µm	d_p=738 µm	d_p=1206 µm	
SP(BJH)	91%	19%	9%	58%
PPPM(BJH)	93%	24%	12%	54%
SP(MIP)	95%	34%	18%	46%
RPM	97%	51%	30%	33%
PPPM(MIP)	98%	67%	45%	19%
MD	100%	98%	95%	17%
SP(fitted)	99%	85%	70%	1%
Experiment	100%	85%	70%	-

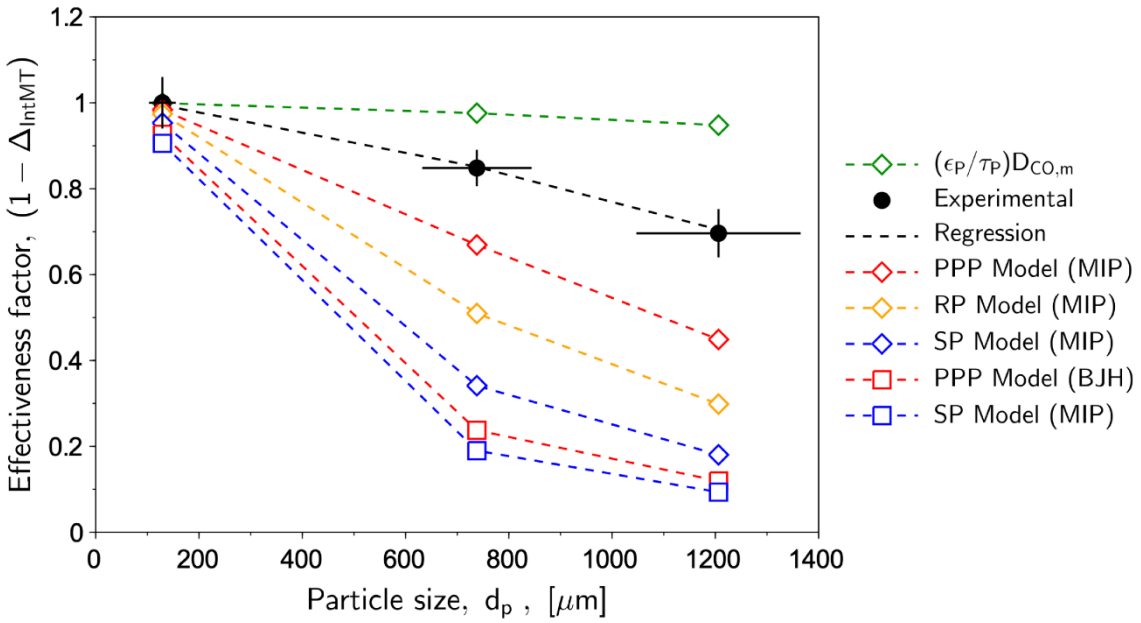

*Figure 2I – Comparison of experimental and model effectiveness factors of the WGS reaction over the UMW catalyst at **300 °C** and TOS ≤ 48 h*

*Table 3I – Comparison of experimental and model effectiveness factors of the WGS reaction over the UMW catalyst at **325 °C** and TOS ≤ 48 h*

Model	Internal mass transfer effectiveness factor, η_{IntMT}, [%]			MARR
	d_p=129 µm	d_p=738 µm	d_p=1206 µm	
SP(BJH)	86%	13%	7%	63%
PPPM(BJH)	89%	16%	9%	60%
SP(MIP)	93%	24%	13%	53%
RPM	96%	39%	23%	41%
PPPM(MIP)	98%	56%	36%	28%
MD	100%	97%	93%	18%
SP(fitted)	99%	82%	68%	4%
Experiment	100%	87%	65%	-

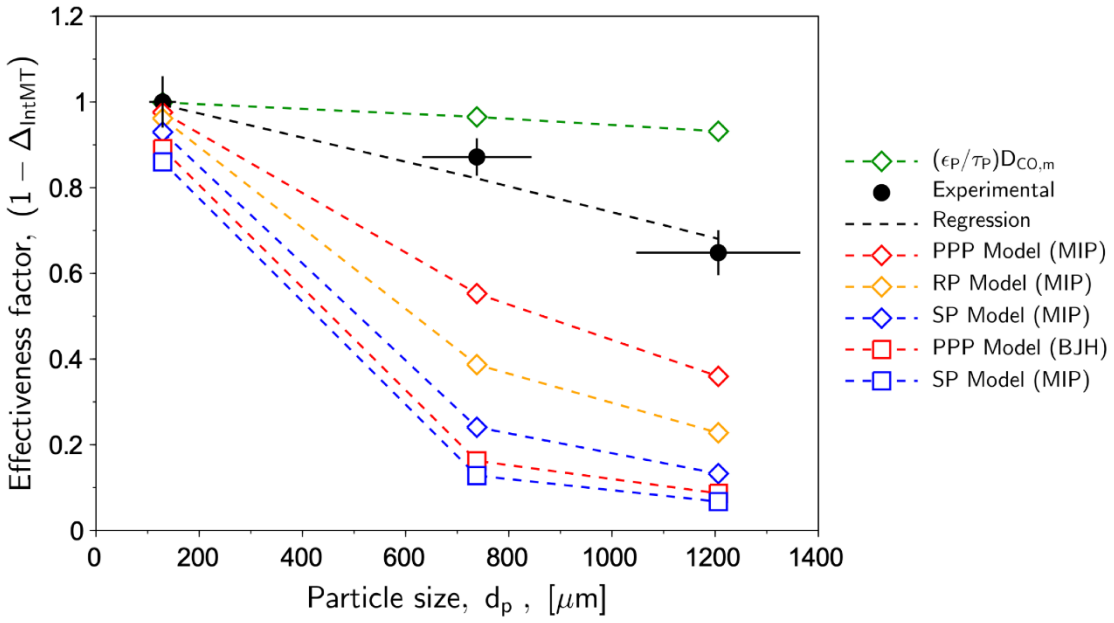

*Figure 3I – Comparison of experimental and model effectiveness factors of the WGS reaction over the UMW catalyst at **325 °C** and TOS ≤ 48 h*

Appendix J: Ethics form

Application for Approval of Ethics in Research (EiR) Projects
Faculty of Engineering and the Built Environment, University of Cape Town

APPLICATION FORM

Please Note:
Any person planning to undertake research in the Faculty of Engineering and the Built Environment (EBE) at the University of Cape Town is required to complete this form **before** collecting or analysing data.The objective of submitting this application *prior* to embarking on research is to ensure that the highest ethical standards in research, conducted under the auspices of the EBE Faculty, are met. Please ensure that you have read, and understood the **EBE Ethics in Research Handbook**(available from the UCT EBE, Research Ethics website) prior to completing this application form: http://www.ebe.uct.ac.za/usr/ebe/research/ethics.pdf

APPLICANT'S DETAILS		
Name of principal researcher, student or external applicant		Dawid Kruger
Department		Chemical engineering
Preferred email address of applicant:		Krgdaw001@myuct.ac.za
If a Student	Your Degree: e.g., MSc, PhD, etc.,	MSc
	Name of Supervisor (if supervised):	Prof. JCQ Fletcher
If this is a researchcontract, indicate the source of funding/sponsorship		N/A
Project Title		Design of a tubular fixed-bed micro-reactor for use in heterogeneous catalyst testing

I hereby undertake to carry out my research in such a way that:

- there is no apparent legal objection to the nature or the method of research; and
- the research will not compromise staff or students or the other responsibilities of the University;
- the stated objective will be achieved, and the findings will have a high degree of validity;
- limitations and alternative interpretations will be considered;
- the findings could be subject to peer review and publicly available; and
- I will comply with the conventions of copyright and avoid any practice that would constitute plagiarism.

SIGNED BY	Full name	Signature	Date
Principal Researcher/ Student/External applicant	Dawid Kruger		**22 May 2017**

APPLICATION APPROVED BY	Full name	Signature	Date
Supervisor (where applicable)	JACK C.Q. FLETCHER		22 May 2017
HOD (or delegated nominee) Final authority for all applicants who have answered NO to all questions in Section1; and for all Undergraduateresearch (Including Honours).	ERIC VAN STEEN		22 May 2017
Chair : Faculty EIR Committee For applicants other than undergraduate students who have answered YES to any of the above questions.			

Page **1** of **1**